

GARCIA

CENTER FOR POLYMERS AT
ENGINEERED INTERFACES

 Stony Brook
University



“The program has no set time limits. Research is a lifelong experience and we hope to remain a resource to our students long after ‘graduation’

The Garcia Center for Polymers at Engineered Interfaces was founded in 1996 and is named after the late Queens College professor Narciso Garcia, who was a pioneer in the integration of education and research. The Center focuses on the integration of materials research with tissue engineering, biomaterials, drug delivery systems, sustainable energy, nanocomposites, and recently, additive manufacturing. The Center also supports innovation through entrepreneurship and has multiple collaborations with industry and national laboratories, both in the US and abroad.

The research scholar program offers the opportunity for high school teachers, undergraduate, and high school students to perform research on the forefront of polymer science and technology together with the Garcia faculty and staff. Students work as part of focus research teams and are taught to make original contributions of interest to the scientific community. In addition to entering national competitions, the students are encouraged to publish in refereed scientific journals, present their results at national conferences, and develop patents to protect their intellectual property.

Our goal is to convey to the students the excitement we enjoy daily in research and provide for them a supportive network within the scientific community. Research is a lifelong experience and we hope to remain a resource to our students long after “graduation”.



Jonathan Sokolov



Miriam Rafailovich

High School Students



Alagappan, Vimala



Balsam, Abraham



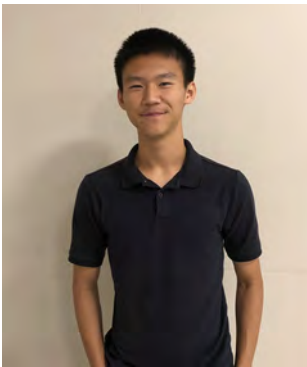
Bian, Carter



Bliznakov, Todor



Cai, Frank



Cai, George



Chai, Esther



Chan, Christopher



Chen, Yijun



Cheng, Kimberley



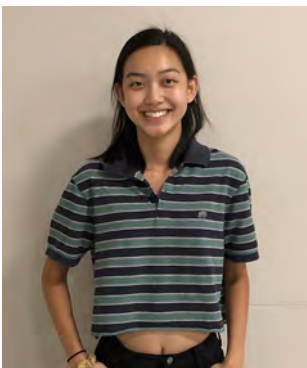
Cheng, Richard



Choo, Dianne



Christianson, Finnur



Cong, Rhea



Cox, Jack



Cui, Audrey

High School Students



Dhulipalla, Suraj



Duong, Teresa



Eisenberg, Ethan



Garg, Nyle



Gopal, Megha



Grajower, Meirav



Gu, Kevin



Gulzar, Saba



Guo, Ellen



Hamerman, Hannah



Han, Michael



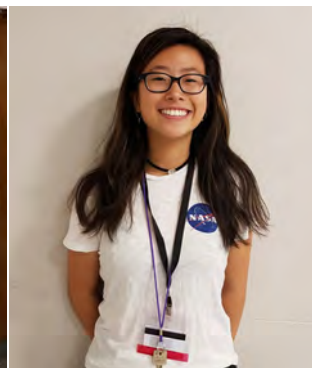
Huang, Larry



Huq, Zahin



Kim, Eric



Kong, Christine

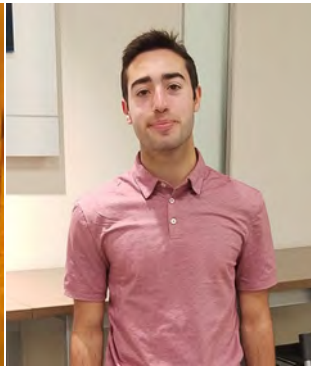


Korn, Elizabeth

High School Students



Kwandou, Alexander



Lederer, David



Lederer, Jonathon



Lee, Clara (Dokyung)



Leger, Luca



Lessler, Stella



Levy, Victoria



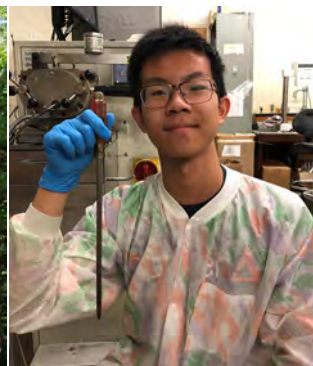
Li, Jasmine (Lisha)



Li, Jeffrey



Li, Mingkang



Li, Richard



Li, Songtao



Liu, Addison (Yeongsing)



Liu, Qinxì



Luo, Daniel



Ma, Carl (Zijian)

High School Students



Meehan, Ryan



Mehta, Dipen



Mehta, Jalaj



Mehta, Somya



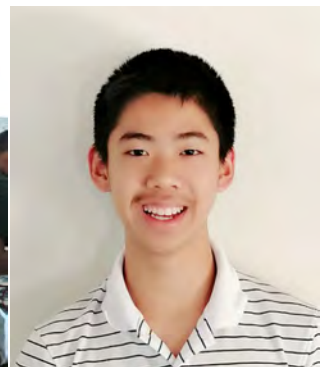
Milan, Roberto



O'Keefe, Edward



Padwa, Shmuel



Pan, James (Bole)



Pan, Luisa



Pandey, Ikshu



Paramesh, Rithu



Pollner, Alina



Rai-Gersappe, Diya



Rajan, Surya



Ramrakhiana, Sahana



Raniwala, Rishabh

High School Students



Rao, Avinash



Sacolick, Ilana



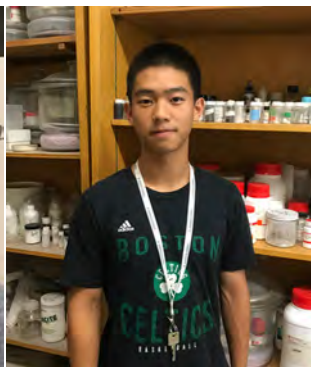
Salunke, Nikita



Sandhu, Bhawan



Shanmugam, Mukil



Shen, Hans



Silverstein, Emily



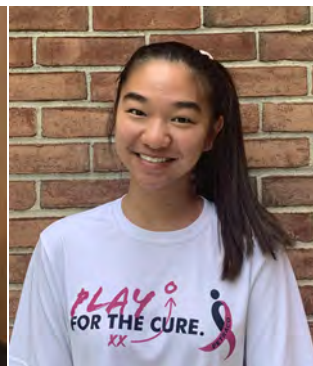
Stabile, Michael



Stabile, Nicholas



Steifel, Lauren



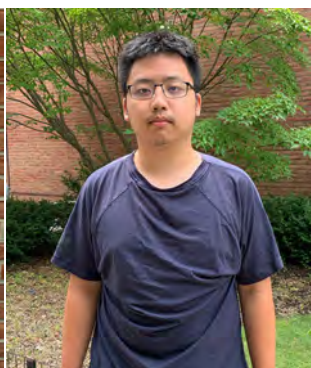
Tian, Katherine



Walsh, Emma



Wolberg, Jeffrey



Wu, Songze

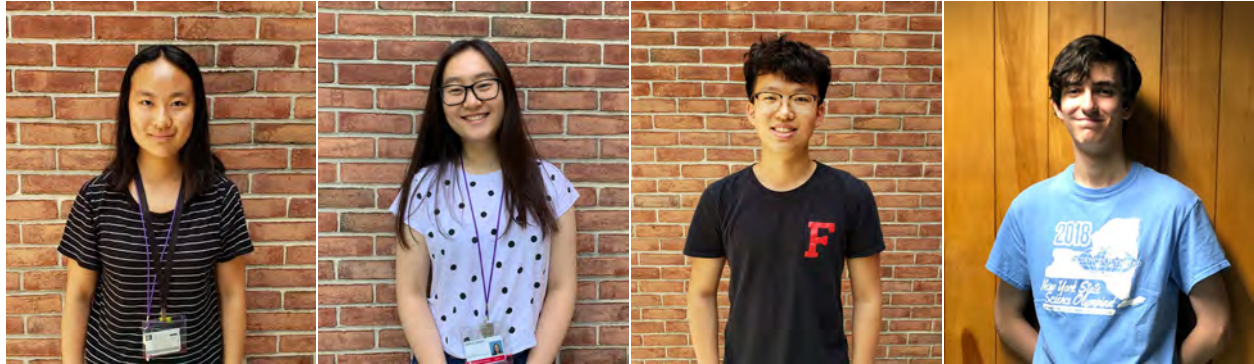


Xiang, Eric



Xing, Kathy

High School Students



Yang, Doris

Yang, Kerui

Yang, Kevin

York, Aidan



Zhang, Mark

Zhu, Aris

Zhu, Jocelyn

Research Experience for Undergraduates (REUs)



Akhter, Atif

Azim, Adeel

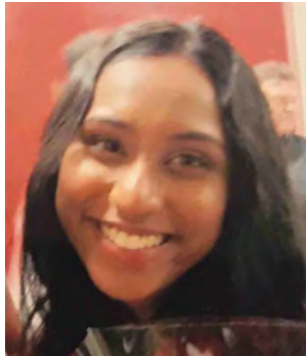
Christie, Olias

Del Valle, Anthony

Research Experience for Undergraduates (REUs)



Essuman, Bernard



Etwaru, Karena



Franquero, Angelina



Ginez, Anthony



Huq, Zahin



Jennings, Joseph



Lam, Bill



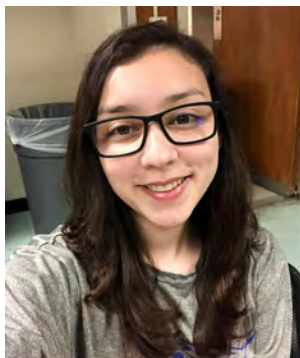
Linskens, Kelvin



Marcelin, Jonathan



Meacham, Rachel



Paz, Rachell



Quinto, Lisa



Semel, Jessica



Su, Vivian



Graduate Students



Chuang, Ya-Chen



Feng, Kuan-Che



Hofflich, Jessica



Li, Juyi



Li, Kao



Lin, Yu-Chung



Raut, Aniket



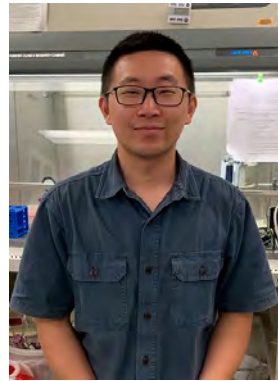
Shmueli, Yuval



Wang, Likun



Xue, Yuan



Yang, Fan



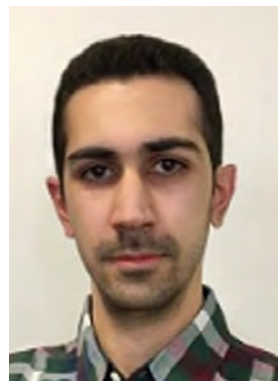
Yin, Yifan



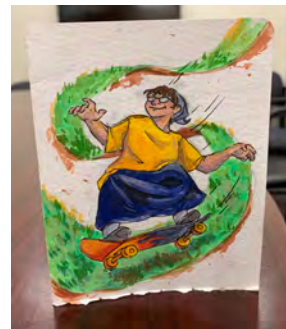
Zhou, Yuchen



Zuo, Xianghao



Koosha, Farzad



Faculty/Staff



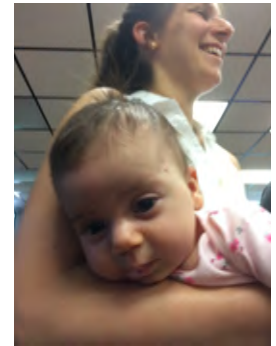
Isseroff, Rebecca



Bertolotti, William



Weiss, Herb



Recruit, Fresh :)



Bliznakov, Stoyan



Sadasivan,
Chandramouli



Cuiffo, Michael



Nitodas, Steve



Gersappe, Dilip



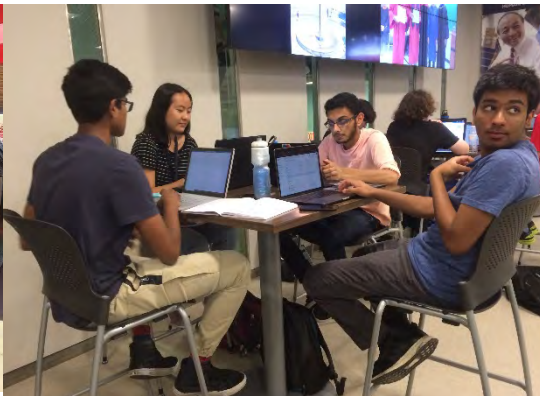
Jerome, John



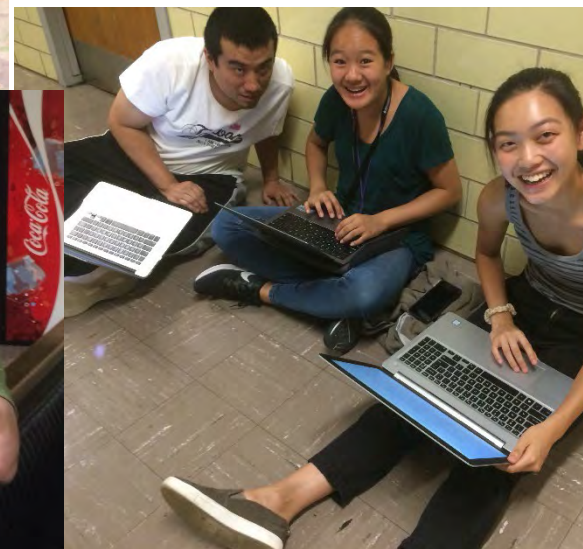
Walker, Steven



Simon, Marcia



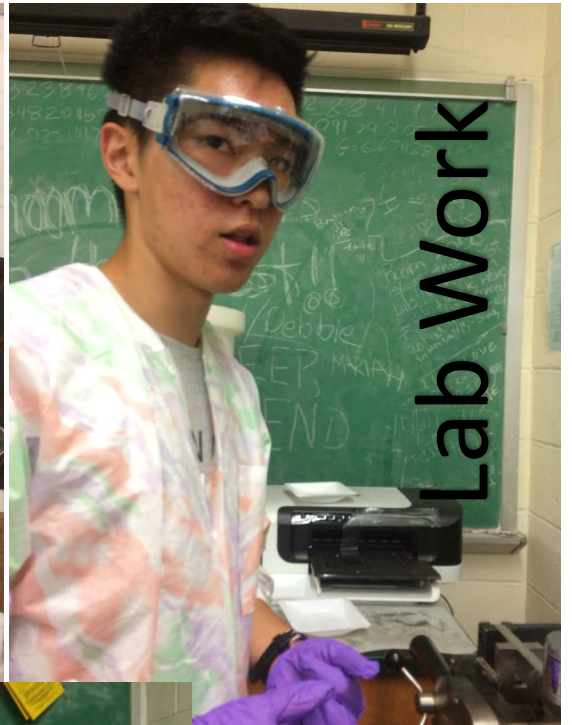
Friends





Dunkin' and Softball





Lab Work

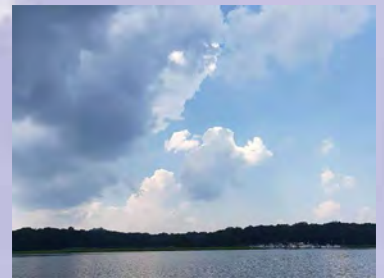


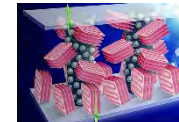


Outdoors



Canoeing!

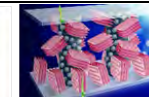




Attendance at the Daily 10:00 AM Group Meeting is Mandatory

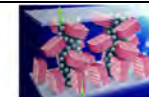
Daily Schedule of Activities

	MONDAY	TUESDAY	WEDNESDAY	THURSDAY	FRIDAY
	6/24		6/26	6/27	6/28
<p><u>Week of 6/24</u> Homework: Select peer reviewed paper and prepare ppt presentation for journal club on Monday. Instructions: Talks are 5 minutes long, maximum 6 viewgraphs; Viewgraph 1: title, citation, your name, high school Viewgraph 2: Introduction, motivation Viewgraph 3: Materials and methods (summary of most important) Viewgraphs 4-5: results, (data) discussion Viewgraph 6: Conclusion (summary), did you like the paper? (critique)</p>			<p>4:00 PM Housing Check in Begins</p>	<p>10:00am -10:10 Introduction to Garcia</p> <p>10: 10am-10:20 am Judith Berhannan Dean of Admissions Welcome to Stony Brook</p> <p>10:30 am-11:00 am Groups 1-4 ID Cards at SAC Groups 5-8: Intro to theory and modeling, Dr. Dilip Gersappe</p> <p>11:00 am-11:30am Groups 4-8 ID Cards at SAC Groups 1-4: Intro to theory and modeling, Dr. Dilip Gersappe</p> <p style="color: red;">11:30-12:30 Lunch at East Side Dining</p> <p>12:45 pm- 1:45 pm Dr. Srinivas Pentyala: The Why of Research</p> <p>1:45 pm -2:40 pm Dr. Tim Benseman CUNY-Queens College Terahertz radiation imaging</p> <p>2:40 pm- 3:30 pm Dr. Sunil Sharma Dr. Priyanka Sharma Cellulose Chemistry</p> <p>3:30 pm-4:00 pm Yuval Shmueli 3-D FDM Printing</p>	<p>10:00am General meeting Statistics Lecture I</p> <p>10:30-12:30 Library/Data Mining/SBU ID problems DoIT, Maoro Nicoletto Clara Yuet , Jin Guo Yuval Shmueli,</p> <p style="color: blue;">12:30 Working Lunch PIZZA (from Hunki's)</p> <p>12:30pm- 1:30pm Mariah Geritano SKYPE Tour or the Boston Children's Hospital 3-D Printing Simulation Laboratory</p> <p>1:30-2:00 Highlights of Science Research on Hydrogen Fuel Cells –former Garcia students Audrey Shine, Plainview HS Danielle Kelly, Friends Academy HS</p> <p style="color: blue;">2:00 Dismissal to LIRR Have a good weekend!!</p>



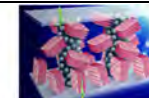
Mandatory meeting for all: daily at 10:00 AM

	MONDAY	TUESDAY	WEDNESDAY	THURSDAY	FRIDAY
I. This week we begin lab work. Starting Tuesday morning, please wear proper laboratory attire: (1) Closed toe shoes. (2) NO shorts (3) NO tank tops. You will get your own lab coat and goggles which must be work in the labs at all times.	7/1 10:00am -10:05 General Meeting 10: 15-11:00 Dr. Chang Yong Nam, BNL Atomic Layer Deposition Journal Club 11:00 am-12:50 pm Divide into 8 groups and report to designated rooms for presentations with your REUs and grads. 12:50-1:30 pm LUNCH At East Side Dining with your group	7/2 10:00am General meeting 10:10 AM-1:00 PM Mandatory Safety Training for all Garcia REU and HS students Note: Water, snacks, in the back of the room—important to be alert and pay attention. 1:00-1:45 pm Lunch at East Side Dining 1:45-2:15 PM Dr. Mircea Cotlet BNL-CFN 2:15-3:10 PM Mrs. Rebecca Isseroff Lawrence High School 1. Magic of Graphene 2. Keep a Lab Notebook 3. MRS conference 3:10-4:00 Groups 1-4 Get their boxes and prepare solutions 3:10- 3:50PM **Groups 5-8 Experiment overview/ Ellipsometry/ 3:50 -4:40 PM Prepare solutions ** Late session for groups 5-8	7/3 10:00am - 10:15 General meeting 10:15-4:00 PM Spin Casting Experiment And hands on safety training specific to Garcia labs	7/4 Enjoy The Holiday! 	7/5 10:00am General meeting Writing the lab reports 10:05-10:45 AM Dr. Marcia Simon, SDM “Printing Skin” 10:45-2:00 PM Facilities tour AFM - Ya-Cen Chuang LB trough – Aniket Raut Zeta potential/UV/VIS- Fan Yang Cell Lab/ Kuan-Che Feng Rheology/Bioprinter- Juyi Li Electrospinning - Kao LI, Fuel cells/TGA - Likun Wang Tensile/ Impact/Extrusion Xianghao Zuo Confocal microscope – Yuchen Zhuo UV vis and DLS - Fan Yang 12:15 PIZZA working lunch (Hunkis)
II. Written individual lab reports are due on Monday, July 8 th —uploaded under your name in the spin casting folder for your group.	1:30-2:15 pm Dr. Steve Schwarz, Queens College, CUNY Rheology of Entangled Polymers 2:15 -3:00 pm Dr. Stoyan Bliznakov Hydrogen Fuel Cells 2:00-3:15pm Mandatory EH&S training for Grads				
III. Quiz on Monday morning covers lab safety and facilities.	3:00-4:00 PM Dr. Adriana Pinkas Sarafova, SCC 3-D printing with Dental Pulp Stem Cells				
IV. Please prepare Group presentations for Monday morning.					




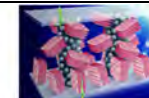
Mandatory meeting for all: daily at 10:00 AM

	MONDAY	TUESDAY	WEDNESDAY	THURSDAY	FRIDAY
Notes:	7/8	7/9	7/10	7/11	7/12
Safety Quiz moved to Tues.	10:00am -10:05 General Meeting	10:00am General meeting/science moment	10:00am General meeting/science moment	10:00am General meeting/science moment	10:00am General meeting/science moment
Study materials will be provided.	10:05-10:15 AM Group Picture in Lobby	10:15-11:00AM Dr. Ying Liu-EH&S Writing the SOP	10:15-11:00 Dr. Robert Harrison Institute for Advanced Computational Science	10:15-10:45 Dr. Sima Mofakham Neuroscience Finalize SOP and upload to your project folder.	10:10 5 minute project updates 1.Polymer Blends—Xianghao's groups
Lab reports must be uploaded by 11:59 PM Monday 7/8.	10:15-11:00 AM Dr. Peter Brink, HSC Swimming with Sharks While curing cancer	11:00-11:30 Safety Quiz	11:00--SELECTION OF PROJECTS/WRITING SOP		2. Gels for fire retardance—Yuan's groups
Before starting lab work:	11:00-11:45 AM Dr. Jonathan Sokolov DNA Science	11:30-12:00 10 minute research talks III	Lunch as coordinated with your projects	Lab work PROPER LAB ATTIRE	3. 3-D Skin printing—Juyi/VIP/Dr. Simon groups
(a) Pass Safety Quiz (b) Write SOP with your graduate student supervisor	11:45 -12:10 PM 10 minutes Research Talks part I	1. Yuan Xue 2. Ya-Chen Chuang			
Tuesday: Last day of Research Bootcamp. Last day of Lunch with Groups...Take an REU out for Lunch to say thank you! Once you select a research project—coordinate your time with other members of the team.	1. Juyi Li—Hydrogels and bioprinting	12:00PM-12:45 Take Your REU Out for Lunch Day	Lab work PROPER LAB ATTIRE		Hunkies Pizza Lunch in Lecture Hall 145
	2. Likun Wang—Fuel Cells	3.			Lab work PROPER LAB ATTIRE
	12:00-12:45 Lunch	12:45-1:30PM Research Talks Part IV			REUs Please have pics of your groups completed.
	12:45-2:30PM Presentations of Groups I-VIII	1. Fan Yang 2. Kao Li 3. Kuan-Che Feng			Save the date next week: July 17 @10:AM Dr. Mary Truhlar, Dean of School of Dental Medicine – Preparing for a Career in Dentistry
	2:30-3:00 Dr. Stephen Walker, Microbiology	1:30 -4:00 PM SELECTION OF PROJECTS			Upcoming events next week: Evening Baseball Game Bring Instruments—Dr. Jerome is beginning his musical ensemble
Research Rules	3:00-4:00 10 minute Research Talks Part II				
1. All Groups remain in lecture hall 145 till they are called out by their Grad/Staff leader.	1. Yuan Xue 2. Ya-Chen Chuang 3. Fan Yang 4. Xainghao Zuo 5. Kuan-Che Feng				
2. NO One works alone in the labs without a supervisor (21+) in the room.					
3. Everyone must attend 10 o'clock meeting					


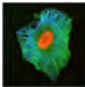





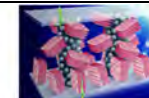
Mandatory meeting for all: daily at 10:00 AM

	MONDAY	TUESDAY	WEDNESDAY	THURSDAY	FRIDAY
<p>Notes:</p> <p>Research Rules</p> <ol style="list-style-type: none"> All Groups remain in lecture hall 145 till they are called out by their Grad/Staff leader. NO One works alone in the labs without a supervisor (21+) in the room. Everyone must attend 10 o'clock meeting. Every group will present a status report before the end of the program. Garcia values continual learning. We will continue to have lectures, which you have the option of attending if you are not scheduled for work with your mentor. Some lectures are still MANDATORY for everyone. They will be marked in red and starred; <p>** Mandatory lecture</p> <p>REUs: Please complete uploading the head shots of yোগroups and upload head shots of yourselves and your grad students as well!</p>	<p>7/15</p> <p>10:00am -10:05 General Meeting</p> <p>**10:10-10:50 AM Prof. Brooke Ellison Engineering Ethics/Science with Social Responsibility</p> <p>11:00 Dr. Marcia Simon will speak to the neural group on protocols for differentiation of DPSC along neurogenic lineage.</p> <p>Lab work PROPER LAB ATTIRE</p>	<p>7/16</p> <p>10:00am General meeting/science moment: Young's Contact Angle</p> <p>Lab work PROPER LAB ATTIRE</p>  <p>6:30PM-8:30PM Night Fishing and Bagel Sunset Dinner on the Celtic Quest. Meet in Lecture Hall 145 at 5:30. Buses leave SAC loop at 5:45.</p>	<p>7/17</p> <p>10:00 am General Meeting 10:05-10:20 am Dr. Mary Truhlar <i>Dean, School of Dental Medicine</i> Exploring careers in dentistry</p> <p>Lunch as coordinated with your projects schedule</p> <p>Lab work PROPER LAB ATTIRE</p>	<p>7/18</p> <p>10:00am General meeting/science moment</p> <p>10:05-10:20 Grace Agnetti, Assistant Dean for Admissions <i>Renaissance School of Medicine</i> Exploring careers in medicine</p> <p>Lunch as coordinated with your projects schedule</p> <p>Lab work PROPER LAB ATTIRE</p>	<p>7/19</p> <p>10:00am General meeting/science moment</p> <p>10:00-11:00AM Dr. Lev Neymotin-BNL emeritus Effects of Nuclear Radiation Nuclear Dilemma: Energy vs. Weapons. Neither?</p> <p>11:00-11:50AM</p> <ol style="list-style-type: none"> Supercapacitor group Xianghao's thin film crystallization group CASA Group Yuan's flame retardant group <p>Hunkies Pizza Lunch in Lecture Hall 145</p> <p>Lab work PROPER LAB ATTIRE</p>



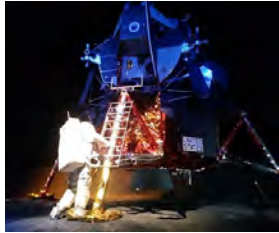
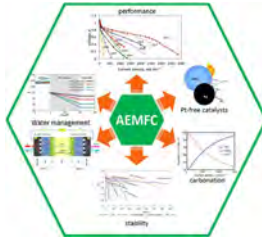


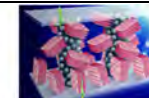
Mandatory meeting for all: daily at 10:00 AM

	MONDAY	TUESDAY	WEDNESDAY	THURSDAY	FRIDAY
Upcoming Events:	7/22	7/23	7/24	7/25	7/26
<p>BNL Summer Sundays Trip: July 28th –visit to the Center for Functional Nanomaterials. With Drs Chang-Yong Nam and Mircea Cotlet Sign up sheet on Google Drive. Buses leave Stony Brook at 10:00 and return at 3:00 PM</p>  <p>July 28 Exploring the Ultra Small Tour the Center for Functional Nanomaterials.</p> <p>Canoe Trip 7/31 or 7/30, weather permitting. Stay tuned for details.</p> <p>Research Rules 1. All Groups remain in lecture hall 145 till they are called out by their Grad/Staff leader. 2. NO One works alone in the labs without a supervisor (21+) in the room. 3. Everyone must attend 10 o'clock meeting. 4. Only ** red lectures are mandatory</p>	<p>10:00am -10:15 General Meeting Atomic Force Microscopy</p> <p>Lunch as coordinated with your projects schedule</p> <p>Lab work PROPER LAB ATTIRE</p>	<p>10:00am General Meeting 10:05-10:20AM</p> <p>12:00 PM Dr. Jerry Cymerman: Dental shadowing opportunities at the Stony Brook Dental Clinic</p> <p>Lunch as coordinated with your projects schedule</p> <p>Lab work PROPER LAB ATTIRE</p>	<p>10:00 am General Meeting</p> <p>Lunch as coordinated with your projects schedule</p> <p>5:00 PM Softball Game Cells vs Cells</p>    <p>Meet in Lobby in front of Lecture Hall 145</p> <p>Lab work PROPER LAB ATTIRE</p>	<p>10:00am General meeting/science moment</p> <p>**Dr. Rina Tannenbaum FTIR and RAMAN spectroscopy</p> <p>Lunch as coordinated with your projects schedule</p> <p>Lab work PROPER LAB ATTIRE</p>	<p>10:00am</p> <p>**Donna Tuminello Intellectual Property</p> <p>General meeting/science moment</p> <p>10:00-11:30 AM</p> <ol style="list-style-type: none"> 1. DNA group 2. Theory group 3. Kao Li's cell groups 4. Yuchen's group <p>Outdoor BBQ</p>  <p>Lab work PROPER LAB ATTIRE</p>







Mandatory meeting for all: daily at 10:00 AM

	MONDAY	TUESDAY	WEDNESDAY	THURSDAY	FRIDAY
<p>Upcoming Events:</p> <p>Please be prompt on days of scheduled trips. Buses will leave promptly.</p> <p>Labs are closed till 4 PM on Wednesday to allow for maintenance.</p> <p>INVITATIONS for symposium will be uploaded: Please send to parents, teachers, friends, and family. We need to have RSVP for the end of summer symposium on 8/8/19</p> <p>Research Rules</p> <ol style="list-style-type: none"> 1. All Groups remain in lecture hall 145 till they are called out by their Grad/Staff leader. 2. NO One works alone in the labs without a supervisor (21+) in the room. 3. Everyone must attend 10 o'clock meeting. 4. Only ** red lectures are mandatory 	<p>7/29</p> <p>10:00am -10:15 General Meeting Electron Microscopy— TEM vs SEM Yuan Xue--AERTC</p>  <p>Lunch as coordinated with your projects schedule</p> <p>Lab work PROPER LAB ATTIRE</p>	<p>7/30</p> <p>10:00am General Meeting</p> <p>Canoe Trip Today Bob's canoe rental Buses leave at 10:00 AM. We are aiming to return at 2:00PM to Stony Brook</p> <p>Do NOT bring computers, electronics, backpacks, etc on boats.</p> <p>Bring water bottles, sunscreen, ...we will also have water bottles, snacks, Hunki's bagel lunch</p>  <p>Lab work PROPER LAB ATTIRE</p>	<p>7/31</p> <p>10:00 am General Meeting</p> <p>Garcia Educational Enrichment trip:</p> <p>Cradle of Aviation Museum Special tour of Grumman Lunar Lander and IMAX Theater. Bagel Lunch from Hunkis</p> <p>Museum security does not allow Backpacks</p>  <p>REMEMBER the Materials Challenge!! PPT viewgraph: Science in the Service of Society Describe A Material or Technology Developed for the Manned Space Program which is now in civilian use. (a) Describe the technology, (b) what was its function in the space program, and (c) what is it used for today. Evidence based..with references. Prizes for the best entries.</p> <p>Labs Closed for Clean Up till we return at 4 PM</p>	<p>8/1</p> <p>10:00am General meeting/science moment</p> <p>Special Seminar: Anion-Exchange Membrane Fuel Cells Dario R. Dekel Technion – Israel</p>  <p>Lunch as coordinated with your projects schedule</p> <p>Lab work PROPER LAB ATTIRE</p>	<p>8/2</p> <p>10:00am</p> <p>General meeting/science moment</p> <p>10:00-11:30 AM</p> <ol style="list-style-type: none"> 1. Aneurism group 2. Nanotoxicology group(Fan Yang's group) 3. Kao Li's cell groups 4. Fan Yang's DISC movie group 5. Hydrogen cellulose fuel cell <p>Hunki's Pizza Lunch</p> <p>Lab work PROPER LAB ATTIRE</p>



Mandatory meeting for all: daily at 10:00 AM

	MONDAY	TUESDAY	WEDNESDAY	THURSDAY	FRIDAY
Upcoming Events:	8/5	8/6	8/7	8/8	8/9
<p>Abstracts due Monday at 5 PM. REMEMBER:</p> <ul style="list-style-type: none"> - One per project -Title, authors, address page --MAX one page with ONE inch margins, Minimum 10pt font. -Must have one or more of following; (a)figures with figure captions, mentioned in text. (b) peer reviewed reference, MLA format. <p>Symposium 10AM-1PM, Formal music and science presentations. RSVP: 8/7/ 4 PM Bring Family, friends, teachers.</p> <p>GARCIA continues after 8/9 BUT- (1) dorms close after 8/9. (2) No 10AM meetings in 145. (3) Meet/snacks in 210.</p> <p>Research Rules—valid after formal program is over----</p> <ol style="list-style-type: none"> 1. Everyone must wear proper PPE at all times. 2. NO One works alone in the labs without a supervisor (21+) in the room. 	<p>10:00am General Meeting Science Moments by students: (a) Ya-Chen’s groups (b) DNA project</p> <p>12:00 in Lecture Hall 145 Dr. Marcia Simon will review principals of RT-PCR.</p> <p>Lunch as coordinated with your projects schedule</p> <p>Lab work PROPER LAB ATTIRE</p>	<p>10:00am General Meeting Science Moment (a) Likun’s groups (b) Aerogel group (c) Stoyan’s group</p> <p>Lunch as coordinated with your projects schedule</p> <p>Lab work PROPER LAB ATTIRE</p>	<p>10:00 am General Meeting (LAST ONE) Announcement of Best REU and Grad Mentor Awards.</p> <p>Science moments: Kuan-Che’s students—2 groups: PLA ALD and PLA gels Jonathan Lederer and Avi Balsam—RGO/Enzymatic activity Biosensor project</p> <p>SYMPOSIUM ppt due 2PM to projectionist</p> <p>Lunch as coordinated with your projects schedule</p> <p>Have any non-perishable food left? Don’t throw it out—We are collecting donations for Island Harvest in room 145.</p> <p>Lab work PROPER LAB ATTIRE</p>	<p>10:00am-2:00 pm Garcia Symposium: Science and Music</p>    <p>Summer 2019</p> <p>Lab work PROPER LAB ATTIRE</p>	<p>10:00am General meeting Trip to ICL-Ardsley, NY</p>  <p>Lunch sponsored by ICL.</p> <p>Presentations: Yuan’s Flame retardant groups Likun’s Hydrogen/cellulose groups</p> <p>Return to SBU at 3PM</p> <p>Lab work PROPER LAB ATTIRE</p>

Invitation



Stony Brook University



*Annual Summer Scholar
Research Symposium & Musicale
Thursday, August 8th, 2019
10:00am — 2:00pm
Student Activity Center, Ballroom A
Buffet Luncheon: Wing Wan of West Hempstead
Guest Speaker*

Steven C. Vaccarelli

Vice President | Trust Officer

**BROWN BROTHERS HARRIMAN TRUST
COMPANY, N.A.**

Please RSVP before Tues August 6, 2019

Via email to :

Michael.Cuiffo@stonybrook.edu

Summer Symposium

2019

GARCIA

CENTER FOR POLYMERS AT
ENGINEERED INTERFACES

 Stony Brook
University

9:30 AM	Breakfast
9:50 AM	Musical Presentation Arranged by Professor John Luckner Jerome and Garcia Students
10:00 AM	Mr. Steven C. Vaccarelli Vice President, Senior Trust Officer, BBH
10:10 AM – 10:25 AM	Materials Research for Biomedical Applications Chairs: Karena Etwaru and Angelina Franqueiro Cornell University, Ithaca, NY
	<i>Characterization of Salicylic Acid and Calcium Hydroxide Paste (CASA) as a Novel Antimicrobial Medicament for Endodontic Applications</i> Aris Zhu , Hamilton High School, Chandler, AZ Jeffrey Wolberg , HAFTR High School, Cedarhurst, NY
	<i>Titanium Dioxide Nanoparticles Increase Risk of Bacterial Infection in Human Cells</i> Alina Pollner , Canyon Crest Academy, San Diego, CA
	<i>Modification of Thrombin Enzymatic Activity Using Graphene Oxide and Partially Reduced Graphene Oxide Nanoparticles</i> Abraham Balsam , Rambam Mesivta, Lawrence, NY Jonathan Lederer , Hebrew Academy of the Five Towns and Rockaway, Cedarhurst, NY
	<i>Using Digital Imaging Skin Correlation to Predict Comatose Recovery</i> Rachell Paz , Suffolk Community College, Selden, NY Anthony Ginez , Nassau Community College, Garden City, NY



10:25 AM – 10:35 AM	Medical Hydrogels and Bioprinting Chair: Adeel Azim and Zahin Huq , Stony Brook University
	<i>Development of Novel Cerebral Aneurysm Embolization Method via Injection of Pluronic® F-127 Multiblock Copolymer Hydrogel</i> Finnur Christianson , Ponte Vedra High School, Ponte Vedra, FL Kevin Yang , Fairview High School, Boulder, CO Rithu Paramesh , Presentation High School, San Jose, CA Diya Rai-Gersappe , Huntington High School, Huntington, NY Ikshu Pandey , East Meadow High School, East Meadow, NY
	<i>Measuring Collagen Contraction and Keratinocyte Colony Efficiency for the Viability of Bioprinting Skin Using Extrusion-Based Printing vs. Traditional Skin Grafting Methods</i> Christopher Chan , Hicksville High School, Hicksville, NY Teresa Duong , St. Anthony’s High School, Melville, NY Saba Gulzar , New Hyde Park Memorial High School, New Hyde Park, NY Katherine Tian , Ward Melville High School, East Setauket, NY
	<i>Analyzing and Comparing 3D Bioprinted Organotypic Dermis and Epidermis to Native Skin</i> Dokyung Lee , Daegu International School, Daegu, South Korea Stella Lessler , Yeshivah of Flatbush Joel Braverman High School, Brooklyn, NY Somya Mehta , Hicksville High School, Hicksville, NY
10:35 AM – 10:45 AM	Hydrogels for Flame Retardant Applications Chairs: Pik Hoi Lam , Caltech and Lisa Quinto , Stony Brook University
	<i>Enhancing the Flame Retardancy of Biodegradable Poly(vinyl alcohol) Hydrogels with Resorcinol Bis(diphenyl phosphate) Coated Starch</i> Jalaj Mehta , Hauppauge High School, Hauppauge, New York Lauren Stiefel , Samuel H. Wang Yeshiva University High School for Girls, Holliswood, NY
	<i>Synthesis of A Novel Flame-retardant Hydrogel for Skin Protection Using Xanthan Gum and Resorcinol Bis(diphenyl phosphate)-coated Starch</i> Mingkang Li , Shanghai Star-river Bilingual School, Shanghai, China Bole Pan , Guangzhou Tianhe Foreign Language School, Guangzhou, China
	<i>Development of a Hydrogel-based Intumescent Flame Retardant System for Limiting Wildfire Propagation</i> Audrey Cui , Monta Vista High School, Cupertino, CA Kimberley Cheng , Princeton High School, Princeton, NJ Frank Jin Rui Cai , Arcadia High School, Arcadia, CA



10:45 AM – 10:55 AM	<p>DNA Chip Technologies Chairs: Anthony Del Valle, Stony Brook University, Joseph Jennings, Nassau Community College</p>
	<p><i>A Novel Method to Apply Restriction Enzymes Through Low Volume Chambers for DNA Fragmentation in Next Generation Sequencing Library Preparation</i> Kerui Yang, Edina High School, Edina, MN Qinxi Liu, Shenzhen Middle School, Shenzhen, Guangdong Jocelyn Zhu, Amador Valley High School, Pleasanton, CA</p>
	<p><i>Temperature- and Solubility-Dependent Desorption of Linearly Combed DNA from Polymer Substrates for Ordered Fragmentation and Sequencing</i> Ellen Guo, The Harker School, San Jose, CA Luisa Pan, The Harker School, San Jose, CA Kathy Xing, Leland High School, San Jose, CA</p>
	<p><i>Gel and Electric Field-Based Desorption of DNA from PMMA-Coated Silicon Surfaces to Optimize Sequencing Accuracy</i> Elizabeth Korn, Plainview-Old Bethpage John F. Kennedy High School, Plainview, NY</p>
10:55 AM – 11:05 AM	<p>Theory and Modeling Chairs: Kelvin Linskens, Stony Brook University</p>
	<p><i>Molecular Dynamics Simulation of Biopolymer-based Pore Fluids</i> Jeffrey Li, Gilman School, Baltimore, MD</p>
	<p><i>Optimizing Graphite Electrode of Lithium-ion Batteries with Lattice Boltzmann Modeling</i> Yijun Chen, Shenzhen Middle School, Shenzhen, China</p>
	<p><i>Lattice Boltzmann Modeling of Hydrogen Ion Transport in a Proton Exchange Membrane Fuel Cell</i> Alexander Kwandou, Bellarmine College Preparatory, San Jose, CA</p>
11:05 AM – 11:15AM	<p>Nanocomposites and FDM printing Chair: Bernard Essuman and Steve Nitodas, Stony Brook University</p>
	<p><i>Optimizing Thermal and Mechanical Properties of Poly(Lactic Acid) / Polypropylene / Graphene Nanocomposite Polymer Blends in Fused Deposition Modeling (FDM) Systems</i> Larry Huang, Wilton High School, Wilton, CT Richard Li, Conestoga High School, Berwyn, PA Addison Liu, Unionville High School, Kennett Square, PA Nikita Salunke, Evergreen Valley High School, San Jose, CA</p>



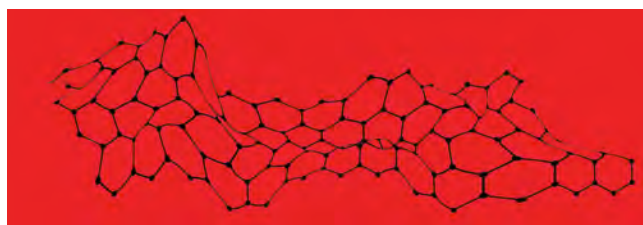
	<p><i>Mechanical and conductivity study of the 3D printed PBAT/PLA/graphene nanocomposites</i></p> <p>Da Hyun (Dianne) Choo, Kent School, Kent, CT Zhehua (Eric) Xiang, Lawrence Woodmere Academy, Woodmere, NY</p>
	<p><i>Studying the Crystal Formation and Interdiffusion Mechanisms of PLA Thin Films</i></p> <p>Suraj Dhulipalla, Eastlake High School, Sammamish, WA Mukil Shanmugam, Redmond High School, Redmond, VA Doris Yang, Lake Oswego High School, Lake Oswego, OR</p>
11:15 AM – 11:30 AM	<p>Dental Pulp Stem Cells: Mechanical and Chemical Sensing Chairs: Jessica Hofflich, Stony Brook University, Atif Akhter, Cornell University, and Rachel Meacham, Nassau Community College</p>
	<p><i>Elucidating the Effects of Direct Contact of Dental Pulp Stem Cells Cultivated Under Various Physical Parameters on Lineage Specification Pathways</i></p> <p>Yihan Shen, St. Andrew's School, Middletown, DE Zijian Ma, Tianjin Nankai High School, Tianjin, China</p>
	<p><i>Determining DPSC Differentiation Pathways and Biomineralization on ALD TiO₂ PB Thick and Thin Films</i></p> <p>Megha Gopal, New Hyde Park Memorial High School, New Hyde Park, NY</p>
	<p><i>Investigating the Mechanics and Differentiation of Dental Pulp Stem Cells on Polybutadiene-Polystyrene Substrate Nanopatterns</i></p> <p>Meirav Grajower, Yeshiva University High School for Girls, Queens, NY Ilana Sacolick, Hebrew Academy of the Five Towns and Rockaway, Cedarhurst, NY</p>
	<p><i>The Effect of Fibrin on the Differentiation of Human Dental Pulp Stem Cells</i></p> <p>Victoria Levy, Saint Anthony's High School, South Huntington, NY Vimala Alagappan, Friends Academy, Locust Valley, NY</p>
11:30 AM – 11:50 AM	<p>Differentiating Dental Pulp Stem Cells on Scaffolds Chair: Jonathan Marcelin and Jessica Semel, Stony Brook University</p>
	<p><i>Optimization of 3D-Printed Scaffolds for Dental Pulp Stem Cell Differentiation via Surface Coating of Proteins and Titanium Dioxide</i></p> <p>Esther Chai, Townsend Harris High School, Flushing, NY Richard Cheng, Clayton High School, St. Louis, MO Rhea Cong, Huron High School, Ann Arbor, MI</p>
	<p><i>Effect of PLA Scaffold Roughness on Dental Pulp Stem Cell (DPSC) Differentiation and Growth in an In Vitro Setting</i></p> <p>Roberto Milan, South Side High School, Rockville Centre, NY Todor Bliznakov, Ward Melville High School, East Setauket, NY</p>

	<p><i>Determining Discrepancies in the Migrational Behavior of Osteosarcoma and Dental Pulp Stem Cells by Comparing Their Movement</i></p> <p>Hannah Hamerman, Yeshiva University High School for Girls, Holliswood, NY Sahana Ramrakhiani, Sachem North High School, Lake Ronkonkoma, NY Emily Silverstein, Hebrew Academy of the Five Towns and Rockaway, Cedarhurst, NY</p>
	<p><i>Investigating Neurogenic Differentiation of Dental Pulp Stem Cells using Novel PLA and Graphene Thin-Film and Electrospun Fiber Scaffolds in Vitro</i></p> <p>Dipen Mehta, George Walton Comprehensive High School, Marietta, GA Michael Stabile, Plainedge High School, N. Massapequa, NY Nicholas Stabile, Plainedge High School, N. Massapequa, NY Daniel Luo, Monroe-Woodbury High School, Central Valley</p>
	<p><i>Utilization of Patch Clamping to Investigate the Influence of Graphene on Transmembrane Ion Current in HeLa Cells and the Efficacy of Novel Fluorescent Dye</i></p> <p>Daniel Luo, Monroe-Woodbury High School, Central Valley, NY Dipen Mehta, George Walton Comprehensive High School, Marietta, GA Michael Stabile, Plainedge High School, N. Massapequa, NY Nicholas Stabile, Plainedge High School, N. Massapequa, NY</p>
11:50 AM – 12:00 PM	<p>Perovskites and Graphene: Photovoltaics and Energy Storage</p> <p>Chair: William Bertolotti, Plainedge High School Science Research Coordinator</p>
	<p><i>Optimization of EDLC Supercapacitors via a Novel Comparison of Acetonitrile Versus Diethyl Carbonate - Ethyl Carbonate - Tetraethylammonium Tetrafluoroborate Electrolytes along with the effects of Graphite-Active Carbon versus Carbon Nanotube-Active Carbon versus Carbon Nanotube-Graphene Nanoplatelet in Supermaterial Electrodes</i></p> <p>Shmuel Padwa, Bronx High School of Science, Bronx, NY Rishabh Raniwala, Wilton High School, Wilton, CT Nyle Garg, Greenwich High School, Greenwich, CT</p>
	<p><i>Preparation of MAPbI₃ Perovskite via Hot-Casting Technique for Photovoltaic Application</i></p> <p>Jasmine Li, Fairview High School, Boulder, CO Aidan York, Kellenberg Memorial High School, Uniondale, NY</p>
	<p><i>Stability Enhancement of Perovskite Solar Cells Using Mixed Cation/Halide Perovskite</i></p> <p>Ethan Eisenberg, George W. Hewlett High School, Hewlett, NY Jack Cox, South Side High School, Rockville Centre, NY</p>



12:00 PM- 12:30 PM	Fuel Cell Technologies Chair: Aniket Raut and Priyanka Sharma, Stony Brook University
	<i>Enhancement of Quaternized Ammonium Polyaromatic Anion Membrane Performance in Alkaline Fuel Cells by Deposition of Graphene Oxide and Catalyst Ink Optimization</i> Avinash Rao , Dougherty Valley High School, San Ramon, CA Michael Han , Dougherty Valley High School, San Ramon, CA Carter Bian , Cupertino High School, Cupertino, CA
	<i>Facile Synthesis of Carbon Aerogel and Application as Catalyst Support to Increase Performance of Proton Exchange Membrane Fuel Cells</i> Kevin Gu , Deerfield Academy, Deerfield, MA Eric Kim , Stuyvesant High School, New York, NY
	<i>Citric Acid Crosslinking of Carboxycellulose Nanofiber Membranes to Enhance Proton Exchange Membrane Fuel Cell Performance</i> George Cai , Wayzata High School, Plymouth, MN Songze Wu , High School Affiliated to Renmin University of China, Beijing, China Songtao Li , Princeton International School of Science and Mathematics, Princeton, NJ
	<i>Enhancing the Performance of Novel Cellulose Membranes for the Proton Exchange Membrane Fuel Cell</i> Christine Kong , Commack High School, Commack, NY Bhawan Sandhu , Lawrence High School, Cedarhurst, NY
	<i>Optimization of Pt/C Catalyst Nanofibers Electrospun on Nafion 117 Membranes in Polyelectrolyte Membrane Fuel Cells</i> Surya Rajan , California High School, San Ramon, CA Edward O'Keefe , Ridgewood High School, Ridgewood, NJ David Lederer , Hebrew Academy of the Five Towns and Rockaway, Cedarhurst, NY
	<i>Reduction of Carbon Monoxide Poisoning in Proton Exchange Membrane Fuel Cells via Application of Gold/Ruthenium Nanoparticle Monolayer</i> Luca Leger , Medfield High School, Medfield, MA Ryan Meehan , Sachem High School East, Farmingville, NY Mark Zhang , Green Valley High School, Henderson, NV
12:30 PM	<i>Buffet Luncheon Catered by WingWan of West Hempstead</i>

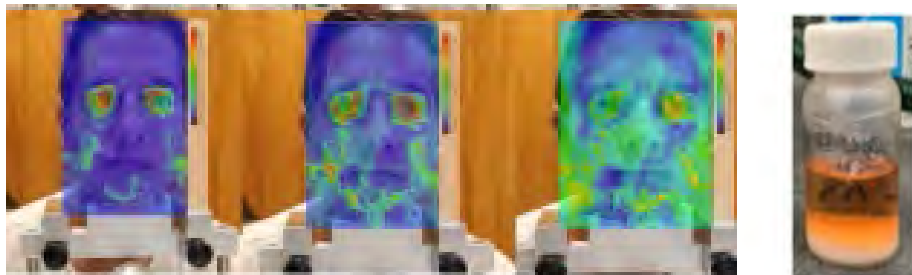
We gratefully acknowledge the Louis Morin Charitable Trust



Session 1:

Materials Research for Biomedical Applications

Chairs: Fan Yang, Farzad Koosha



Characterization of Salicylic Acid and Calcium Hydroxide Paste (CASA) as a Novel Antimicrobial Medicament for Endodontic Applications

Aris Zhu¹, Jeffrey Wolberg², Karena Etwaru³, Fan Yang⁴, Farzad Koosha⁵, Stephen Walker⁶, Miriam Rafailovich⁴, Marcia Simon⁶

¹Hamilton High School, Chandler, AZ 85248, ²HAFTR High School, Cedarhurst, NY, 11516, ³Cornell University, Ithaca, NY 14850, ⁴Department of Materials Science and Chemical Engineering, Stony Brook University, NY 11794, ⁵Department of Endodontics, Stony Brook University, NY 11794 ⁶Department of Oral Biology and Pathology, Stony Brook University, NY 11794

Endodontic infections are primarily caused by persistent bacterium *Enterococcus faecalis* and fungus *Candida albicans*. Currently, calcium hydroxide is routinely used as a disinfectant in endodontic procedures despite its inefficacy against both microbes.^[1] Additionally, its high pH contributes to dental pulp necrosis. To improve antimicrobial properties and neutralize the pH, salicylic acid was added to calcium hydroxide in a 3.7: 1 mass ratio to formulate CASA. This study characterizes the antimicrobial properties and cytotoxicity of CASA.

To assess the effectiveness of CASA against common endodontic pathogens, agar plates containing CASA or calcium hydroxide were incubated for 24 hours with *Enterococcus faecalis*, *Candida albicans*, *Staphylococcus aureus*, *Escherichia coli*, *Streptococcus gordonii*, *Lactobacillus salivarius*, and *Actinomyces viscosus*.^[2] Zones of inhibition were subsequently measured to quantify antimicrobial properties. For all the tested microbes, CASA consistently yielded larger zones of inhibition compared to calcium hydroxide (Fig. 1), suggesting CASA is the more effective antimicrobial agent.

However, further analysis was needed to determine whether the supernatant or precipitate of CASA contributes to its antimicrobial nature (Fig. 2). To determine the antibacterial properties of each CASA component, different concentrations of supernatant and precipitate were suspended in liquid growth media containing *E. faecalis* or *C. albicans* with 0.2 OD at 600 nm. After 24 hours, live and dead *E. faecalis* and *C. albicans* were stained using green and red fluorescent proteins, respectively. The precipitate had a greater ratio of dead to live microbes than the supernatant for both *E. faecalis* and *C. albicans* (Fig. 3), indicating the precipitate contributes most to the antimicrobial properties of CASA.

In order to be considered for clinical use, CASA must not only be antimicrobial but also non-cytotoxic to dental pulp stem cells (DPSC). Cytotoxicity was measured over a four-day period by counting DPSC with 0.25 mg/mL of CASA in media. The results show doubling times of control DPSC and DPSC with CASA are both approximately 27 hours, suggesting CASA is not cytotoxic and will not cause dental pulp necrosis if used for endodontic procedures.

Further investigations may use x-ray diffraction and ¹H NMR spectroscopy to elucidate the chemical structure and composition of the CASA supernatant and precipitate. Additional studies may determine the effect of CASA on DPSC differentiation for clinical knowledge.

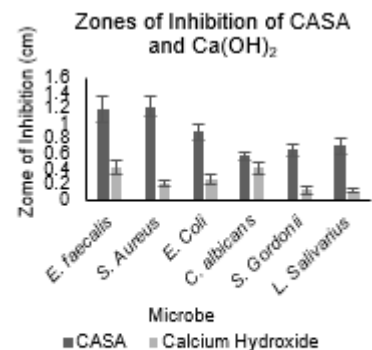


Figure 1: Graph of zones of inhibition of CASA and Ca(OH)₂ incubated with various microbes.



Figure 2: Photograph of CASA supernatant (top) and precipitate (bottom).

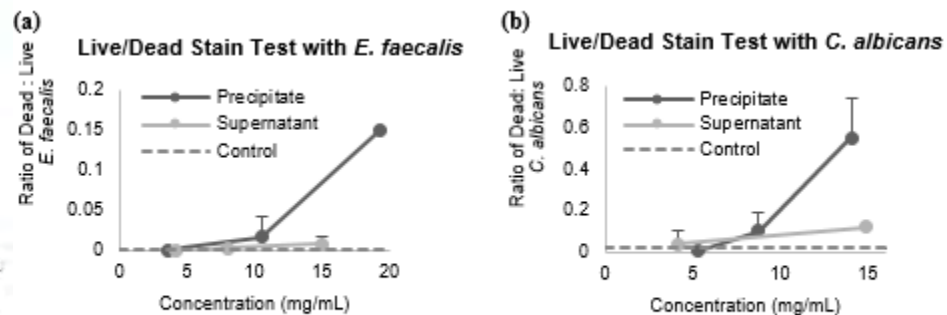


Figure 3: Antimicrobial efficacy of different concentrations of CASA supernatant and precipitate on (a) *C. albicans* and (b) *E. faecalis*.

[1] Mohammadi, Z., & Dummer, P. M. H. (2011). Properties and applications of calcium hydroxide in endodontics and dental traumatology. *International Endodontic Journal*, 44(8), 697-730. doi:10.1111/j.1365-2591.2011.01886.x

[2] Narayanan, L. L., & Vaishnavi, C. (2010). Endodontic microbiology. *Journal of conservative dentistry: JCD*, 13(4), 233-239. doi:10.4103/0972-0707.73386

Titanium Dioxide Nanoparticles Increase Risk of Bacterial Infection in Human Cells

By Alina Pollner¹, Angelina Franqueiro², Fan Yang³, Miriam Rafailovich³

¹Canyon Crest Academy, San Diego, California

²Cornell University, Ithaca, New York

³Department of Materials Science and Chemical Engineering, Stony Brook University, Stony Brook, NY

Titanium dioxide (TiO₂) nanoparticles are widely used in many cosmetic products, most notably sunscreen and toothpaste, for their white pigment and UV radiation blockage capabilities. As roughly four million tons of titanium dioxide particles are produced worldwide annually, a comprehensive review of their potential cytotoxic effects is needed. Previously, exposure to TiO₂ nanoparticles (NP) increased HeLa (cervical cancer) cells' susceptibility to *Staphylococcus aureus* infection[1]. *Staphylococcus aureus* and *Enterococcus faecalis* (*E. faecalis*) are some of the most successful human pathogens, and are present in millions of humans. Here, we evaluated the effect of TiO₂ nanoparticles (NP) on the proliferation of dental pulp stem cells (DPSC), fibroblasts, and human umbilical vein endothelial cells (HUVEC) and susceptibility to infection by *S. aureus* and *E. faecalis*.

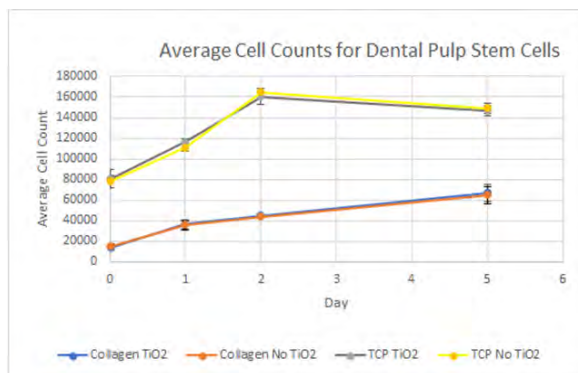


Figure 1: Average cell counts for DPSC as measured by Alamar Blue Assay and hemocytometer. Nanoparticle exposure did not affect proliferation.

Cells were exposed to *S. aureus* and *E. faecalis* (at a ratio of 1:1,000 cells to bacteria) for 90 minutes and then analyzed by a confocal microscope. For *S. aureus*, dental pulp stem cells exposed to TiO₂ NP had on average 545% more bacteria attached to their surface ($p < 0.0001$) as seen in Figure 2. Fibroblasts exposed to TiO₂ NP similarly had 286% more bacteria ($p = 0.0001$) than unexposed fibroblasts (Figure 2). Unlike DPSC and fibroblasts, HUVEC cells exposed to NP did not have a statistically significant difference in bacterial attachment with *S. aureus* as compared to HUVEC cells without exposure to NP. For *E. faecalis*, there was not a statistically significant difference in bacterial attachment for cells that were exposed to NP.

These results suggest that exposure to TiO₂ nanoparticles may increase the cells' risk of bacterial infection. Further data, such as the measurement of colony forming units (CFU), are needed to support these findings. Future research involves investigating mechanisms that cause cells to be more susceptible to the bacteria (such as Lactate Dehydrogenase assays), NP skin permeability studies, and engineering solutions for prevention.

Cell proliferation was measured using the Alamar Blue assay, which measures the viability of cells through the reduction of resazurin to resorufin, and a hemocytometer over a five-day period. Using a concentration of 0.4 mg/ml rutile TiO₂ NP, cell counts were measured and compared to standard samples. As shown in Figure 1, the addition of TiO₂ NP did not affect cell proliferation of dental pulp stem cells, grown on either collagen or tissue culture plastic (TCP).

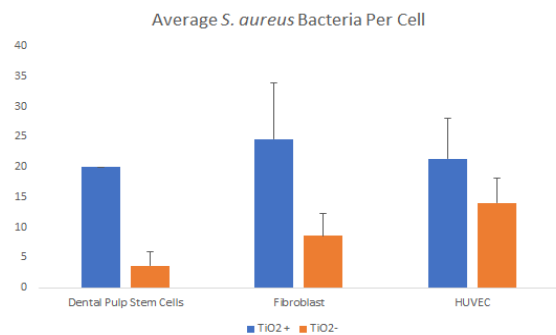


Figure 2: Average *Staphylococcus aureus* bacteria per cell, as measured by confocal microscopy.

Modification of Thrombin Enzymatic Activity Using Graphene Oxide and Partially Reduced Graphene Oxide Nanoparticles

Abraham Balsam, Jonathan Lederer, Mrs Rebecca Isseroff, Dr Yuval Shmueli, Dr Miriam Rafailovich
Rambam Mesivta, Lawrence, NY, Hebrew Academy of the Five Towns and Rockaway, Cedarhurst, NY, Lawrence
High School, Lawrence, NY, Stony Brook University, Stony Brook, NY

Graphene and its water-soluble derivative, graphene oxide (GO), have unique physical and chemical properties. GO, in particular, possesses a single-layered, two-dimensional (2-D), sp² hybrid structure studded with charged functional groups, offering a unique double-sided, easily accessible substrate for multivalent functionalization and efficient loading of molecules from small organic materials to biomacromolecules. Many of its effects on biological material remain unknown, so we researched how GO and prGO (partially reduced Graphene Oxide) affect enzymatic activity. We chose to test was thrombin, the enzyme responsible for catalyzing hemostasis which prevents one from losing an excessive amount of blood. In severe circumstances, such as in car accidents or post surgery, hemostasis could be too slow to fully repair the vessel in time, and it would be helpful to introduce an external substance that would hasten blood coagulation. Additionally, in cases of thrombosis, when blood unnecessarily clots and the circulatory system is disrupted, introducing a substance that would inhibit blood coagulation would allow for a non-invasive treatment. We tested to see if GO and prGO would be capable of exhibiting either of these characteristics when interacting with thrombin.¹

Thrombin activates hemostasis by transforming fibrinogen into a fibrin network. We utilized rheology in order to test the onset of the formation of the fibrin clot. We determined that 30 u/ml of thrombin was an appropriate concentration as it began to produce a clot about 6 min after thrombin was dispensed into the fibrinogen solution. Our control consisted of 3 ml of 10mg/ml bovine fibrinogen dissolved in pure PBS. The experimental groups were: 1) 3 ml of 10 mg/ml bovine fibrinogen dissolved in a solution containing 1mg/ml GO in PBS 2) 3 ml of 10 mg/ml bovine fibrinogen dissolved in a solution containing 1mg/ml prGO, reduced by 12 millimolar NaBH₄, in PBS.

We observed 2 parameters from the rheology graphs which resulted: 1) The time the sample took to begin to clot, determined by the time at which a spike, or a sharp increase in slope, was discerned on the logarithmic graph of the modulus of the sample. 2) The modulus of the sample after clotting.

Figure 1 shows the discrepancy between the gelation time of the control and GO. It indicates that GO delayed the onset of gelation by 35.7% when compared to the control. The fibrinogen solution without GO began to clot at 350 seconds and the solution with GO began to clot at 475 seconds. This can be beneficial for counteracting thrombosis. We predict that prGO will enhance thrombin's activity and this would assist the onset of hemostasis. We continue to search for optimal parameters which will allow prGO to enhance the activity of thrombin. In the future we hope to characterize GO and prGO with XPS, SEM, and AFM in order to determine the properties responsible for causing its effects on thrombin.

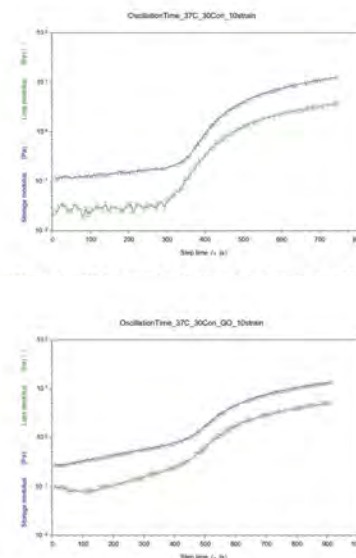


Fig 1B. This graph shows the rheology of GO in PBS mixed with a fibrinogen solution. Elastic modulus (Y-axis) indicates the strength of the clot over time (X-axis)

¹ Yang, Xinjian, et al. "Contrasting Modulation of Enzyme Activity Exhibited by Graphene Oxide and Reduced Graphene." *Chemical Communications*, vol. 49, no. 77, 2013, p. 8611., doi:10.1039/c3cc44632h.

² Kaibara, M. "Rheology of Blood Coagulation." *Biorheology*, vol. 33, no. 2, 1996, pp. 101–117., doi:10.1016/0006-355x(96)00010-8.

Using Digital Imaging Skin Correlation to Predict Comatose Recovery

Anthony Ginez¹, Rachell Paz², Fan Yang³, Miriam Rafailovich³

¹Nassau Community College, 1 Education Dr, Garden City, NY 11530; ²Suffolk County Community College, 533 College Rd, Selden, NY 11784; ³Department of Material Science and Chemical Engineering, Stony Brook University, Stony Brook, NY 11794

Digital Imaging Speckle Correlation (DISC) is a well-known method of measuring and graphing displacements and facial strains by analyzing a set of still images, especially in mechanical testing. Other applications include studying the recovery of skin after use of Botox or skin tightening cream, facial recognition software, and clinical diagnostics. The project focuses on honing a new application, the tracking of micro expressions in comatose patients to better predict their rate of recovery. This is possible because facial skin is directly attached to underlying muscles. Using the subject's pores as "speckles," we are able to graph and map the micro movements that may be undetectable by the human eye. It is known that recovery rates can vary between patients, at times with no obvious correlation. By imaging and recording the trends in healthy volunteers as a control, we hope to develop the code and procedure used to record signs of consciousness in affected patients.

Our recording is done by a Nikon D300 as an unedited video. In order to calculate displacement, we needed to cut the file into individual photos. These are then sorted by the timestamp of the associated presentation, which in turn is connected to the slide shown; good, bad, and neutral. The now sorted photos are averaged as a unit and compared to a predetermined 'neutral photo', seen in Figure 1. The average is plotted and graphed as a heat map as shown here.

The displacement is measured and graphed with the intensity of color reflecting the degree of displacement. Warmer tones represent more distortion from the original neutral photo.

During testing, it was seen that the head needed to be in a still position for the entire duration of the recording session. In order to keep the head as still as possible, we created a special chin rest that attached to the camera facing the subject. Talking, head tilting or an over enthusiastic smirk would move the entire face a millimeter or more. To our eyes these slight shifts make for good communication in a natural setting, but with the project focus in mind the shifts become detrimental to an accurate response, attributable to a wide error margin in our final project. Something else we noticed in the above pictures was the concentration of distortion in the cheeks and forehead, seen by the intensity of the heat map. When analyzing the "bad" photos, the forehead is noted as a major area of interest. Conversely, when looking at the "good" slides, the cheeks show more displacement as compared to the neutral slide.

In order to predict the recovery rate of comatose patients, more data is needed from our control group. This data can then be compared to the recorded response of affected in-patients and record if there are results correlative to healthy, wake patients. Similarly to how we predicted the recovery rates of botox patients, we can attempt to graph the recovery of comatose patients. By imaging them daily and comparing their results, we can measure whether their reaction, if there is one, strengthens over time. As with all studies, a larger sample size is ideal to better generalize for the public. More work will have to be done, but these are only the instrumental first steps.

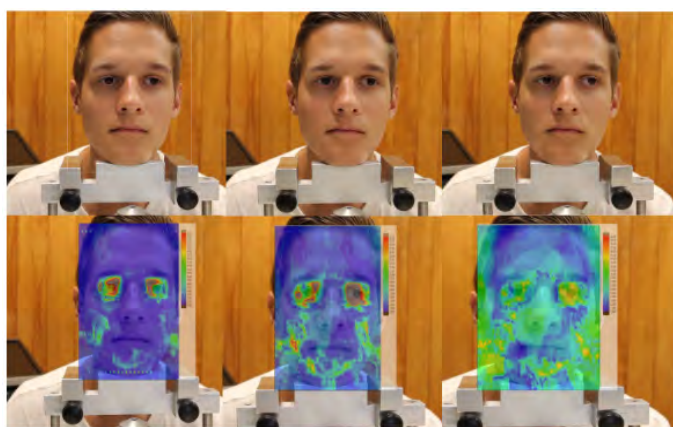
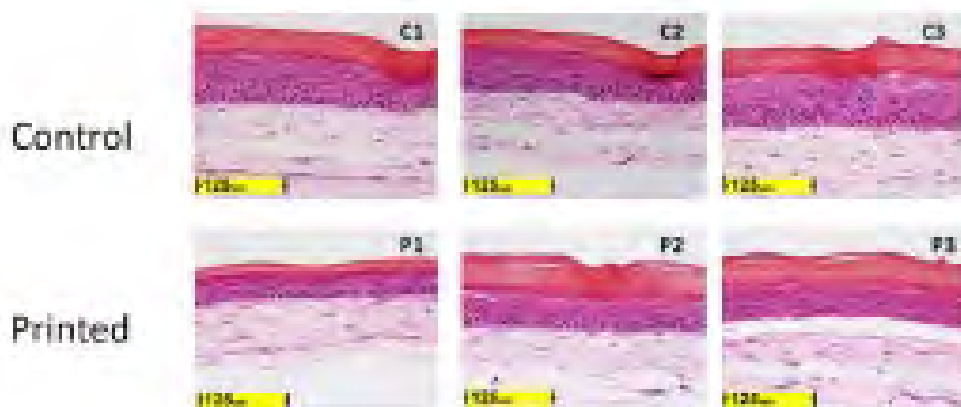


Figure one: Neutral slide shown (left) Good image (middle) Bad image (right)

1. Divya Bhatnagar, et al. "An in vivo analysis of the effect and duration of treatment with botulinum toxin type A using digital image speckle correlation" 8, Apr. 2013 <https://www.ncbi.nlm.nih.gov/pubmed/23565582>
2. Satprem Pamudurthy, et al. "Dynamic Approach for Face Recognition using Digital Image Skin Correlation" AVBPA 2005 https://link.springer.com/chapter/10.1007/11527923_105
3. E. Guan, et al. "Determining the Mechanical Properties of Rat Skin with Digital Image Speckle Correlation" 10 Oct. 2003 <https://www.ncbi.nlm.nih.gov/pubmed/15056999>
4. Divya Bhatnagar, et al. "An Analysis of Facial Nerve Function in Patients with Vestibular Schwannomas Using Digital Image Speckle Correlation" Feb. 20
5. Isabelle Afriat Staloff, et al. "An in vivo study of the mechanical properties of facial skin and influence of aging using digital image speckle correlation" May 2008. <https://www.ncbi.nlm.nih.gov/pubmed/18412553>

Session 2: Medical Hydrogels and Bioprinting

Chair: Juyi Li



Development of Novel Cerebral Aneurysm Embolization Method via Injection of Pluronic® F-127 Multiblock Copolymer Hydrogel

Finnur Christianson¹, Kevin Yang², Rithu Paramesh³, Diya Rai-Gersappe⁴, Ikshu Pandey⁵, Juyi Li⁶, Chander Sadasivan⁷, Miriam Rafailovich⁶
¹Ponte Vedra High School, Ponte Vedra, FL 32081, ²Fairview High School, Boulder, CO 80305, ³Presentation High School, San Jose, CA 95122, ⁴Huntington High School, Huntington, NY 11743, ⁵East Meadow High School, East Meadow, NY 11554, ⁶Department of Mat. Sci. & Chem. Eng., Stony Brook University, Stony Brook, NY 11790, ⁷Department of Neurological Surgery, Stony Brook University, Stony Brook, NY 11790

Endovascular embolization is a recently developed minimally invasive technique used for treatment of cerebral aneurysms¹. The technique involves embolization of the injured artery with metallic or hydrogel coils to occlude the vessel and induce thrombosis. However, this technique is limited by the packing density achieved by the coils, and currently results in a high recurrence rate of 17%². Hydrogels are networks of polymer chains that are biocompatible and highly absorbent, and therefore can be injected directly into aneurysms to occlude the vessel. In this study, we therefore developed a novel aneurysm occlusion technique through injection of a shear thinning hydrophilic triblock copolymer, Pluronic® F-127³.

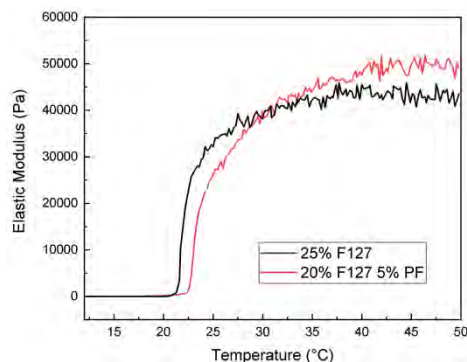


Figure 1. Temperature dependent rheological tests conducted on Pluronic hydrogels with and without multiblock copolymer PF127.

Pluronic® F-127 hydrogels were synthesized at concentrations of 20%, 25% and 30% w/v, and contrast agent iopromide was added at concentrations of 20% and 30% v/v to 20% F-127 for angiography. To increase rigidity, 1% and 5% w/v PF-127 multiblock copolymer was added to F-127 to achieve final hydrogel concentration of 25%⁴. Various rheological techniques, including amplitude sweep, single frequency, and temperature dependent tests were conducted to determine the viscoelastic range and elastic modulus as a function of temperature of each gel. After the sol-gel transition temperature was reached, the elastic modulus of the 25% F-127 hydrogel changed from <10 Pa to a maximum of 43 kPa, while the 20% F-127 5% PF multiblock copolymer solution reached a maximum of 51 kPa after the sol-gel transition at 25 °C (Fig 1).

Deionized water at 37 °C was circulated by a peristaltic pump with a mean flow rate of 4.06 cc/sec through a silicone model of a saccular cerebral aneurysm in order to simulate blood flow in a carotid artery. A catheter was then threaded into the model aneurysm through silicone tubing simulating the vasculature of a human body. Incorporating a red dye additive into the hydrogels and recording the color density in the aneurysm over time indicated that greater concentrations of F-127 hydrogel successfully occluded the aneurysm for longer time spans and were injectable for concentrations up to 30% w/v. The addition of multiblock copolymer PF-127 at concentrations of 1% and 5% resulted in occlusion times of 31 minutes and 61 minutes, respectively (Fig 2a). The 5% multiblock copolymer showed a nearly fivefold improvement over the occlusion time of 25% w/v F-127 without multiblock copolymer (occlusion time of 13 minutes) (Fig 2b). However, excessive concentrations of multiblock copolymer at 25% w/v were too stiff for injection through a catheter.

Due to their biocompatibility and absorbent properties, coupled with high elastic moduli and shear thinning properties, hydrogel injection for aneurysm embolization has great potential for intracranial aneurysm treatment. This study shows the effectiveness of a novel temporary embolization method, with promise for future improvement through addition of fibrinogen with thrombin coagulant or other crosslinking polymers to ensure effective permanent embolization.

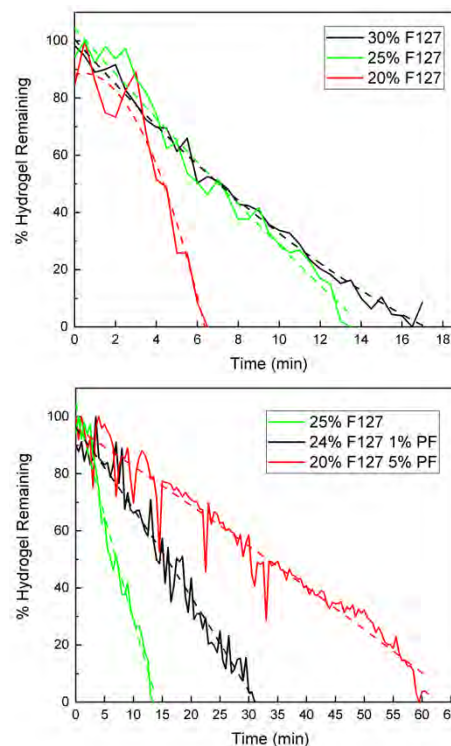


Figure 2. Effect of concentration of (a) Pluronic F127 and (b) multiblock copolymer on aneurysm occlusion time.

¹ Molyneux, A., Kerr, R., & Yu, L. (2005). International Subarachnoid Aneurysm Trial (ISAT) of Neurosurgical Clipping Versus Endovascular Coiling in 2143 Patients With Ruptured Intracranial Aneurysms: A Randomised Comparison of Effects on Survival, Dependency, Seizures, Rebleeding, Subgroups, and Aneurysm Occlusion. *ACC Current Journal Review*, 14(12), 52. doi:10.1016/j.accreview.2005.11.083

² Knap, D., Gruszka, W., Sieroń, D., Gruszczyńska, K., Zawadzki, M., Zbroszczyk, M., & Baron, J. (2017). Evaluation of Endovascular Embolization of Cerebral Aneurysms by Hydrogel Coils. *Polish journal of radiology*, 82, 203–208. doi:10.12659/PJR.895675

³ Shirwaiker, R., Purser, M., & Wysk, R. (2014). Scaffolding hydrogels for rapid prototyping based tissue engineering. *Rapid Prototyping of Biomaterials*, 176–200. doi:10.1533/9780857097217.176

⁴ Jun Jiang, Miriam H. Rafailovich, Ram Malal, Chunhua Li, Min Y. Lin, Ralph H. Colby, ... Daniel Cohn. (2008). Rheology of Thermoreversible Hydrogels from Multiblock Associating Copolymers. *Macromolecules*, 41(10), 3646–3652.

<https://doi.org/10.1021/ma800192m>

Measuring Collagen Contraction and Keratinocyte Colony Efficiency for the Viability of Bioprinting Skin Using Extrusion-Based Printing vs Traditional Skin Grafting Methods

Christopher Chan¹, Teresa Duong², Saba Gulzar³, Dokyung Lee⁴, Stella Lessler⁵, Somya Mehta¹, Katherine Tian⁶, Adeel Azim⁷, Olias Christie⁷, Michael Cottone⁷, Philip Cottone⁷, Michael Gozelski⁷, Zahir Huq⁷, Vivian Su⁷, Juyi Li⁷, Marcia Simon⁷, and Miriam Rafailovich⁷
¹Hicksville High School, Hicksville, NY 11801, ²St. Anthony's High School, Melville, NY 11747, ³New Hyde Park Memorial High School, New Hyde Park, NY 11040, ⁴Daegu International School, Daegu, South Korea 41021, ⁵Yeshivah of Flatbush Joel Braverman High School, Brooklyn, NY 11230, ⁶Ward Melville High School, East Setauket, NY 11733, ⁷Department of Materials Science and Chemical Engineering, Stony Brook University, Stony Brook, NY 11790

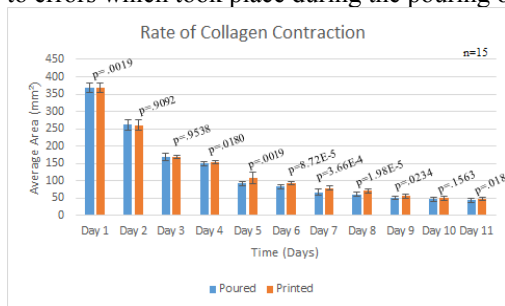
Multiple methods through tissue engineering have been applied to construct skin grafts for treatment. However, several disadvantages accompany these methods, such as immune reactions, transmission of diseases, and shortages of donor skin. A novel technique - bioprinting - would alleviate the majority of these complications.¹ Bioprinting skin holds great potential for application in treatments as it would not only eliminate the need for donors, but it would also prevent homogeneity issues accompanied by current methods. Bioprinting allows for faster integration with the host tissue, lower risk of rejection and uniform tissue growth in vivo.² Currently, extrusion-based printing is found to be the most feasible bioprinting technique in terms of vertical configuration and allowing a larger variety of bioink, including more cell-dense bioinks; however, present limitations include lower cell survivability due to the shear stress that occurs during printing.² We aimed to evaluate the cell survivability rates, comparing poured and printed samples.

Two essential components in artificial skin constructs include the extracellular matrix (collagen and fibroblasts) and keratinocytes. In order to test the viability of each of these components once passed through the bioprinter nozzle, the collagen contraction, as well as the damage to the keratinocyte cell membranes, was observed. The collagen gels were first prepared to have a final concentration of 1.2 mg/mL and a concentration of 7.5×10^4 cells/well for three plated and three poured samples. The associated volumes of each of the materials, shown in *Table 1*, were combined along with cells to create a collagen gel solution. Three samples were printed at a pressure of 10 kPa and three samples were plated to observe the effect of shear force on cell survivability. This gel solution was then placed in the incubator at 37 °C to set and the contraction rate of the collagen gel was measured and compared using EVOS imaging. Damage to the keratinocytes, on the other hand, was observed using trypan blue dye. This method allows us to count the intact and damaged cells and compare the printed (1 kPa) and poured samples. After letting these keratinocytes grow in a KC+ Medium for two weeks, a colony efficiency test was conducted to determine the effect of bioprinting on the functionality of the cells.

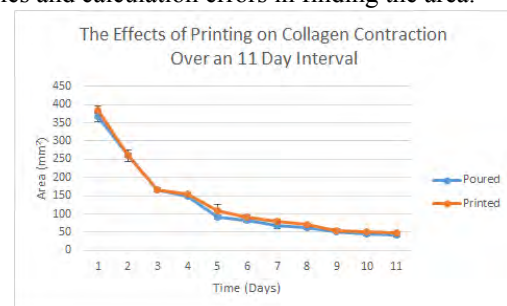
Table 1: Volumes for collagen gel components

Material	Amount/20 mL
10x EMEM	2.0 mL
L-glutamine (.2M)	166µL
FBS	2.0 mL
Na ₂ CO ₃	568 µL
Collagen (5.44 mg/mL)	4.4 mL
PBS	10.0 mL
NaOH	Until pH = 7

The results of the collagen contraction experiment showed that the contraction rates look fairly similar, as seen in *Figure 1*. However, after doing two-sample t-tests assuming unequal variances for each day, *Figure 2* shows that most of the samples actually contracted quite differently. We believe these differences most likely occurred due to errors which took place during the pouring or printing of the samples and calculation errors in finding the area.



Figures 1 (left) and 2 (right): Graphs of collagen contraction in printed samples vs time as well as collagen contraction in poured samples vs time



Future research would include repeating this experiment to discern if these differences occurred due to experimental errors, or if poured and printed samples truly have a statistically significant difference in collagen contraction rates. We would also like to test multiple trials involving varying pressures through the bioprinter nozzle as varying pressures would affect cell survivability.

¹Augustine, Robin. "Skin bioprinting: a novel approach for creating artificial skin from synthetic and natural building blocks." *Progress in biomaterials* vol. 7,2 (2018): 77-92. doi:10.1007/s40204-018-0087-0

²Kačarević, Željka P et al. "An Introduction to 3D Bioprinting: Possibilities, Challenges and Future Aspects." *Materials* (Basel, Switzerland) vol. 11,11 2199. 6 Nov. 2018, doi:10.3390/ma11112199

Analyzing and Comparing 3D Bioprinted Organotypic Dermis and Epidermis to Native Skin

Christopher Chan¹, Teresa Duong², Saba Gulzar³, Dokyung Lee⁴, Stella Lessler⁵, Somya Mehta¹, Katherine Tian⁶, Adeel Azim⁷, Olias Christie⁷, Michael Cottone⁷, Philip Cottone⁷, Michael Gozelsk⁷, Zahin Huq⁷, Vivian Su⁷, Juyi Li⁷, Marcia Simon⁷, and Miriam Rafailovich⁷

¹Hicksville High School, Hicksville, NY 11801, ²St. Anthony's High School, Melville, NY 11747, ³New Hyde Park Memorial High School, New Hyde Park, NY 11040, ⁴Daegu International School, Daegu, South Korea 41021, ⁵Yeshivah of Flatbush Joel Braverman High School, Brooklyn, NY 11230, ⁶Ward Melville High School, East Setauket, NY 11733, and ⁷Department of Materials Science and Chemical Engineering, Stony Brook University, Stony Brook, NY 11790

3D bioprinting has exhibited promise for creating a functional skin equivalent, potentially helping treat patients with major burns and severe surgical wounds via a skin graft. However, the use of bioprinting to create skin organotypic holds many engineering and biological challenges, such as the body's potential allergenic reaction to printed skin¹. In order to attempt to accurately replicate human skin, we must print a skin organotypic that contains both a dermal and epidermal layer². Therefore, the purpose of this experiment is to compare different combinations of printed and plated skin in order to assess the possibility of bioprinting skin.

Four varying combinations of three different samples of dermal and epidermal organotypic were created in 6-well plates with 24mm diameter wells: first layer of collagen printed and second layer collagen plated, both first and second layer collagen printed, both first and second layer of collagen plated, and first layer of collagen plated with the second layer of collagen printed. For the first layer of the dermis, we printed (at 10 kPa) and plated 1 mL of 2mg/mL concentration of rat tail collagen solution in each well (*Table 1*).

After allowing the collagen to gel, we created a solution for the second layer of our samples (*Table 2*). The second layer of collagen consisted of 1.2mg/mL concentration of the same collagen and different chemical compounds mentioned above. Additionally, cells at a concentration of 2.5×10^4 cells/mL were added to the solutions. We then printed (at 10 kPa) or plated 3 mL of the solution into each sample based on the different combinations. For one week after, we changed the media every other day: 2mL on top of the insert and 3mL on the bottom of the insert.

Table 1: Collagen solution for first layer

Materials	Per 13ml
10X EMEM	1.3ml
Glutamine (.2M)	108.29µl
FBS	1.3ml
Na ₂ CO ₃	367.9µl
Collagen(4.82mg/ml)	5.4ml
PBS	4.5ml to 13ml
NaOH	Until Ph = 7

Table 2: Collagen solution for second layer

Materials	Per 28ml
10X EMEM	2.8ml
Glutamine (.2M)	232.4µl
FBS	2.8ml
Na ₂ CO ₃	792.4µl
Collagen(4.82mg/ml)	7ml
PBS	14ml to 27ml
NaOH	Until Ph = 7

Three days into the week, a metal ring was added to each insert. Following the seven days, we then printed (at 0-1 kPa) 50µl of keratinocyte cells at a concentration of 600×10^4 cells per mL in the metal ring, serving as the epidermis. After two weeks of changing the media and allowing the keratinocyte cells to properly develop, the artificial skin was then extracted from the inserts and sent to a lab for H&E staining.

In January 2019, Stony Brook University students conducted a similar experiment in which three samples of entirely printed skin and three samples of entirely plated organotypic were grown. From the results of their experiment (*Figure 1*), we expect the layers that were placed through the printer nozzle to be generally thinner than the layers plated without being placed through a pressurized environment. However, due to the recent data acquired via a collagen contraction experiment, we do expect the cells to react normally in every other way aside from the thickness of the dermis.

DERMAL EQUIVALENT FOR PRINTED COMPARED TO CONTROL (POURED)

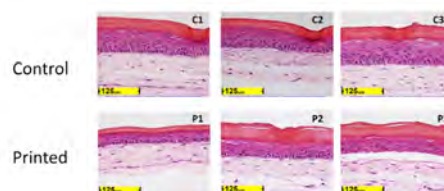


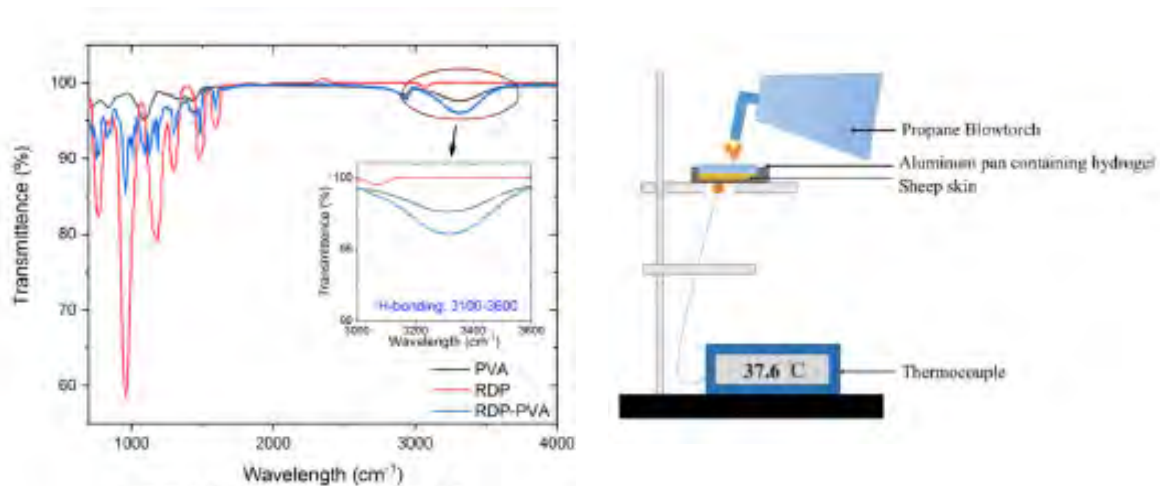
Figure 1: Results from Stony Brook University experiment

[1] van der Veen, Vincent C., et al. "Biological Background of Dermal Substitutes." *Burns*, vol. 36, no. 3, Jan. 2010, pp. 305–321. EBSCOhost, doi:10.1016/j.burns.2009.07.012.

[2] Cubo Mateo, Nieves, et al. *3D Bioprinting of Functional Human Skin: Production and in Vivo Analysis*. 2016. EBSCOhost, search.ebscohost.com/login.aspx?direct=true&db=edsbas&AN=edsbas.9414310F&site=eds-live&scope=site.

Session 3: Hydrogels for Flame Retardant Applications

Chair: Yuan Xue



Enhancing the Flame Retardancy of Biodegradable Poly(vinyl alcohol) Hydrogels with Resorcinol Bis(diphenyl phosphate) Coated Starch

Jalaj Mehta¹, Lauren Stiefel², Yuan Xue³, Miriam Rafailovich³

¹Hauppauge High School, Hauppauge, New York 11788, ²Samuel H. Wang Yeshiva University High School for Girls, Holliswood, New York 11423, ³Department of Materials Science and Chemical Engineering, Stony Brook University, Stony Brook, New York 11794

Flame retardant components are necessities to a firefighter's protective gear, such that more eco-friendly advancements in this technology have become more pertinent in an effort to better ensure the safety of both firefighters and victims in fire. Conventionally, flame retardants have been created from only slightly biodegradable superabsorbent polymers with extremely high water content[1]. Generally these superabsorbent polymers are derived from acrylic acid and acrylamide and unless these are oligomers it is likely that they are not biodegradable[2,3]. In lieu of these facts the primary goal of this research was to synthesize a biodegradable hydrogel flame retardant that is as efficient as its less environmentally friendly equivalents.

To create the hydrogel samples we used a cyclic freezing and defrosting procedure consisting of 24 hours in a -20 degree Celsius freezer and then 1 hour of defrosting at room temperature 3 times for each set of samples. Our samples consisted of various concentrations of starch, resorcinol bis(diphenyl phosphate) (RDP), and RDP-coated starch suspended/dissolved in multiple bases that were created through the addition of poly(vinyl alcohol) (PVA) and RDP-coated PVA in deionized water. The samples created can be seen in Figure 1.

Starch and RDP were chosen as a result of their performance as flame retardants and chemicals with excellent charring both in our preliminary testing with gelatin based hydrogels and in previous literature. We also suspected that the free hydroxyl groups on starch and the double bonded, outstretched oxygen on RDP would interact well, likely through hydrogen bonds, with the surface of the PVA molecules in the PVA based hydrogel. The PVA was also chosen as a result of its positive performance and flame retardant properties along with strong mechanical properties and flexibility in literature[4,5,6].

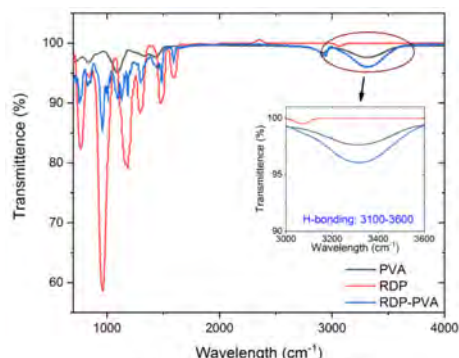


Figure 2. FTIR spectrum of RDP/PVA

Starch and RDP were chosen as a result of their performance as flame retardants and chemicals with excellent charring both in our preliminary testing with gelatin based hydrogels and in previous literature. We also suspected that the free hydroxyl groups on starch and the double bonded, outstretched oxygen on RDP would interact well, likely through hydrogen bonds, with the surface of the PVA molecules in the PVA based hydrogel. The PVA was also chosen as a result of its positive performance and flame retardant properties along with strong mechanical properties and flexibility in literature[4,5,6].

We derived from the FTIR results in Figure 2 that hydrogen bonds were present in the PVA and RDP-PVA, and learned that the gels were mainly shear-thinning through the rheological studies. Overall samples *R* and *O* performed the best in terms of the completeness of the char layer formed, the lowest max temperatures, both being below 65°C (the temperature for a burn to almost instantaneously be second degree), the amount of gel remaining with *R* having .60 grams of gel remaining and *O* having .51 grams remaining. Additionally these two samples displayed clear shear-thinning which is useful for flame retardants. Compared to previous results, our gels are better while still retaining their biodegradable nature, as they keep the temperature under 65 degrees Celsius for longer than 200 seconds[7]. With the knowledge that the hydrogels synthesized in this experiment behave in the ways described and that 4% RDP-PVA with RDP-Starch hydrogels and 4% PVA with RDP-Starch hydrogels perform the best, in future studies we aim to test additional concentrations of RDP-PVA, starch, RDP-starch, and PVA to determine the optimal combination for a flame retardant.

- [1] "Ultimate Biodegradation of Ingredients Used in Cleaning Agents." *ScienceDirect*, Elsevier Science B.V., 19 Oct. 2007, www.sciencedirect.com/science/article/pii/B9780444516640500206. [2] "US5087513A - Flame Retardant Film and Composite Containing Superabsorbent Polymer." *Google Patents*, Google, patents.google.com/patent/US5087513A/en. [3] "Iranian Polymer Journal - Home Page." *Iranian Polymer Journal - Home Page*, journal.ippi.ac.ir/. [4] Cheng, Zhihan, et al. "Sustainable, Low Flammability, Mechanically-Strong Poly(Vinyl Alcohol) Aerogels." *Polymers*, MDPI, 5 Oct. 2018, www.ncbi.nlm.nih.gov/pmc/articles/PMC6403961/. [5] Bright, Danielle A., et al. "Resorcinol Bis(Diphenyl Phosphate), a Non-Halogen Flame-Retardant Additive - Bright - 1997 - Journal of Vinyl and Additive Technology - Wiley Online Library." *Journal of Vinyl and Additive Technology*, John Wiley & Sons, Ltd, 16 Apr. 2004, onlinelibrary.wiley.com/doi/pdf/10.1002/vnl.10184 [6] "Improved Flame-Retardant and Tensile Properties of Thermoplastic Starch/Flax Fabric Green Composites." *Carbohydrate Polymers*, Elsevier, 16 Mar. 2017, www.sciencedirect.com/science/article/pii/S0144861717302928. [7] "Fire-Resistant Hydrogel-Fabric Laminates: A Simple Concept That May Save Lives." *ACS Applied Materials & Interfaces*, pubs.acs.org/doi/abs/10.1021/acsami.5b10538.

	Controls	5% RDP	16.7% RDP-starch
1% PVA	A	B	C
1% RDP-PVA	D	E	F
2% PVA	G	H	I
2% RDP-PVA	J	K	L
4% PVA	M	N	O
4% RDP-PVA	P	Q	R

Fig. 1: Hydrogel sample make-ups and concentration

Synthesis of A Novel Flame-retardant Hydrogel for Skin Protection Using Xanthan Gum and Resorcinol Bis(diphenyl phosphate)-coated Starch

Mingkang Li^{1, a}, Bole Pan^{2, a}, Lisa Quinto³, Jalaj Metha⁴, Lauren Steifel⁵, Yuan Xue^{3*}, Miriam Rafailovich^{3*}

¹ Shanghai Star-river Bilingual School, Shanghai 201108, China ² Guangzhou Tianhe Foreign Language School, Guangzhou 510627, China ³ Department of Materials Science and Chemical Engineering, Stony Brook University, NY 11794, USA ⁴ Hauppauge High School, 500 Lincoln Blvd, Hauppauge, NY 11788, USA ⁵ Yeshiva University High School for Girls, 86 Palo Alto Street, Holliswood, NY 11423, USA

Firefighters continually endanger their lives in order to rescue others. This can leave them with severe burns; in 2017 alone, 2,835 U.S. firefighters suffered from burn-related injuries [1]. Developing a flame-retardant hydrogel for skin protection would greatly reduce these risks. This research presents the synthesis of said hydrogel using biodegradable, non-toxic materials: xanthan gum (XG) and resorcinol bis(diphenyl phosphate) (RDP)-coated starch [2].

To synthesize the flame-retardant hydrogel for skin, RDP and starch (weight ratio of 3:7) were mixed, stirred, centrifuged, and dried to obtain RDP-coated starch. RDP-coated XG was also prepared in a weight ratio of 1:3. The powders were combined with deionized water and put into an incubating waver at 45 °C for 10 hours to form the hydrogel samples. Different gel formulations varied in 2 aspects: 1) the concentration of XG or RDP-XG (at 1 wt.%, 2 wt.%, and 2.5 wt.%) and 2) with or without 10 wt.% RDP-coated starch. All samples were characterized with burn tests, Thermal Gravimetric Analysis (TGA), Fourier-transform Infrared Spectroscopy (FTIR), viscometry, and goniometry.

The set-up of the flammability assessment is demonstrated in Figure 1. Sheepskin was embedded in aluminum pans, covered with hydrogel, and burned continuously for 150s.

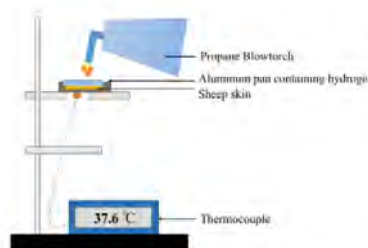


Fig.1. Illustration of the set-up for burn tests

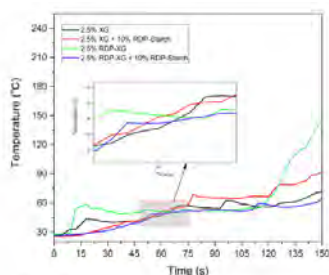


Fig.2. Increase in temperature over time for 2.5 wt.% hydrogel samples in burn test for sheepskin

Results from the test showed that the 2.5 wt.% RDP-XG+10 wt.% RDP-coated starch had the best performance, forming a uniform char layer which protect the underlying gel layers and skin. The sample outperformed its pure XG gel counterpart by 29% in terms of the final temperature. The best-performing hydrogel remained below 45 °C for over 50 seconds and below 55 °C for 114 seconds upon direct heating with a propane torch, whose flame temperature can reach approximately 1000 °C. Similar tests are also conducted on chicken skin covered with hydrogels. The thermal stabilities of pure XG gel, XG gel with RDP-starch, RDP-XG gel, and RDP-XG gel with RDP-starch were investigated through TGA. As depicted in Figure 3, the gel samples without RDP-starch were almost completely decomposed after a single-stage thermal decomposition between approximately 90 °C and 110 °C, which was mainly attributed to the loss of water in the hydrogels [3]. The starch-containing gels, on the other hand, underwent two-stage thermal degradation, one at around 110 °C, and another between 250 °C and 360 °C, before losing most of its weight. The addition of RDP-starch significantly increased the thermal stability of our hydrogel, by reducing weight loss at both stages of decomposition.

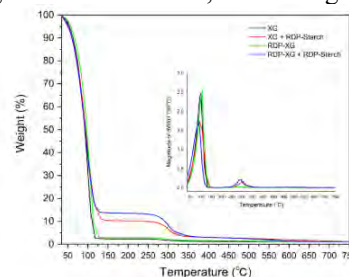


Fig.3. TGA curves for the 2.5 wt.% hydrogels

FTIR spectra identified the presence of hydrogen bond between RDP/starch and RDP/XG. Data from the viscosity tests revealed that all samples displayed shear-thinning behavior. From viscometry, gel viscosity increases as the concentration of XG increases, whereas the presence of RDP reduces the gel's viscosity; the addition of starch increases the viscosity overall. Moreover, through goniometry we determined the contact angle of gels on sheepskin surface, which demonstrated the hydrophilicity of the XG gels. The feasibility of the gel's application is supported by its thermal stability, flame retardancy, shear-thinning and hydrophilic properties, which indicated that the flame retardant RDP-XG/RDP-starch gel was easily spreadable and safe to use as a protective measure for not just firefighters but also for commercial use. Further studies could examine skin irritation and toxicity of the hydrogels, compare their limiting oxygen indices through cone calorimetry, and establish a heat transfer model to further evaluate their thermal protective performance.

^aThese authors contributed equally to this work

[1] Fahy, R. F., LeBlanc, P. R., & Molis, J. L. (2017). Firefighter fatalities in the United States. Quincy, MA: NFPA.

[2] Ju, Y., et al. (2015). The flame-retardance polylactide nanocomposites with nano attapulgite coated by resorcinol bis(diphenyl phosphate). *Journal of Vinyl and Additive Technology*, 22(4), 506-513. doi:10.1002/vnl.21469

[3] Rusu, A. G., Popa, M. I., Lisa, G., & Vereștiuc, L. (2015). Thermal behavior of hydrophobically modified hydrogels using TGA/FTIR/MS analysis technique. *Thermochimica Acta*, 613, 28-40. doi:10.1016/j.tca.2015.05.018

[4] Geh, K., et al. (2019). Development of a sprayable hydrogel formulation for the skin application of therapeutic antibodies. *European Journal of Pharmaceutics and Biopharmaceutics*, 142, 123-132. doi:10.1016/j.ejpb.2019.06.015

Development of a Hydrogel-based Intumescent Flame Retardant System for Limiting Wildfire Propagation

Audrey Cui¹, Kimberley Cheng², Frank Jin Rui Cai³, Pik Hoi Lam⁴, Lisa Quinto⁵, Yuan Xue⁵, Miriam Rafailovich⁵

¹Monta Vista High School, Cupertino, CA 95014 ²Princeton High School, Princeton, NJ 08540 ³Arcadia High School, Arcadia, CA 91007 ⁴California Institute of Technology, Pasadena, CA 91125 ⁵Department of Materials Science and Chemical Engineering, Stony Brook University, Stony Brook, New York 11790



Figure 1 Top: fresh gel
Middle: charring while burning
Bottom: char after 3 min of burning

Due to global warming, wildfires are becoming increasingly prevalent and destructive — \$5.1 billion lost in the past decade¹. To limit the spread of wildfires, we developed an eco-friendly, hydrogel-based fire retardant solution that can be sprayed upon vegetation. Our testing focused on dried grass, as dry grass is a major fuel source that sustains and propagates wildfires².

The addition of water to Xanthan Gum (XG) forms a hydrogel, whose ~90% water content makes it naturally fire resistant. However, the pure XG gel won't be effective after the water being evaporated. In order to increase the flame retardancy of XG gel for both wet and dry application conditions, an intumescent fire retardant (IFR) system with resorcinol diphenyl phosphate (RDP) as acid source and starch as charring agent was suspended in the XG gel matrix³. Due to RDP's high mobility, it was first coated onto XG and starch surface with a 1:3 and 3:7 weight ratio, respectively. The intensity increase in the hydrogen bonding region on the FTIR spectrum, shown in fig. 3,

confirmed the successful coating of RDP onto the starch and XG surface. The fire retardancy of candidate gels was assessed by measuring the percent mass loss after 1, 2, and 3 minutes of using a propane torch to burn samples of grass coated in a thin layer of gel; test setup is shown in fig. 1. Burn test results showed that the gel formulation of 1g/100ml RDP-XG gel with 10 wt.% RDP-starch yielded the highest percent of weight remaining in both wet and dry conditions, shown in fig. 2. Rheology results also proved that this formulation is shear thinning and has one of the lowest viscosities, which is promising for spray application. Thus, we identified the 1g/100ml RDP-XG with 10 wt.% RDP-starch as the most effective flame retardant gel formulation, whose FR property was not compromised even following the complete evaporation of its water content.

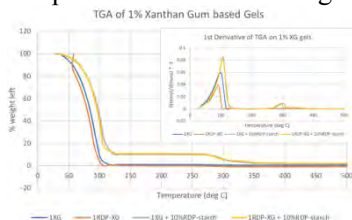


Figure 4. TGA results of 1% gels

TGA supported the addition of starch as a charring agent, as shown by the elevated char residue between 150-350°C in fig. 4. Through the successful bonding of RDP onto the XG and starch surface, RDP is immobilized inside the gel matrix, which increased its stability. The plasticizing effect of RDP also effectively decreased the gel viscosity.

In the future, in order to better quantify the effectiveness of our solutions, we plan to run cone calorimetry of our solutions on compression molded grass, which would characterize the heat release process of gel on grass during combustion. Limited oxygen index, which is level of oxygen necessary for a fire to persist, will also be measured.

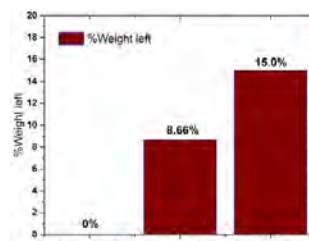


Figure 2. Burning test result of grass control, freshly applied gel and overnight dry gel

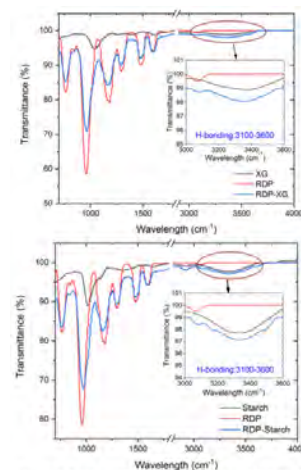


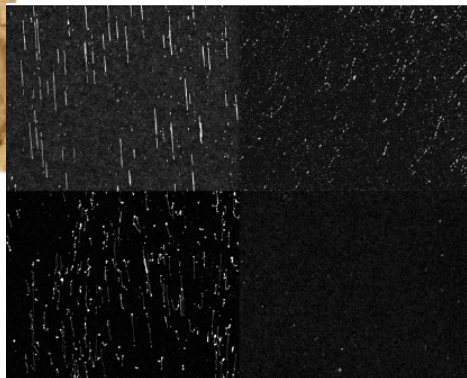
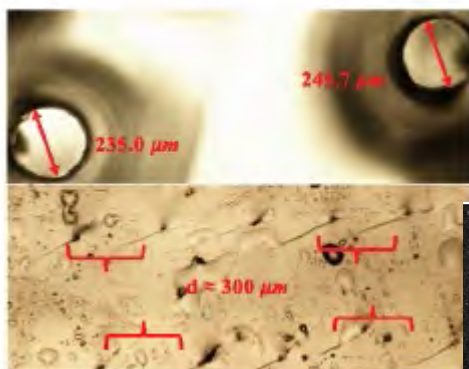
Figure 3. FTIR spectrum of RDP/XG and RDP/starch

¹ “Facts Statistics: Wildfires.” *III*, Insurance Information Institute.

² Donovan, Victoria M, et al. “Surging Wildfire Activity in a Grassland Biome.” *Geophysical Research Letters*, vol. 44, no. 12, 7 June 2017, pp. 5986–5993.

³ Chen, Xingyou, and Chen, Yinghong. “Synthesis of a Hydrogen-Bonded Complex Intumescent Flame Retardant through Supramolecular Complexation and Its Application in LDPE Foam.” *RSC Advances*, Royal Society of Chemistry, 19 June 2017.

Session 4: DNA Chip Technologies



A Novel Method to Apply Restriction Enzymes Through Low Volume Chambers for DNA Fragmentation in Next Generation Sequencing Library Preparation

Kerui Yang¹, Qinxi Liu², Jocelyn Zhu³, Joseph Jennings⁴, Dr. Jonathan Sokolov⁵, Anthony Del Valle⁵

¹Edina High School, 6754 Valley View Rd, Edina, MN 55439, ²Shenzhen Middle School, Shenzhen, Guangdong, ³Amador Valley High School, 1155 Santa Rita Rd, Pleasanton, CA 94566, ⁴Nassau Community College, NY 11530, ⁵Dept. of Materials Science and Chemical Engineering, Stony Brook University, Stony Brook, NY

Significant progress has been made in the past few decades in genome sequencing technologies. Next Generation Sequencing (NGS) Technology is highly valued for DNA sequencing as it provides a platform to tackle greater and more diverse genomic sequencing¹. A common method for sequencing, Nextera™ technology utilizes Transposome™ complexes to randomly cut and tag DNA². However, an ordered method of fragmenting DNA would offer significant advantages in simplifying the assembly problem of sequencing. Microfluidic channels have been used to diffuse an enzyme solution via capillary force in a vacuum, but due to the attraction of enzymes to the channel walls, the distance of enzyme diffusion is limited. An alternate method in which restriction enzymes are stamped onto microfabricated surfaces has a low success rate since a liquid environment must be maintained during the fragmentation process.

In this project, we aim to develop a novel method to effectively apply cutting enzymes onto PMMA surfaces combed with λ DNA. Using 1mm long low-volume-chambers in PDMS (Polydimethylsiloxane), in theory, the restriction enzyme solution should be able to diffuse more efficiently in comparison to it diffusing through the longer microfluidic channels. The first step was to produce uniform rows of microchambers in PDMS for enzyme delivery. Initially, chambers were created via a micro-needle ($d=250\mu\text{m}$) penetrating three layers of PDMS. It was observed that uniformly spaced cracks were created instead of circular chambers (Fig. 1). In order to produce regular micropatterns, a molding device was engineered so the PDMS would cure around pre-located, upright needles. Through observation with an optical microscope, circular chambers with diameters conforming to those of the needles were successfully observed (Fig. 1).

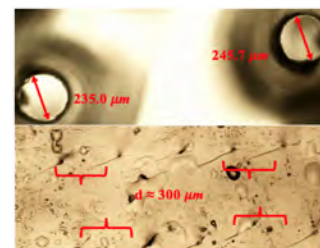
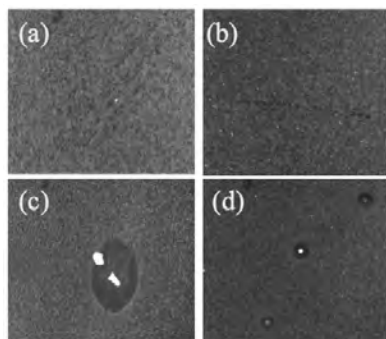


Figure 1. On the bottom: cracking in PDMS caused by the mechanical needle machine. On the top: uniform circular holds created by molding technique.



Figures 2a, 2c, 2d showcases the enzyme cutting areas for the test with molded PDMS holes. **Figures 2b, 2d** showcases the enzyme cutting areas for the test with the needle machine PDMS holes.

A PDMS peel test was subsequently conducted to confirm that the enzyme was digesting the DNA instead of the PDMS ripping the DNA off of the surface of PMMA. There was a difference in the amount of observable DNA on the PMMA surface before and after the test under the same exposure time ($\approx 805\text{ms}$). However, after increasing the exposure time ($\geq 1.4\text{s}$), more visible λ DNA molecules were observed, suggesting that the SybrGold dye for λ DNA labelling might be weakened after being in contact with PDMS.

Enzyme digestion tests were run utilizing a vacuum filling method to transfer DNase I (RNase-free) solution through PDMS chambers and a heating plate for enzyme activation and inactivation. Fabricated PDMS micro-channels produced by both mechanical needle poking and molding devices were tested. For the PDMS treated with mechanical poking, two types of enzymes digestion traces were observed: circular and linearly fragmented dots (Fig. 2). The intermittent linear pattern was possibly caused by the potentially high viscosity of DNase I solution and varying spaces within the PDMS cracks. Successfully digestion of DNA was observed using the molding-device fabricated holes (Fig. 2). The bright spots visible at the center of holes in Figure 2(c) and 2(d) are believed to be cut DNA fragments concentrated by the flow pattern of evaporating solutions (during the enzyme deactivation step).

Potential future research includes DNA fragmentation and desorption on PAA (Polyacrylic Acid) substrate using low-volume chambers and microfabrication of PDMS hole patterns using a femtosecond fiber laser.

¹Goodwin, Sara, John D. McPherson, and W. Richard McCombie. "Coming of age: ten years of next-generation sequencing technologies." *Nature Reviews Genetics* 17.6 (2016): 333.

²Caruccio, Nick, Haiying Grunenwald, and Fraz Syed. "Nextera™ technology for NGS DNA library preparation: simultaneous fragmentation and tagging by in vitro transposition." *Nature Methods* 16.3 (2009).

Temperature- and Solubility-Dependent Desorption of Linearly Combed DNA from Polymer Substrates for Ordered Fragmentation and Sequencing

Ellen Guo¹, Luisa Pan¹, Kathy Xing², Anthony del Valle³, Dr. Jonathan Sokolov⁴

¹The Harker School, San Jose, CA ²Leland High School, San Jose, CA ³Stony Brook University, Stony Brook, NY ⁴Department of Materials Science & Chemical Engineering, Stony Brook University, Stony Brook, NY

Accurate DNA sequencing proves invaluable to fields ranging from archaeology to biotechnology.¹ Despite the successes of fast and cost-effective short-read technologies, current methods require chemical or physical fragmentation in solution that loses information about spatial organization, necessitating costly computational reassembly or simply overlooking structural rearrangements, duplications, inversions, and mobile elements.^{2,3,4} To combat this issue, Cho and colleagues immobilized DNA on polymethylmethacrylate (PMMA) surfaces by molecular combing and cutting the strands with a soft lithography stamp.³

However, removal of the DNA from the PMMA surface involves extremely complex downstream methods and reagents like chloroform that need further purification.³ Thus, this study aims to first, simplify PMMA desorption and second, explore the potential of a second substrate: polyacrylic acid (PAA), a polymer with a solubility switch.⁵

PMMA and PAA solutions were spun onto silicon wafers at varying speeds, annealed in a vacuum oven at different temperatures and lengths of time, and dipped in various concentrations of λ DNA solution to comb the molecules; PAA wafers were rendered insoluble by immersion in CaCl₂ prior to dipping. We employed fluorescence microscopy and imaging to analyze the linearity, uniformity, and overall success of combing. Then the samples were desorbed. PMMA wafers were submerged in various buffer solutions and heated at different temperatures for times ranging from 30 minutes to overnight. PAA samples were soaked in NaCl to initiate ion exchange and dissolve the polymer, thus removing the DNA. Samples were again analyzed with fluorescence microscopy at the same locations as prior to desorption. Quantitative image analysis was achieved with ImageJ.

Qualitative observation of the PMMA samples reveals successful combing at an optimal DNA concentration of 0.5 μ g/mL for desorption tests. On the other hand, the DNA immobilized on PAA was often inconsistent in density and direction, even at the optimal conditions of 180nm thick PAA layers, overnight vacuum anneal at 130°C, and 10 mm/s velocity of combing. However, DNA desorption from PMMA proved more difficult than from PAA. Despite the desorption of PMMA at various temperatures, times, and pH resulting in an overall decrease in average amount of adsorbed DNA of up to 91.52% at 60°C and three hours soaking in NEB 3-1 buffer (pH ~7.9), we observed a reduction in the linearity of desorbed DNA, indicating unideal breakages. Conversely, all DNA was successfully removed by complete dissolution of the PAA substrate within seconds. See Figure 1 for details.

In conclusion, both the improved PMMA and the new PAA methodologies present promising strategies for ordered fragmentation in DNA sequencing, though future research should be done to improve the desorption of DNA from PMMA and molecular combing onto PAA. Furthermore, other polymers with solubility switches, such as chitosan or polyethyleneimine (PEI), may provide viable options as well.

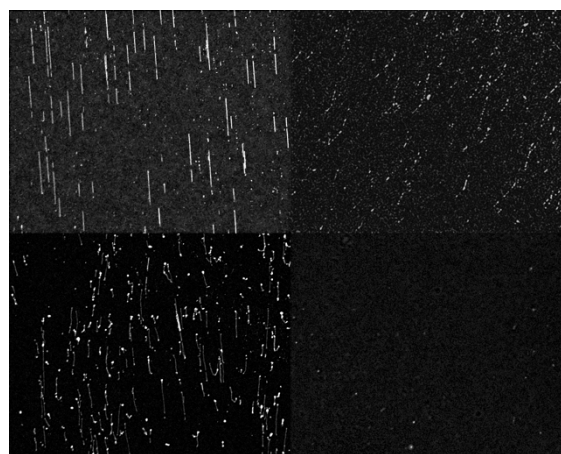


Figure 1. Top left: PMMA dipped in DNA, before desorbing. Top right: PMMA dipped in DNA after desorbing at 60°C for 3 hours in NEB 3-1. Bottom left: PAA dipped in DNA, before desorbing. Bottom right: PAA dipped in DNA after desorbing for 10 seconds in 24 mM NaCl.

¹ França, Lilian TC, Emanuel Carrilho, and Tarso BL Kist. "A review of DNA sequencing techniques." *Quarterly reviews of biophysics* 35.2 (2002): 169-200.

² Chin, Chen-Shan, et al. "Nonhybrid, finished microbial genome assemblies from long-read SMRT sequencing data." *Nature methods* 10.6 (2013): 563.

³ Cho, N., et al. "Fragmentation of Surface Adsorbed and Aligned DNA Molecules using Soft Lithography for Next-Generation Sequencing." *J. Biosens. & Bioelectro* 8 (2017).

⁴ Eisenstein, Michael. "Startups use short-read data to expand long-read sequencing market." (2015): 433.

⁵ Linder, Vincent, et al. "Water-Soluble Sacrificial Layers for Surface Micromachining." *small* 1.7 (2005): 730-736.

Gel and Electric Field-Based Desorption of DNA from PMMA-Coated Silicon Surfaces to Optimize Sequencing Accuracy

Elizabeth Korn¹, Anthony Del Valle², Jonathan Sokolov², and Miriam Rafailovich²

¹Plainview-Old Bethpage John F. Kennedy High School, Plainview, New York 11803

²Department of Materials Science and Chemical Engineering, Stony Brook University, Stony Brook, New York 11790

Following the success of the Human Genome Project in 2003, DNA sequencing has been applied successfully to whole genome genotyping, mutation detection, carrier screening, detection of inherited disorders, and DNA library preparation.¹ Unfortunately, current sequencing methods are limited to DNA fragments at most a few kilobases long and result in many inaccuracies due to random cutting and the repetitive nature of DNA.² In one practice called molecular combing, a substrate is slowly pulled out of a DNA solution, depositing DNA molecules linearly on its surface. This offers the advantage of controlled cutting of DNA to then be sequenced in an orderly fashion.³ PMMA-coated silicon wafers have been effectively used for both DNA combing and cutting; however, they have presented issues in the removal of DNA fragments for subsequent replication and sequencing.

In order to address this issue of desorbing the DNA from the polymer coated silicon wafer, we decided to use agarose gels and create an electric field to draw the DNA off the surface. This setup relies on the same electromotive force that is employed in gel electrophoresis to move the DNA molecules through the gel matrix due to the negative charge of DNA. We cleaved 0.5 in x 0.5 in silicon wafers and spun cast them with varying concentrations of PMMA and PAA. PAA samples resulted in nonlinear DNA deposition and were not selected to be used in this experiment. Through testing several combinations of PMMA and DNA concentrations, it was determined that the 1 $\mu\text{g}/\text{mL}$ λ DNA solution on 80-100 nm PMMA-coated silicon produced the best samples. Successful samples were dipped in the DNA solution, which was first heated at 60°C for 30 minutes to eliminate formation of DNA dimers. DNA-dipped samples were assigned to four different treatments. Some were placed in wells and covered with 4 mm thick 3% agarose gels made with NEBuffer 3.1 and incubated in a 60°C oven overnight. Others were placed in a well with an electric field parallel to the sample at field strengths for different lengths of time, with and without a gel. All samples were then re-dyed in diluted SYBR gold solutions, washed with DNase reaction buffer, and blown dry with nitrogen gas. A Leica TCS SP2 confocal microscope was used to photograph 8 areas on each sample before and after DNA was desorbed and ImageJ was used to quantify the percent change in DNA on the samples.

As shown in Figure 1, the samples that were placed in an electric field desorbed significantly better than those that did not, regardless of the voltage, running time, or presence of a gel. Compared to the 79.1% DNA desorbed on the sample that sat with a gel in the oven overnight, the other samples which electrophoresed at .55 V/mm for 10 minutes, .39 V/mm for 15 minutes, and .55 V/mm for 10 minutes with a gel experienced a greater percent DNA desorption at 92.0%, 96.5%, and 97.8%, respectively. Among those three, the lower voltage for a longer time resulted in less remaining DNA, and the sample that was in contact with a gel had the least remaining DNA. This suggests that electrophoresis is a viable method of removing cut DNA from PMMA for replication and sequencing of systematically cut fragments, resulting in a more accurate technique for sequencing long DNA molecules.

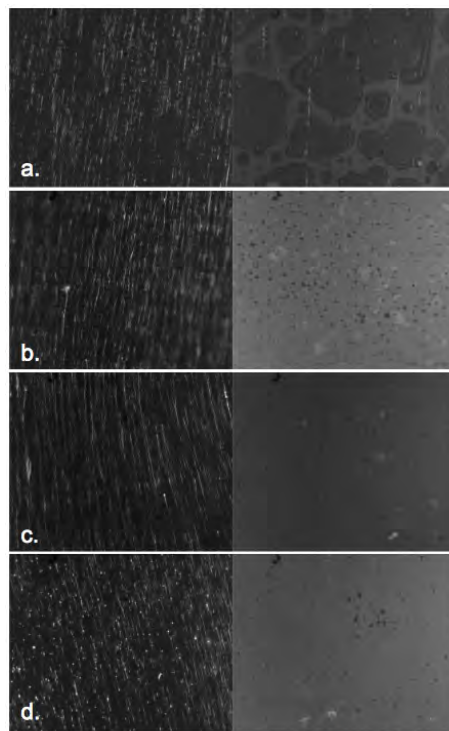


Figure 1- Confocal microscope images (63x) of samples before (left) and after (right) desorption with only a gel (a), 7 volts for 10 minutes (b), 5 volts for 15 minutes (c), and 7 volts for 10 minutes with a gel (d).

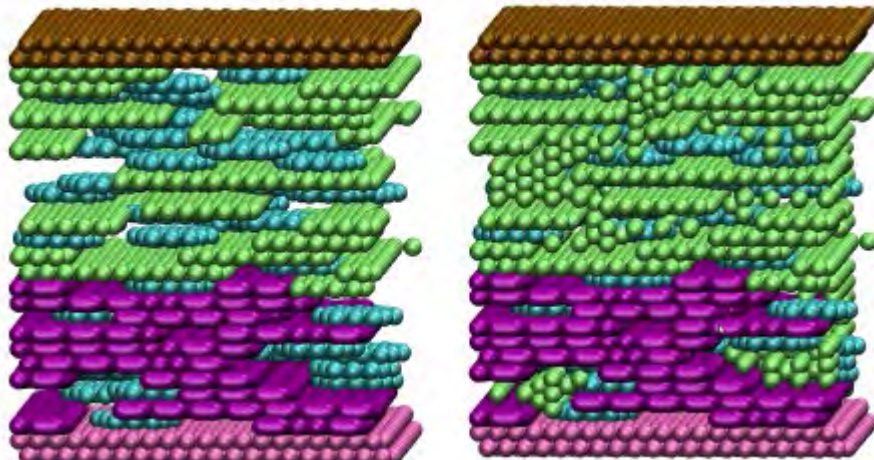
[1] Pareek, Chandra Shekhar, et al. "Sequencing Technologies and Genome Sequencing." *Journal of Applied Genetics*, vol. 52, no. 4, 2011, pp. 413–435., doi:10.1007/s13353-011-0057-x.

[2] Goodwin, Sara, et al. "Coming of Age: Ten Years of next-Generation Sequencing Technologies." *Nature Reviews Genetics*, vol. 17, no. 6, 2016, pp. 333–351., doi:10.1038/nrg.2016.49.

[3] Allemand, J.f., et al. "PH-Dependent Specific Binding and Combing of DNA." *Biophysical Journal*, vol. 73, no. 4, Oct. 1997, pp. 2064–2070., doi:10.1016/s0006-3495(97)78236-5.

Session 5: Theory and Modeling

Chairs: Hongyu Li
Shoumik Saha
Zhuolin Xia



Molecular Dynamics Simulation of Biopolymer-based Pore Fluids

Jeffrey Li¹, Kelvin Linskens², Shoumik Saha², Dilip Gersappe², Miriam Rafailovich²

¹Gilman School, Baltimore, MD 21210

²Department of Materials Science and Chemical Engineering, Stony Brook University, Stony Brook, NY 11794

Given the ubiquity of soil as a structural material in both civil and geotechnical engineering, it is imperative to have a comprehensive understanding of its mechanical properties under a range of conditions. Soil by itself possesses little merit as a foundational material and thus often has its mechanical strength augmented through the addition of various fillers, the most common of which is cement. Cement-based fillers significantly improve soil's mechanical performance, but this comes at the cost of a large environmental impact¹. As such, efforts are being made to develop more sustainable methods of soil reinforcement. One fast-emerging technique is the addition of biopolymer pore fluids that modify the internal structure of the soil and thus supplement its mechanical strength. Although the efficacy of such methods has been experimentally demonstrated², the mechanisms by which reinforcement is achieved are not well understood. In this study, we help to answer such questions by using coarse-grain molecular dynamics techniques as implemented in the LAMMPS code package³ to simulate the behavior of a pore fluid composite consisting of various concentrations of nanoplatelet clay fillers, biological polymers, and water under different levels of mechanical strain. Scripts were developed to randomly

generate the positions of the contents of the pore fluid. Any remaining space inside the simulation domain was filled using either a simple cubic, pseudo-BCC, or pseudo-HCP packing method (see Fig. 1) to achieve any solvent concentration up to the theoretical maximum allowed by the system - thus replicating a variety of real-world conditions. These generated samples were then equilibrated in both a canonical ensemble and a piston model, after which they were sheared at different speeds to simulate realistic weight-bearing scenarios.

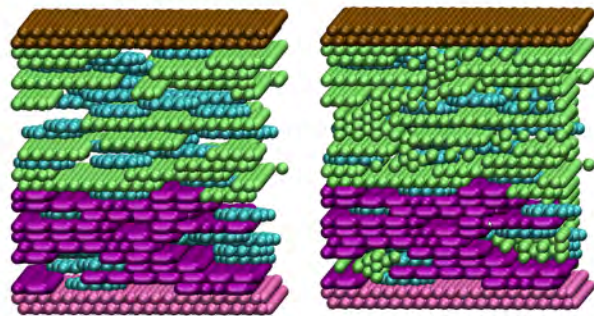


Figure 1 | Effect of explicit solvent generator script. Left | Original pore fluid with solvent in green, clay nanoparticles in blue, and biopolymers in purple. **Right |** Pore fluid with 696 additional solvent particles generated by a pseudo-BCC packing method. This increases the density at the center of the system to 0.8, which aligns with both QFT predictions and the established experimental literature.

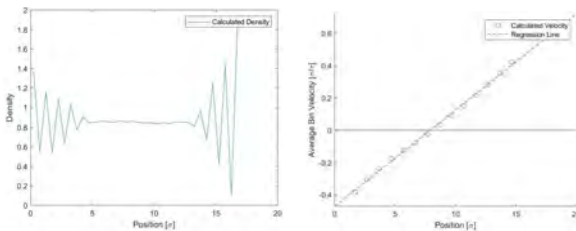


Figure 2 | Rheological properties of soil sample with twenty (20) nanoplatelets and fifty percent (50%) by volume biopolymer concentration. Left | Density profile across height of soil sample - note that the density at the center of the sample is around 0.8 and thus in agreement with QFT prediction. **Right |** Average particle velocity across height of soil sample - note the close fit to the LSRL model and occurrence of zero (0) velocity at half of the height of the sample.

In order to better understand the rheological properties of the pore fluid, we calculated the internal system density, pressure, viscosity, and velocity profiles (see Fig. 2) and kept track of possible microstructure formation for each simulation. Our findings provide valuable insight on how to improve the mechanical properties of soil - a practice which has, until now, had little to no theoretical basis for its selection of treatments. Knowledge of this nature will

help scientists better understand soil phenomena and thus allow them to engineer informed solutions better tailored to individual situations.

¹ Naeimi, Maryam & Haddad, Abdolhosein. (2018). Investigation on the Environmental Impact of Soil Improvement Techniques: Comparison of Cement Grouting and Biocement. 10.1007/978-981-13-0128-5_53.

² Latifi, Nima & Horpibulsuk, Suksun & L. Meehan, Christopher & Abd Majid, Muhd.Zaimi & Tahir, Mahmood & Tonnizam Mohamad, Edy. (2016). Improvement of Problematic Soils with Biopolymer—An Environmentally Friendly Soil Stabilizer. Journal of Materials in Civil Engineering. 29. 10.1061/(ASCE)MT.1943-5533.0001706.

³ S. Plimpton, Fast Parallel Algorithms for Short-Range Molecular Dynamics, J Comp Phys, 117, 1-19 (1995).

Optimizing Graphite Electrode of Lithium-ion Batteries with Lattice Boltzmann Modeling

Yijun Chen¹, Zhuolin Xia², Dilip Gersappe², Miriam Rafailovich²

¹Shenzhen Middle School, Shenzhen, Guangdong

²Department of Materials Science and Chemical Engineering, Stony Brook, NY 11790

Graphite is a widely used material for the anode of Li-ion batteries. There have been various attempts to optimize the electrode performance, and one of the goals is to achieve a higher final charge density, which is mainly concerned with suppressing the plating of Li metal, or the formation of dendritic structure [1]. Instead of focusing on the performance of electrode-electrolyte interface of the Li-ion batteries, this study aims to optimize the morphology of electrode under multiple conditions by simulating its influence on intercalation reactions in the graphite electrode with Lattice Boltzmann Method.

The 3D printing technology offers people more control on the structure of electrodes, and previous work tests two types of morphologies, which are random and sorted; in this study, we adopt the general reaction model developed by Ning Sun [1], and add a cluster counting algorithm to check if the generated morphology is appropriate. Besides, we create a parameter called density distribution factor to describe the general structure of the graphite electrode (Figure 1). The according morphology can be easily manufactured with current technologies. The diffusivity of Li atoms in graphite is set at $1e-6$ mm^2/s [2]. Other material parameters such as electrode density are altered to see the performance of electrodes under different charging conditions. In

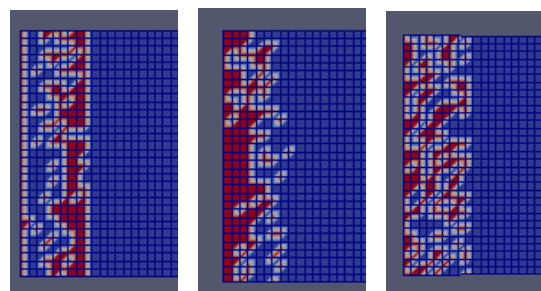


Figure 1: 2D slices of graphite morphologies at different density distribution factor with electrode density of 50% and 1C-rate current. From left to right, the factors are -4, 4 and 0. The factor determines whether the graphite density is higher near the current collector (left) or the electrolyte (right).

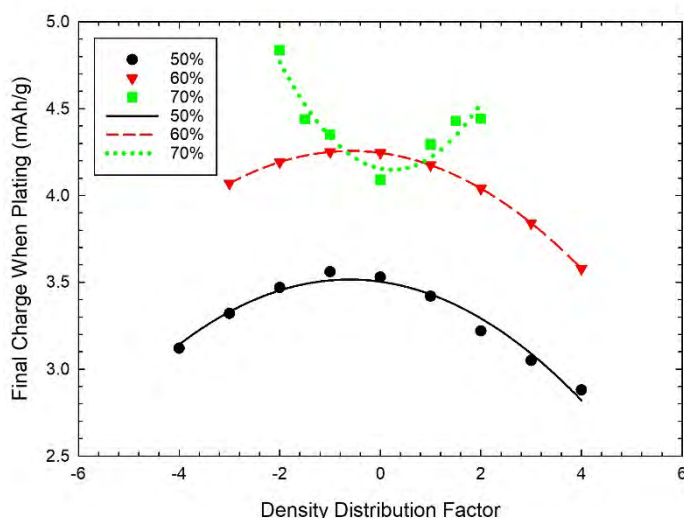


Figure 2: The final charge density when plating at different density distribution factors and electrode densities of 50%, 60% and 70% in simulation with 1C-rate current

the end, we analyze the results in terms of final charge density, charging time, and actual current.

We show that the capacity of the Li-ion batteries has a functional relationship with the density distribution factor. By simulating electrode densities of 50%, 60% and 70%, we show a quadratic relationship between the final charge and the density distribution factor, and the fitted curve changes from concave down to concave up at 70% (Figure 2). Besides, we see a linear relationship between the charging time and the total charge, which is not a strong function of the electrode density, while the actual current is higher when the electrode density is higher, because of the higher mass density. These results can be used to better design the morphology of graphite anodes for superior performance.

[1] Sun, Ning. *Application of Lattice Boltzmann Methods in Complex Mass Transfer Systems*. 2016. State University of New York at Stony Brook, PhD dissertation.

[2] Yu, P., et al. "Determination of the lithium ion diffusion coefficient in graphite." *Journal of the Electrochemical Society*, vol. 146, no. 1, 1999, pp. 8-14.

Lattice Boltzmann Modeling of Hydrogen Ion Transport in a Proton Exchange Membrane Fuel Cell

Alexander Kwandou¹, Hongyu Li², Dilip Gersappe², Miriam Rafailovich²

¹Bellarmino College Preparatory, San Jose, CA 95126

²Department of Materials Science and Chemical Engineering, Stony Brook University, Stony Brook, NY 11794

Proton exchange membrane fuel cells (PEMFC), better known as hydrogen fuel cells, are energy sources powered by hydrogen gas that can supply the world with clean, sustainable electrical power. First invented by Sir William Grove in 1839, fuel cells have become the center of modern research due to their high efficiency and power density. In order for hydrogen fuel cells to achieve their full potential, a critical improvement needed is to develop new materials for the membrane that controls the transport of ions.

In this project, we investigate the transport properties of the proton exchange membrane, specifically two different membrane structures to find the most efficient one. The underlying principle of this project is the polaron theory which states that waves of movement in a crystal lattice, called polarons, spread particles through deflection and reflection. In our case, protons "hop" from one position to the next by "worming" their way along the backbone of polymer chains¹. The first structure consists of nanometer-sized channels where the chains are all aligned and provide an excellent conduit for transporting protons². The second structure consists of nanocellulose which functions similarly to the first structure, but transports the protons with randomized motion³.

The modeling approach we use in this project is the Lattice Boltzmann Method (LBM), which makes it much simpler to simulate single and multiphase fluids by offering a numerical solution to difficult Navier-Stokes equations. LBM especially excels at simulating complex physical phenomena while proving to be efficient and convenient compared to other methods of modeling. To apply the LBM, we used the program, Palabos, wrote C++ scripts in XCode, and executed those scripts with Unix. After running our simulations on a server, we used Paraview to create 3D models of our system and Matlab to plot the data. Regarding the simulation, we created a lattice of 60x10x60 lattice units and ran the simulation for 30 timesteps, recording the density every timestep. The simulation was created by initializing a higher region of density in the left and by using advection-diffusion and Guo external force fluid dynamics. We then changed the diffusion properties, either patterned or randomized, to simulate the two different structures by having the particles diffuse through the structures.

The diffusion gradient for the two structures can be seen in figure 1 and a 3D model of the nanocellulose structure in action can be seen in figures 2-4. In figure 1, the diffusion gradient for the nanometer-sized channels is greater than that of nanocellulose, and since the gradient is inversely proportional to the diffusion coefficient, the first structure diffuses faster than the second structure, which is to be expected as uniform motion should diffuse more quickly than randomized motion.

Overall, we were able to simulate the polaron theory of proton transport through a membrane and accurately model different transport structures while making the simulation versatile by having the power to change parameters. In the future, we can add a bias for the second structure to coerce particles to diffuse faster.

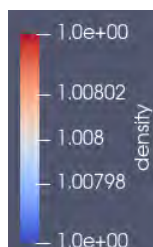


Figure 2 - Timestep 0



Figure 3 - Timestep 15



Figure 4 - Timestep 30

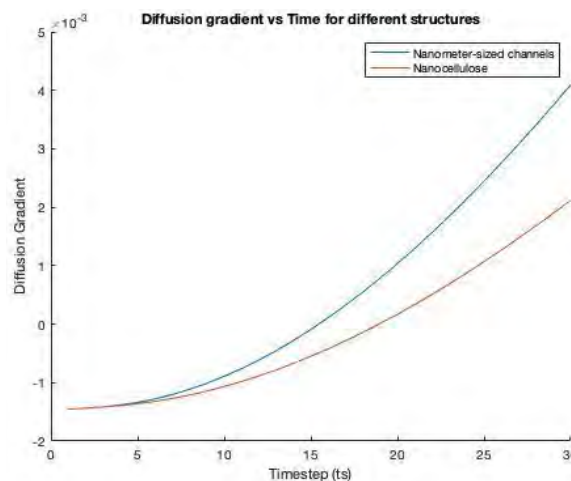


Figure 1 - Diffusion gradient vs Time

[1] How protons move through a fuel cell. (2017, June 21). Retrieved from <https://www.nanowerk.com/nanotechnology-news/newsid=47150.php>

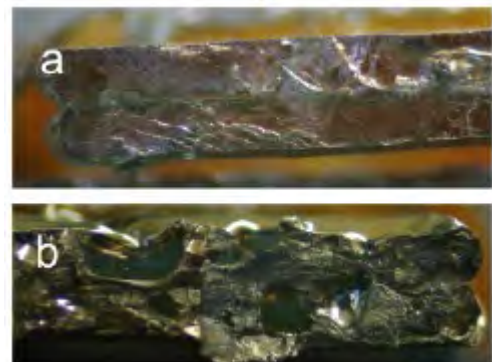
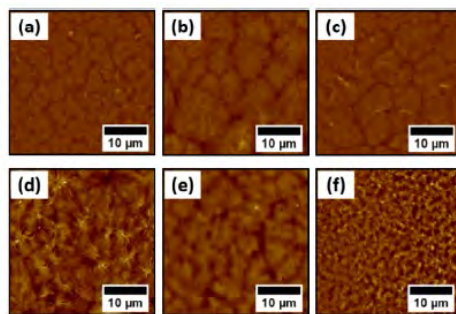
[2] Braun, A. (2017). Swiss team discovers how protons move through fuel cell. *Fuel Cells Bulletin*, (6). [https://doi.org/10.1016/S1464-2859\(17\)30237-7](https://doi.org/10.1016/S1464-2859(17)30237-7)

[3] Bayer, T., Cuning, B. V., Selyanchyn, R., Nishihara, M., Fujikawa, S., Sasaki, K., & Lyth, S. M. (n.d.). High Temperature Proton Conduction in Nanocellulose Membranes: Paper Fuel Cells. *CHEMISTRY OF MATERIALS*, 28(13), 4805–4814.

<https://doi.org/10.1021/acs.chemmater.6b01990>

Session 6: Nanocomposites & FDM Printing

**Chairs: Yu-Chung Lin
Yuval Shmueli
Xianghao Zuo**



Optimizing Thermal and Mechanical Properties of Poly(Lactic Acid) / Polypropylene / Graphene Nanocomposite Polymer Blends in Fused Deposition Modeling (FDM) Systems

Larry Huang^{*1}, Richard Li^{*2}, Addison Liu^{*3}, Nikita Salunke^{*4}, Yu-Chung Lin⁵, Yuval Shmueli⁵,
Steve Nitodas⁵, Miriam H. Rafailovich⁵

¹Wilton High School, Wilton, CT 06897, ²Conestoga High School, Berwyn, PA 19312, ³Unionville High School, Kennett Square, PA 19348, ⁴Evergreen Valley High School, San Jose, CA 95148, ⁵Department of Materials Science and Chemical Engineering, Stony Brook University, Stony Brook, NY 11794

Additive manufacturing, commonly known as 3D printing, has increased in popularity within the last decade¹ due to its versatility and accessibility. Coupled with the rise in polymer blend systems applications and graphene-based devices, this study aims to combine the three in the development of an optimized nanocomposite polymer blend for 3D printing applications.

Polymer composite systems have been especially popular in recent years because of their unique mechanical and thermal properties. This work explores a binary polymer blend of polylactic acid (PLA) and isotactic polypropylene (iPP) with added graphene nanoplatelets (GNPs). This nanocomposite utilizes PLA/iPP immiscibility² to aid in filament fusion and the compatibility of GNPs to enhance thermal conductivity of 3D-prints.

The focus of this study was two-fold: optimizing properties of (1) binary PLA and iPP blends at varying concentrations and (2) PLA/iPP blends with GNPs. Mechanical properties were studied using tensile testing, and thermal properties were studied using forward-looking infrared radar (FLIR) imaging. Raman spectroscopy, optical microscopy (OM) and scanning electron microscopy (SEM) were employed for structural characterization and morphology determination. Tensile testing revealed that in comparison to a control sample of pure PLA, the 99PLA/1iPP and 97.5PLA/2.5iPP concentrations exhibited an increase in Young's modulus, followed by a decrease in modulus with the addition of iPP beyond the 2.5% level. This aligns with the theorized interfacial fusion enhancements that result from iPP migrating to the surface of PLA, as low concentrations of iPP allow for migration due to uniform dispersion with minimal consequences to printability. OM offered insight into the interfilament fusion along the horizontal cleave of a 3D printed sample. Figure 1a. displays the poor interfilament fusion within the 100% PLA sample. As depicted in Figure 1b, the addition of iPP resulted in a total fusion at the interface at the cost of voids due to the poor miscibility of the polymer composite. Raman spectra of filament cross-sections confirm polypropylene filament rings observed during optical microscopy. These polypropylene channels hold promise in facilitating the organization of GNPs, likely boosting thermal conductivity and mechanical properties. Figure 2. shows relative PLA/iPP concentrations and clearly illustrates an iPP phase separation within the PLA matrix. PLA/iPP/GNP blends at multiple ratios were also prepared and 3D printed, using a minimum GNP concentration of 5% weight for weight. Mechanical testing showed a small reduction in the Young's modulus in the composites as compared with pure PLA and the binary blends.

Preliminary FLIR imaging indicated that the addition of graphene to PLA significantly enhances thermal conductivity and the addition of PP to this blend further improves thermal conductivity, supporting the theorized orientation of GNPs within the polymer matrix as a result of its incorporation with PP.

Future research should be conducted to investigate the effects of substituting iPP with polymers such as polybutadiene (PB) and polydimethylsiloxane (PDMS). Additionally, for enhanced FDM capabilities, it may be beneficial to add polybutylene adipate terephthalate (PBAT) as a compatibilizer during blending. To better understand additional properties of the blend, thermogravimetric analysis (TGA) and X-ray diffraction (XRD) analysis would also be advantageous.

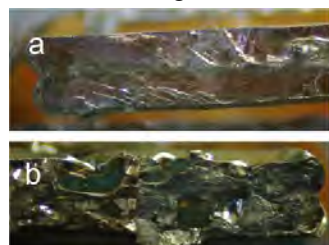


FIG. 1 Optical Microscopy a) Gold plated 100 PLA dogbone cross-section b) Image of 95PLA 5iPP

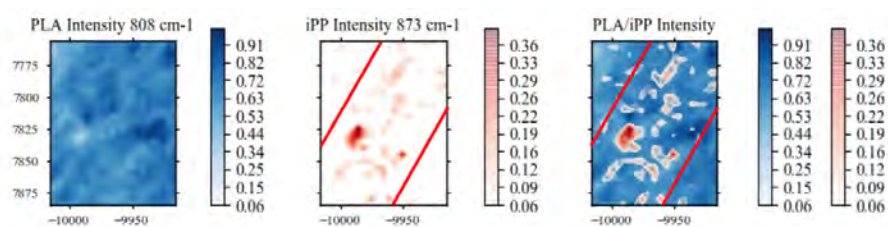


FIG. 2: Raman Spectra of 90PLA/10iPP polymer blend demonstrating aggregation of iPP rings in filament

[1] Wohlers Assoc., "Additive manufacturing & 3D printing state of the industry," 2013, Morgan Stanley Research, September 2013; J.P. Morgan, January 2012.

[2] Choudhary, Priyanka, et al. "Poly(L-Lactide)/Polypropylene Blends: Evaluation of Mechanical, Thermal, and Morphological Characteristics." *Journal of Applied Polymer Science*, vol. 121, no. 6, 2011, pp. 3223–3237., doi:10.1002/app.33866.

Mechanical and conductivity study of the 3D printed PBAT/PLA/graphene nanocomposites

Da Hyun (Dianne) Choo¹, Zhehua (Eric) Xiang², Xianghao Zuo³, Miriam Rafailovich³

¹Kent School, 1 Macedonia Rd, Kent, CT 06757, ²Lawrence Woodmere Academy, Woodmere, NY 11598, ³Stony Brook University, Stony Brook, NY 11794

In recent years, manufacturers are facing the requirements to enhance the thermal and electrical conductivity with reliable mechanical properties since the demand of electrical appliances is increasing. Polystyrene (PS) and its copolymers are among the most used materials of recent products. However, the concern of the environmental pollution caused by styrenic products has attracted more attention from the public and the government. Considering this, we chose a more environmentally friendly PBAT/PLA blend to mix with graphene (GNPs) H-5 to study the mechanical and conductivity performance. Previous study has shown that graphene prefers to stay in PBAT phase than PLA phase, and for the molded samples, they used PLA as a minor domain to confine the arrangement of GNPs H-5^[1]. Inspired by this, we are trying to further orientate the H-5 platelets under the shear force of the nozzle during 3D printing^[2].

The 3D printed samples present a relatively similar impact strength comparable to the molded ones, as shown in Figure 1(a). While in figure 1(b), we can see that the Young's modulus of 3D printed samples performed a higher tensile strength than the molded samples. These results suggest that the polymers made through 3D printing can perform better mechanical properties. In addition, as the concentration of graphene H-5 increases, the impact strength decreases slower than the molded samples, and maintained at 65 J/m, which is much stronger than PS and the tensile strength, increases with the addition of H-5 content.

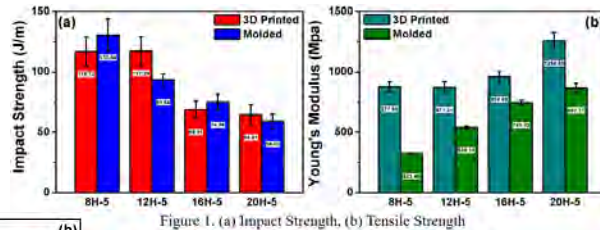


Figure 1. (a) Impact Strength, (b) Tensile Strength

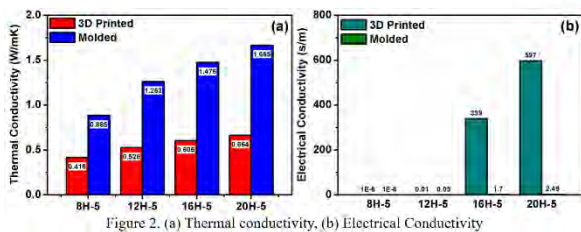


Figure 2. (a) Thermal conductivity, (b) Electrical Conductivity

For the thermal conductivity test, we tested the significance of the direction of graphene platelets can have on conductivity by making the testing direction vertical to the printing direction.

In figure 2(a), we can conclude that the thermal conductivity of the 3D-printed samples is lower than that of molded samples, which can be explained as the printing direction is perpendicular to the testing direction, thus the orientated H-5 pathways is not applied at the direction of the heat diffusion. In the other hand, the electrical conductivity, which is measured in a closed loop and the electrons was transferred right on the printed direction, showed a significant increase, nearly 240 times higher for the 3D-printed 20% H-5 mixed PBAT/PLA blends than the molded sample, as shown in figure 2(b).

The high magnitude and low magnitude SEM image of 69PBAT/23PLA/8H-5 and 60PBAT/20PLA/20H-5 are shown in figure 3(a) - (d). From the low magnitude images, we can see that the printing of 69PBAT/23PLA/8H-5 is better than the 60PBAT/20PLA/20H-5 as the fusion and connections between each layer of the 8H-5 samples are significantly better than those of 20H-5 samples. From figure 3(a) we can hardly tell the boundaries of the layers. In figure 3(b) and 3(d), the orientation of the H-5 platelets was clearly displayed, shown as arrow directions, which is in agree with the enhancement of the mechanical and electrical conductivity.

[1] Weng, Y. X., Jin, Y. J., Meng, Q. Y., Wang, L., Zhang, M., & Wang, Y. Z. (2013). Biodegradation behavior of poly (butylene adipate-co-terephthalate)(PBAT), poly (lactic acid)(PLA), and their blend under soil conditions. *Polymer Testing*, 32(5), 918-926.

[2] Jia, Y., He, H., Geng, Y., Huang, B., & Peng, X. (2017). High through-plane thermal conductivity of polymer based product with vertical alignment of graphite flakes achieved via 3D printing. *Composites Science and Technology*, 145, 55-61

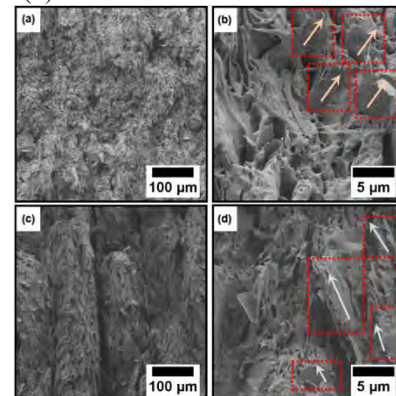


Figure 3. SEM images: (a) Low magnitude of 69PBAT/23PLA/8H-5, (b) High magnitude of 69PBAT/23PLA/8H-5, (c) Low magnitude of 60PBAT/20PLA/20H-5 and (d) High magnitude of 60PBAT/20PLA/20H-5

Studying the Crystal Formation and Interdiffusion Mechanisms of Polylactic Acid Thin Films

Suraj Dhulipalla¹, Mukil Shanmugam², Doris Yang³, Xianghao Zuo⁴, Miriam Rafailovich⁴

¹Eastlake HS, 400 228th Ave NE, Sammamish, WA 98074; ²Redmond HS, 17272 NE 104th St, Redmond, WA 98053; ³Lake Oswego HS, 2501 Country Club Rd, Lake Oswego, OR 97034; ⁴Dept. of Mat. Sci. and Chem. Engineering, Stony Brook University, NY 11794

Polymer thin films are widely utilized as industrial coatings in fields ranging from photovoltaics to organic LEDs. Due to growing environmental concerns, however, petroleum-based plastics commonly used in thin films have come under scrutiny. The thermoplastic polylactic acid (PLA) has emerged as an inexpensive, eco-friendly replacement for nonbiodegradable plastics.^[1] Little is known, however, about the interfacial diffusion or crystal formation in PLA thin films, which are important to the surface performance of confined polymers.

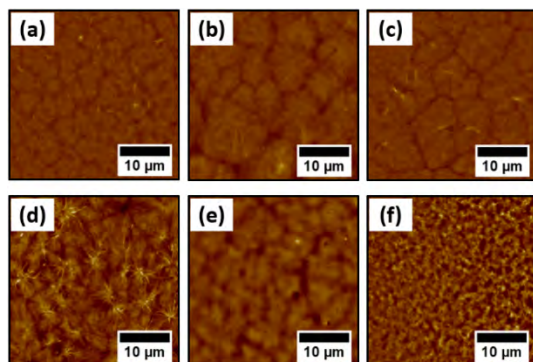


Figure 1 (a) PLA (b) 99PLA/1PS (Mw 9.4k) (c) 99PLA/1PS (Mw 2mil) (d) 99PLA/1dSMMA on PS (e) PS on 99PLA/1dSMMA (f) PS on PLA on PS middle

Table 1: Roughness (10 mg/mL)

Sample Name	Roughness (nm)
PLA Control	14.0
MwPS 9,400	21.1
MwPS 2 million	14.9
PLA/dSMMA on PS	14.7
PS on PLA/dSMMA	10.0

further examine the effect of confinement on PLA crystal formation.

The control group was pure PLA. AFM showed that the surface roughness for the pure PLA was 14.0 nm and that the average crystal size was 4.09 nm. When PS with Mw=9,400 amu was added, the roughness grew 50.7% to 21.1 nm, and the average crystal size grew 66.5% to 6.810 nm. When the polystyrene with Mw 2 million was added, the roughness increased just 6.04% to 14.9 nm, while the crystal size increased 84.7% to 7.554 nm. These results show that the addition of PS consistently increased both the roughness and the crystal size within the thin films; the increase in roughness is due to the rigidity of polystyrene as compared to PLA (Table 1). In addition, they show that larger molecular weight PS additives increase crystal size by a greater amount. Next, the 99 % PLA/1% dSMMA top layer of the bilayer samples with PS on bottom that were analyzed using AFM and SIMS. AFM revealed that the roughness of the surface was 14.7 nm; when the top layer was PS the roughness decreased 31.97% to 10.0 nm (Table 1). In addition, SIMS data from samples with 1%, 2%, and 5% dSMMA annealed at 120°C and 170°C for 1 hour proved that samples with higher SMMA concentration and at higher annealing temperatures saw more interfacial diffusion (Figure 2; Table 2).

SIMS data for the samples with PS on top is currently being generated to confirm the interfacial diffusion phenomenon. AFM performed on the triple layers in a region covered only by the PLA on PS revealed that crystallization on the PLA layer was heavily suppressed even when the PLA was not completely covered by PS (Figure 1f). To continue this study, it is necessary to study the roughness when PLA/dSMMA is the bottom layer and its effects on the interfacial thickness of the bilayer after diffusion. Furthermore, to study the broader applications of the dSMMA compatibilizer, we can use dSMMA and monitor its diffusion when miscible with similar polymers such as PEO and PVDF.

In this study, various PLA, polystyrene (PS) and deuterated styrene methyl methacrylate (dSMMA) blends were examined as confined thin films on different substrates. The first part of this study used atomic force microscopy (AFM) and ellipsometry to determine the impact of polymer chain length on crystal formation and was investigated by comparing PS of molecular weights (Mw) 9.4k and 2 million amu in 99% PLA/1% PS thin films on silicon wafers annealed for 24 hours at 170°C. The second part of this study involved testing different substrates by creating bilayer thin films through a floating procedure. Since PLA and PS are immiscible^[2], dSMMA was

Figure 2

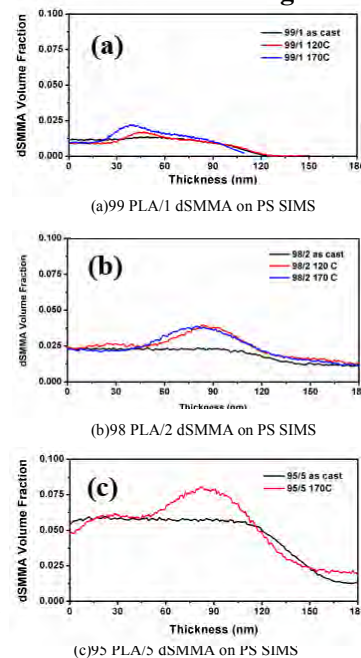


Table 2: dSMMA Interfacial Thickness (nm)

	99/1	98/2	95/5
120°C	25.080	39.937	in progress
170°C	37.456	46.355	57.425

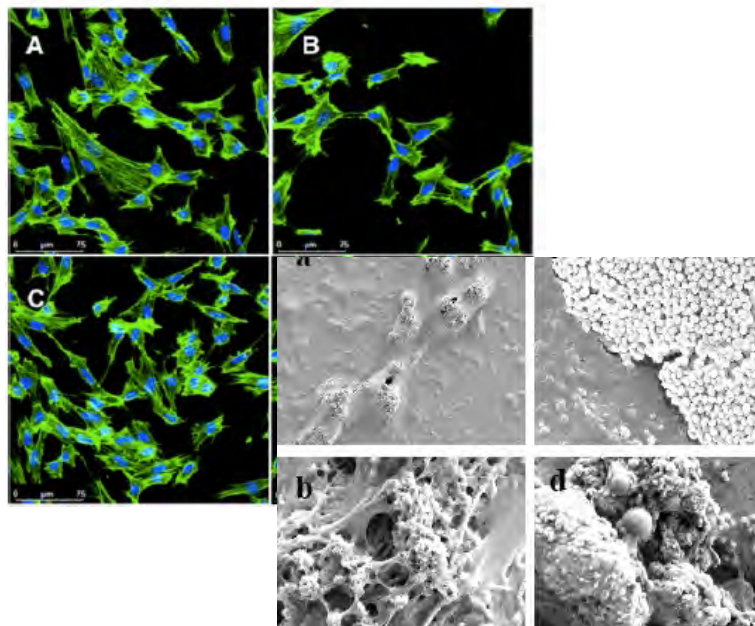
[1] Kikkawa, Yoshihiro, et al. "Crystallization, Stability, and Enzymatic Degradation of Poly(L-lactide) Thin Film," *Biomacromolecules*, 2002.

[2] Guo, Yichen, et al. "Enhancing Impact Resistance of Polymer Blends via Self-Assembled Nanoscale Interfacial Structures," *Macromolecules*, 14 April 2018.

Session 7:

Dental Pulp Stem Cells: Mechanical & Chemical Sensing

Chair: Ya-Chen Chuang
Kao Li



Elucidating the Effects of Direct Contact of Dental Pulp Stem Cells Cultivated Under Various Physical Parameters on Lineage Specification Pathways

Yihan Shen^{1*}, Zijian Ma^{2*}, Jessica Hofflich³, Ya-Chen Chuang^{3,4}, Miriam Rafailovich³, Marcia Simon⁵

¹St.Andrew's School, Middletown, DE19709, ²Tianjin Nankai High School, Tianjin, China

³Department of Materials Science and Chemical Engineering, Stony Brook University, Stony Brook, NY 11794,

⁴ThINC Facility, Advanced Energy Center, Stony Brook University, Stony Brook, NY 11794,

⁵Stony Brook University School of Dental Medicine, Stony Brook, NY 11794,

*Authors have equally contributed to the project

Dental Pulp Stem Cells (DPSCs) have demonstrated immense potential for therapeutic purposes and might be used to treat a myriad of diseases such as neurological disorders and ischemic heart disease¹². Nonetheless, the means through which odontogenic signals transmit in between DPSCs remains enigmatic. As previously demonstrated by Chang, C., et al., besides well-studied chemical-initiating differentiation, differentiation of DPSCs can also be manipulated by polybutadiene(PB) substrate mechanics, as odontogenesis is inhibited by soft, thick PB films while promoted by hard, thin ones³. Therefore, this research was conducted to investigate how physical contact of stem cells cultured on substrates of various stiffness impacts differentiation pathways.

PB was dissolved in toluene at concentrations of 3mg/ml and 20mg/ml, which were then spun cast onto silicon wafers to produce thin (20nm) and thick (200nm) films for cell cultivation. The wafers were designated into 3 groups: contact group composed of one 1cm*2cm thin-film wafer adjoining one thick-film wafer of the same size, non-contact group with thin and thick films on two separate 1cm*2cm wafers in the same well, and 2cm*2cm control group with only thin or thick film. Strain 13 DPSCs were incubated at 37.5 °C with 5% CO₂ and fed every other day with osteogenic medium solution comprised of 89% MEM Alpha medium, 10% Fetal Bovine Serum, 1% Penicillin, L-ascorbic acid, and β-glycerol phosphate. On days 3 and 7, moduli of cells were measured by Atomic Force Microscopy in contact mode. On days 3 and 7, cell samples were first fixed by applying formaldehyde, then stained with AF488 and DAPI, and finally examined by Confocal Microscopy.

One day 3 {Fig.1}, the relative moduli were high for cells on thin films and low for those on thick films. In addition, the moduli of cells in touching group and non-touching group did not vary notably before confluence. Interestingly, the moduli of cells on touching thin films demonstrate a gradual decrease, progressively approaching that of cells grown on thick films. This phenomenon may stem from the various degrees of cell contact according to their respective locations on the film. On day 7, all touching cells exhibited similar low moduli. In images of confocal microscopy on day 3 {Fig.2}, cells on thin films outnumbered those on thick films and meanwhile were more attached and stretched, indicating cells' preference for hard substrates. On day 28 {Fig.3}, biomineralization images suggested that cell on the thin film lost the ability to produce minerals after cell contacts.

On days 3, 7, 14, and 28, RNA was isolated for RT-PCR using QIAzol Lysis Reagent. After purification and cDNA preparation, the expression of early markers, ALP, Runx, and late markers, DSPP, OCN will be measured by qRT-PCR. The latter will serve as indicators of odontogenic and osteogenic differentiation. Additionally, a microarray will be conducted with microRNA kits to explore whether genetic expressions are affected by cell contacts.

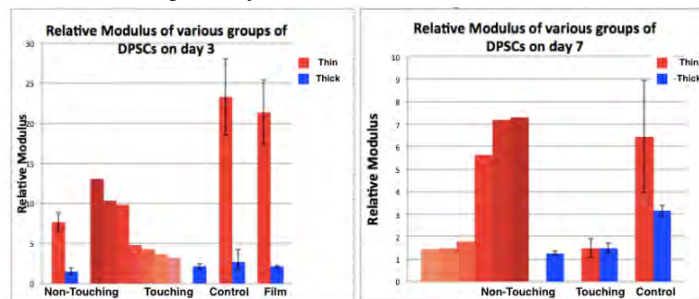


Figure1. Relative Modulus of Various DPSC Samples

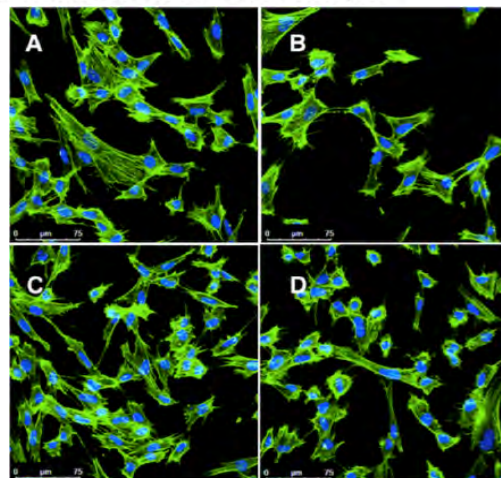


Figure 2. Confocal Microscopy of DPSCs on day 3. Actin stained with AF 488 (green) and Nucleus stained with DAPI(blue). A)Thin Control Group B)Thick Control Group C)Thin Touching Group D)Thick Touching Group



Figure 3. Biomineralization Image captured by Scanning Electron Microscopy on Day 28 of DPSCs from A)NT Thin Films B)NT Thick Films C)T Thin-Thick Films

¹ Potdar, Pravin D., and Yogita D. Jethmalani. "Human dental pulp stem cells: Applications in future regenerative medicine." *World journal of stem cells* 7.5 (2015): 839.

² Chalisserry, Elna Paul, et al. "Therapeutic potential of dental stem cells." *Journal of tissue engineering* 8 (2017): 2041731417702531.

³ Chang, C., et al. "Entangled polymer surface confinement, an alternative method to control stem cell differentiation in the absence of chemical mediators." *Ann J Materials Sci Eng* 1.3 (2014): 7.

Determining DPSC Differentiation Pathways and Biomineralization on ALD TiO₂ PB Thick and Thin Films Megha Gopal¹, Jessica Hofflich², Ya-Chen Chuang², and Miriam Rafailovich²

¹New Hyde Park Memorial High School, New Hyde Park, New York 11040, ²Department of Materials Science and Chemical Engineering, Stony Brook University, Stony Brook, New York 11790

Dental Pulp Stem Cells (DPSC) provide a valuable and enticing avenue for the field of regenerative medicine. In order to better control cell proliferation, studies have been conducted to determine the extent to which environmental factors influence differentiation. Titanium nanoparticles, for example, have synergistic effects on DPSC growth as well as high biocompatibility, so it is frequently used in dental implants [1]. Similarly, cell modulus has close ties to actin formation and density, as well as later stage collagen formation [2]. Hence, there is great need to elucidate a relationship between titanium nanoparticles, template biomineralization, and differentiation of DPSC.

Si wafers were cut and coated with thin (TN) or thick (TK) films of polybutadiene (PB), with PBTN having an average thickness of 24 nm and PBTK thickness 240 nm. Half of the Si wafers with PBTN and half with PBTK, along with untreated Si wafers, were further treated with 80 cycles of Atomic Layer Deposition of TiO₂ at

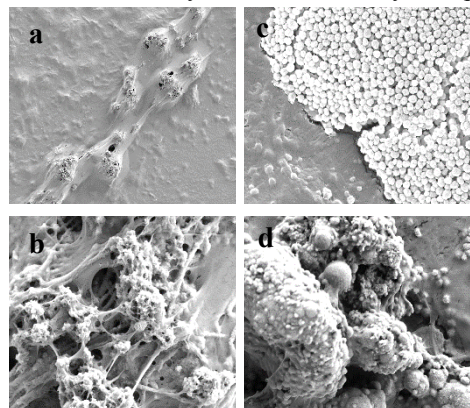


Figure 2 Day 28 SEM images (a) and (b) ALD PBTN, (c) PBTN, (d) ALD PBTK

very similar between PBTK and PBTN groups, leading a conclusion that there was no significant effect of ALD on cell proliferation. Subsequently, confocal images of early-stage DPSC cell division, as referenced in Figure 1, demonstrate similar actin density and length between ALD PBTN and PBTN cells, while ALD PBTK and PBTK cells both exhibited significantly less actin development. Therefore, it may be stated that the titanium nanolayer has minimal effect on cell presentation in the initial period, while substrate thickness is more influential on this early-stage cytoskeleton.

However, when biomineralization data in Figure 2 is presented, it is apparent that the titanium does indeed affect collagen development in later-stage cells, especially in terms of creating templated structures. ALD samples exhibited substantially more collagen banding than the non-ALD samples did, providing reason that TiO₂ is a physiological impetus for DPSCs for this favorable behavior. Thus, it is posited that an ALD coating of titanium nanoparticles on any polymeric substrate will allow for templated biomineralization.

Further research in this project will include extended data analysis and testing. Day 28 and 35 cells will be examined with RAMAN to determine mineral composition. Hydroxyapatite and collagen peak integral ratios will be calculated to have a preliminary sense of differentiation path (i.e. dentin, bone, etc.). This result will be bolstered by RT-PCR of all samples for aforementioned markers.

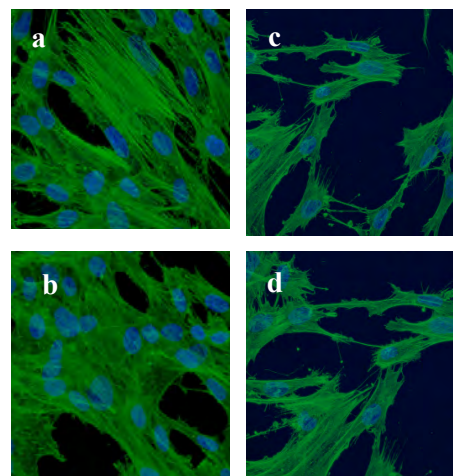


Figure 1 Day 4 Confocal Images of (a) ALD PBTN, (b) PBTN, (c) ALD PBTK, (d) PBTK

Brookhaven National Laboratories. Afterwards, all wafers were cultured with AV3 line human DPSC, held in a medium of 2% DPBS by mass. Culture medium was changed every 2 days through aspiration and pipetting procedures. Data samples were taken 2, 4, 7, 14, 28, and 35 days after culturing.

Confocal microscopy was used with an AF 488 dye for actin and DAPI stain for the nucleus for Day 2, 4, and 7 cells. PCR was used to find general differentiation markers (ALP, RUNX) in day 7 and 14 cells and more specialized markers (DSPP, OCN) in day 28 and 35 cells. Day 28 and 35 cells were also analyzed under Scanning Electron Microscopy (SEM) and RAMAN for biomineralization and collagen formation.

First, cell count and doubling time was analyzed. As per the interval between days 2 and 4 of cell growth, cell doubling time was

[1] Lai, Min, et al. Surface Functionalization of TiO₂ Nanotubes with Bone Morphogenetic Protein 2 and Its Synergistic Effect on the Differentiation of Mesenchymal Stem Cells, vol. 12, no. 4, 11 Mar. 2011, pp. 1097–1105.

[2] Titushkin, Igor, and Michael Cho. “Modulation of Cellular Mechanics during Osteogenic Differentiation of Human Mesenchymal Stem Cells.” *Biophysical Journal*, vol. 93, Nov. 2007, pp. 3693–3702.

Investigating the Mechanics and Differentiation of Dental Pulp Stem Cells on Polybutadiene-Polystyrene Substrate Nanopatterns

Meirav Grajower¹, Ilana Sacolick², Ya-Chen Chuang³, Jessica Hofflich³, Miriam Rafailovich³, Marcia Simon⁴
Yeshiva University High School for Girls, Queens, NY 11423¹; Hebrew Academy of the Five Towns and Rockaway, Cedarhurst, NY 11516²; Department of Material Science and Chemical Engineering, Stony Brook University, NY 11794³; Department of Oral Biology and Pathology, Stony Brook University, NY 11794⁴

Understanding the causes of cell differentiation furthers the field of tissue engineering and contributes to the goal of creating tissue for implantation and bioprinting. This study involves understanding and analyzing how dental pulp stem cells respond to different moduli. In the past, researchers have etched silicon wafers using SIMS in order to achieve a substrate to create differing moduli. In this study, a mixed solution of Polybutadiene(PB) and Polystyrene(PS) was created because there is a repulsion between them which causes them to form protruding structures with a variety of moduli.

The first step of the study was to create solutions of PS and PB with varying ratios and concentrations, spincast the solutions onto silicon wafers, and analyze the height to determine which solution is optimal. Previous researchers measured the height using a concentration of 11 mg/ml of PS with 8 mg/ml of PB in the ratio of 1:3. They found that there was not enough contrast in moduli, so we used a higher concentration of PS in different ratios, using concentrations of 15 mg/ml of PS and 8 mg/ml of PB with concentrations of 3:1, 1:1, and 1:3. The three solutions were spuncast onto silicon wafers and analyzed by atomic force microscopy (AFM), which displayed that the solution with the greatest height and contrast in moduli was the 1:3 ratio at 182.6 nm, as referenced in Figure 1. The cells were cultured onto the 1:3 solution of PS and PB.

Multiple analyses included cell counts, confocal microscopy, and atomic force microscopy. Using ImageJ, cells were counted on days 2, 4, and 7 and it was found that they were growing slower than the control. It was hypothesized that this was because of the uneven topography, which most likely made it more difficult for cell growth. From the confocal images, it was observed that on days 2, 4 and 7 many of the cells were stretched out, indicating that the substrate was compatible, as referenced in figure 2. A small portion of the cells were constricted, suggesting that those cells either found the position or the substrate unsatisfactory.

The moduli of the cells were then tested with AFM. The relative moduli were calculated based on past research¹. It was hypothesized that because PB is soft and PS is hard (PS moduli are 2.28 times greater than the PB moduli), the cells would react similarly, but the results did not follow this pattern. There were three different moduli: soft, medium and hard, as referenced in Figure 3. AFM analysis determined that the average width of the spikes was 0.595 μm . This was compared to the average length of the cell found from the confocal which was 61.43 μm . Because the cell is large enough to cover multiple parts of the substrate, both soft and hard, this may be the reason the cell exhibits a medium modulus. Another possible explanation is that the interaction between the PS and PB produced a medium modulus, to which the cells are responding. On day 28, RT-PCR will be conducted on the mRNA to determine if differentiation occurred, using markers such as ALD, Runx, DSPP, and OCN. Scanning electron microscopy will also be done to visualize each individual cell in its specific place on the substrate.

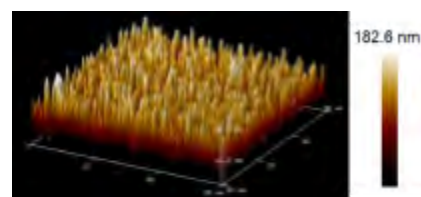


Figure 1. AFM image of 1PS:3PB

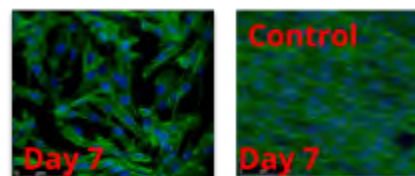


Figure 2. Confocal Microscopy of cells on PS-PB Substrate vs. Cells on Pure PB Substrate



Figure 3. Relative Moduli from AFM. Left Day 4. Right Day 6

¹ "Structure and Nanomechanical Characterization of Electrospun PS/Clay Nanocomposite Fibers." Langmuir. 06 Aug. 2019 <<https://pubs.acs.org/doi/abs/10.1021/la0525022>>.

The Effect of Fibrin on the Differentiation of Human Dental Pulp Stem Cells

Victoria Levy^{1*}, Vimala Alagappan^{2*}, Kao Li³, Miriam Rafailovich³, Rachel Meacham⁴, Atif Akhter⁵

¹Saint Anthony's High School, South Huntington, NY 11747; ²Friends Academy, Locust Valley, NY 11560; ³Department Materials Science and Chemical Engineering, Stony Brook University, NY 11794; ⁴Stony Brook University, NY 11794; ⁵Cornell University, Ithaca, NY 14850;

*primary authors – contributed equally to this work

Due to their accessibility and multipotency, dental pulp stem cells (DPSCs) are of particular interest to researchers, having shown potential for use in regenerative medicine and treatment of various human diseases. A less invasive option compared to bone marrow stromal mesenchymal stem cells, following interaction with growth factors, extracellular matrix proteins, and transcriptional factors, DPSCs are capable of differentiating into various cell types, including odontoblasts, osteoblasts, chondrocytes, cardiomyocytes, and neuron cells. As the regenerative properties of the pulp-dentin complex are dependent on the formation of dentin, a proposed approach for the regeneration of the tissue includes the placement of a scaffold and odontoblast-like cells on open pulp, with the scaffold maintaining cell mobility and promoting differentiation while adhering the cells to its surface^[1]. In addition to having non-toxic degradation products, being cytocompatible, and causing the formation of an extracellular matrix, fibrin, the result of the fibrinogen polymerization under thrombin, has been found to be highly suitable in supporting dental tissue formation and improving cell-dentin interactions^[2]. As a result, this study sought to determine the effects of fibrin on the proliferation and differentiation of dental pulp stem cells, an investigation with, as indicated above, potential applications in odontogenic and osteogenic regenerative medicine.

Prior to the collection of data indicating these effects of fibrin on human DPSCs, gelatin-fibrinogen hydrogels were created using 15% gelatin and 12 mg/mL bovine fibrinogen cross-linked by 10% mTG (microbial transglutaminase) and thrombin, respectively. Gelatin hydrogels were created as a control, fibrinogen being replaced by PBS (phosphate-buffered saline) and thrombin not being used. Those samples which did not undergo rheology were plated at 4×10^3 cells/cm³ with cultured 13 y.o. DPSCs (Figure 1). The stem cells, plated on the hydrogels, were then provided with α -MEM (containing 10% FBS, Pen Strep, L-ascorbic acid, and β -glycerol phosphate) and were incubated at 37°C and 5% CO₂ until observation on Days 11 and 28.

In the meantime, rheology has been performed on the gelatin and gelatin-fibrinogen gels, to see if there is any significant difference between the elastic and viscous moduli of the two gels. An amplitude sweep test of three samples of each of the two gels was carried out, and the viscous and elastic moduli measured by taking the average of these values before the breaking point at which the gel deteriorated. The recorded modulus for gelatin and gelatin-fibrinogen gels was the average modulus of the three gels of the respective composition. The viscous moduli of the gelatin and gelatin-fibrinogen gels were 176.95 Pa and 92.70 Pa respectively, and the elastic moduli 6301.44 Pa and 6857.27 Pa. A t-test showed that there was no significant difference between the two gels for each modulus at an alpha level of 0.05. Due to the high price of collagen, gelatin was used in its place because the fibrinogen would have unfolded the collagen in the gels anyway. In future studies, collagen will be used, so to see the effect of switching gelatin for collagen, rheology will also be carried out on collagen gels and the values compared.

On Days 11 and 28, the methods of observation will be SEM, confocal microscopy, and RT-PCR. The proliferation of the cells will be measured by the microscopy, and the extent of differentiation will be determined by the presence of certain genetic markers of differentiated cells found with the RT-PCR. Further research will include the preparation of gelatin and gelatin-fibrinogen gels containing dexamethasone, a glucocorticoid known to promote osteogenic stem cell differentiation^[3]. The effect of fibrinogen on already prompted cell differentiation will thus be analyzed.

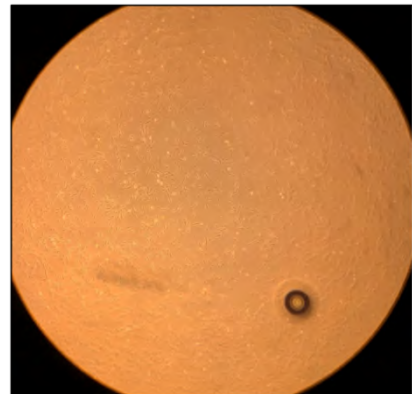


Figure 1. 4x optical microscopy image of 13 y.o. h-DPSCs on gelatin-fibrinogen hydrogel – Day 3 after plating of cells.

[1] Potdar, P. D. (2015). Human dental pulp stem cells: Applications in future regenerative medicine. *World Journal of Stem Cells*, 7(5), 839. doi:10.4252/wjsc.v7.i5.839

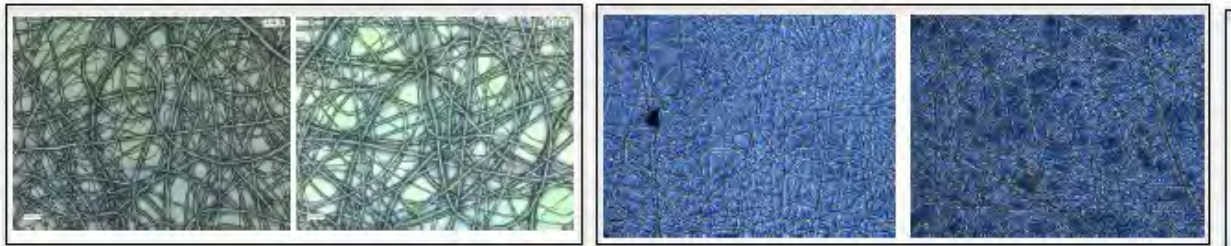
[2] Ducret, M., Montembault, A., Josse, J., Padeloup, M., Celle, A., Benchrih, R., . . . Farges, J. (2019). Design and characterization of a chitosan-enriched fibrin hydrogel for human dental pulp regeneration. *Dental Materials*, 35(4), 523-533. doi:10.1016/j.dental.2019.01.018

[3] Alliot-Licht, B., Bluteau, G., Magne, D., Lopez-Cazaux, S., Lieubeau, B., Daculsi, G., & Guicheux, J. (2005). Dexamethasone stimulates differentiation of odontoblast-like cells in human dental pulp cultures [Abstract]. *Cell and Tissue Research*, 321(3), 391-400. doi:10.1007/s00441-005-1115-7

Session 8:

Differentiating Dental Pulp Stem Cells on Scaffolds

**Chair: Kuan-Che Feng
Kao Li**



Optimization of 3D-Printed Scaffolds for Dental Pulp Stem Cell Differentiation via Surface Coating of Proteins and Titanium Dioxide

Esther Chai¹, Richard Cheng², Rhea Cong³, Kuan-Che Feng⁴, and Miriam Rafailovich⁴

¹Townsend Harris High School, Flushing, NY 11367, ²Clayton High School, St. Louis, MO 63105, ³Huron High School, Ann Arbor, MI 48105, ⁴Department of Materials Science, SUNY Stony Brook, Stony Brook, NY 11790

Tissue engineering, despite substantial advancements in recent years¹, requires significant improvements in order to become a more pervasive methodology in regenerative medicine. One of the most important components that still requires further research is the artificial scaffolds that facilitate cell attachment and growth. In order to better guide and predict the differentiation of human dental pulp stem cells (hDPSCs), this study aimed to parse the relationship between coats of titanium dioxide and various proteins on the surface of these scaffolds and the adhesion, proliferation, and differentiation of hDPSCs.

The structure of this research fell into a three-fold process: creating the scaffolds, plating the cells, and monitoring the growth of the cells over a 35-day duration. In order to construct the scaffolds, we used a Ultimaker 2 Extended+™ 3D FDM Printer to produce standardized, biodegradable polylactic acid (PLA) discs², half of which were then coated with a thin (~5 nm) layer of titanium dioxide by way of Atomic Layer Deposition (ALD). After sterilization, three different proteins were added to the surface of the scaffolds: gelatin (G), collagen gel (CG), or fibronectin (FN). hDPSCs in passage 5 were cultured for four days in cell medium and then transferred to the scaffolds (Day 0).

Scanning Electron Microscopy (SEM) of Day 5 scaffolds allowed the surfaces of the substrates to be visualized, revealing the deposition of titanium dioxide and morphology of the attached cells (Figure 1). In addition, EVOS fluorescence microscopy of DAPI and AF488-stained scaffolds displayed cell nuclei and actin filaments, respectively. From these images, it was determined that hDPSCs typically orient along the 3D-printed filament.

On Days 1, 3, and 5, cells were counted using alamarBlue Cell Viability Reagent in order to calculate plating efficiency and doubling time. This data revealed that the scaffolds coated with fibronectin and ALD supported increased plating efficiency, similar to scaffolds with only ALD (Figure 2). Doubling time was not significantly different for any of the conditions, suggesting that neither the protein coats nor ALD greatly enhanced or reduced the proliferation capacity of the hDPSCs.

The differentiation of the hDPSCs will be closely monitored from Day 10 to 35. Reverse Transcriptase PCR (RT-PCR), the process of reverse transcribing RNA into complementary DNA and the use of DNA polymerase and primers to amplify a DNA sequence³, will divulge any gene expression of osteogenic or odontogenic differentiation markers. The Day 10 early differentiation biomarkers ALP and RUNX2 will be quantified using RT-PCR, and presence of later stage markers osteocalcin and DSPP on Day 28 and Day 35 will clarify osteogenic and odontogenic differentiation on each substrate. Postliminary examination of the scaffolds under the SEM will reveal possible biomineralization, confirming cell viability. Finally, Raman spectroscopy will be performed on the fixed Day 35 hDPSCs to detect the presence of hydroxyapatite and its crystallinity. Osteogenic and odontogenic fates of the cells will manifest as different ratios of enamel to dentin and varying morphologies.

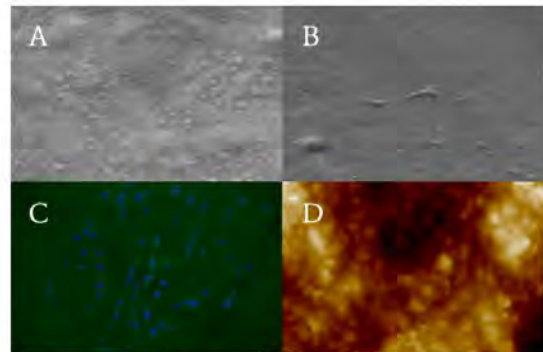


Figure 1. SEM images show (A) deposition of titanium dioxide on a non-coated scaffold and (B) cell adhesion to a FN coated scaffold with ALD. EVOS microscopy visualized cell nuclei and actin filaments on (C) a G coated scaffold with ALD. AFM provided a scan of the surface topography on (D) a non-coated scaffold with ALD.

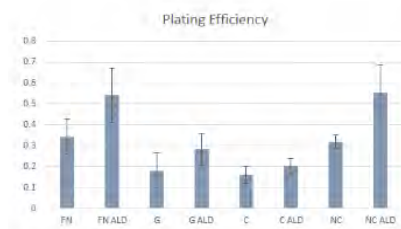


Figure 2. DPSCs plated on FN coated scaffolds with ALD showed a marked increase in plating efficiency in comparison to not coated (control) scaffolds.

[1] Dzobo, Thomford et al. "Advances in Regenerative Medicine and Tissue Engineering: Innovation and Transformation of Medicine." *Stem Cells International*, vol. 2018. doi:10.1155/2018/2495848.3]

[2] Galler, K.m., et al. "Scaffolds for Dental Pulp Tissue Engineering." *Advances in Dental Research*, vol. 23, no. 3, 2011, pp. 333–339., doi:10.1177/0022034511405326.

[3] Ohan, Heikkila. "Reverse transcription-polymerase chain reaction: An overview of the technique and its applications." *Biotechnology Advances*, vol. 11, Issue 1, 1993. doi:10.1016/0734-9750(93)90408-F.

Effect of PLA Scaffold Roughness on Dental Pulp Stem Cell (DPSC) Differentiation and Growth in an In Vitro Setting

Roberto Milan¹, Todor Bliznakov², Johnathan Marcelin³, Kuan-Che Feng³, Miriam Rafailovich³

¹South Side High School, Rockville Centre, NY 11570, ²Ward Melville High School, East Setauket, NY

11733 ³Department of Materials Science and Chemical Engineering, Stony Brook University, Stony Brook, New York 11790

The field of regenerative sciences has been focusing on the use of mesenchymal stem cells due to their ability to differentiate into various cell types. DPSC are the most promising source of stem cells for reasons including their accessibility within the central pulp cavity, the noninvasive surgical process that is utilized to retrieve them, and their multilineage differentiation¹. Our research has to do with the physical mimicking of the extracellular matrix (ECM) by creating scaffolds with varying roughness to create a situation that maximizes cell attachment and promotes the biomineralization of developing cells.

The procedure began with the 3D-Printing polylactic acid (PLA) well plates of varying distances between each line filament in order to create scaffolds with distinct anisotropic surface roughness². We used distances of 0.7 mm, 0.3 mm, and a scaffold created using 150 flow rate making it extremely rough. We used atomic layer deposition, at the parameters of 80°C for 50 cycles, to coat TiO₂ onto a second batch of each roughness. Previous research has hinted that TiO₂ has a positive effect on the adhesion of stem cells and their in vitro differentiation³. In order to view the topography of two of our sample scaffolds, we used Atomic Force Microscopy (AFM) as shown in figure one. AFM also allowed us to calculate each samples RMS value. Both samples had the same distance between filaments but one was coated with ALD of TiO₂ while the other wasn't. In Image A, the scaffold was coated with TiO₂ and had an average RMS of 45.01 nm while in image B the scaffold, which was not coated with TiO₂ had an average RMS of 60.92 nm. This difference in RMS confirmed that ALD of TiO₂ was successful and that ALD of TiO₂ has minimal effect on surface roughness. For cell plating, we created a growth medium comprised of 10% Fetal Bovine Serum, 1% Penicillin-Streptomycin, and 89% alpha Minimum Essential Medium. We then added 500,000 DPSC into 4 flasks containing 25 ml of the growth medium each. After 4 days, we removed the media and added 3.5 mL of trypsin to each flask which dissolved the protein connecting the cells to the flask. We then created a stock solution containing 5x10⁵ cells/mL and poured 1mL into each well that contained our scaffolds.

Plating efficiency and doubling times of the cells on each scaffold were measured with Alomar blue during the first 5-days post-plating; this was quantified using a microplate reader. For day 10 and 28 we will be isolating mRNA and using RT-PCR to quantify the expression of early and late-stage gene markers in osteogenic and odontogenic differentiation. On day 35 we will be using SEM imaging and Raman spectroscopy in order to confirm biomineralization and view the crystalline structure of the differentiated stem cells.

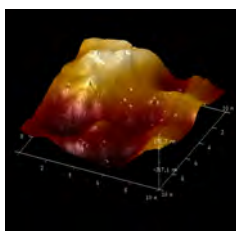


Image A(.3 ALD)

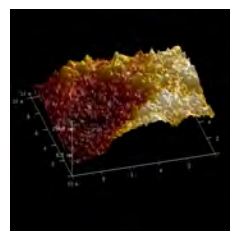


Image B(.3 no ALD)

Figure 1:

[1]Anitua, E., Troya, M., & Zaldueño, M. (2018). *Progress in the use of dental pulp stem cells in regenerative medicine*. *Cytotherapy*, 20(4), 479-498. <https://doi.org/10.1016/j.jcyt.2017.12.011>

[2] Metavarayuth, K., Sitasuwan, P., Lin, Y., Zhao, X., & Wang, Q. (2016). Influence of Surface Topographical Cues on the Differentiation of Mesenchymal Stem Cells in Vitro. *ACS Biomaterials Science & Engineering*, 2(2), 142-151. <https://doi.org/10.1021/acsbiomaterials.5b00377>

[3]Hou, Yanhua et al., "Effects of titanium nanoparticles on adhesion, migration, proliferation, and differentiation of mesenchymal stem cells." *International journal of nanomedicine* vol. 8 (2013): 3619-30. doi:10.2147/IJN.S38992

Determining Discrepancies in the Migrational Behavior of Osteosarcoma and Dental Pulp Stem Cells by Comparing Their Movement

Hannah Hamerman¹, Sahana Ramrakhiani², Emily Silverstein³, Jessica Semel⁴, Kao Li⁴

¹Yeshiva University High School for Girls, Holliswood, NY 11423, ²Sachem North High School, Lake Ronkonkoma, NY 11779, ³Hebrew Academy of the Five Towns and Rockaway, Cedarhurst, NY 11516,

⁴Stony Brook University, Stony Brook, New York 11790

Cell migration is primarily driven by the protein actin, which propels the cell membrane forward from inside of the cell. Healthy cells migrate along the fiber they are resting on, but cancerous cells tend to migrate from the fiber to other areas of the body. Metastasizing cancers are difficult to treat; pathogenic cells deviate from their primary site, blurring the target for traditional cancer treatments such as chemotherapy. Mapping cancer cell migration will aid in the determination of the cells' intended path, which can have applications in cancer research and treatment.

Our interest was to observe and analyze cancer cell migration by comparing the movement of osteosarcoma cells (cell line SAOS-2) to that of healthy dental pulp stem cells (DPSC, strains 13 and AV3). While doing so we were additionally interested in comparing the makeup of different types of cells to understand their patterns of migration; when comparing them we considered actin, the protein specific to cell movement in the two cells.

We grew three cell lines: osteosarcoma SAOS-2, 13- DPSC, and AV3- DPSC, in DMEM and alphaMEM, to evaluate which medium was most favorable for the cell growth of all three lines. Based on the rates of proliferation obtained by counting cells using a hemocytometer, we concluded that DMEM was ideal. In no case were cells overcrowded so that cell movement was not impeded.

After determining conditions for optimal cell growth, we spin casted solutions of chloroform and PMMA onto glass coverslips to plate the cells on [1]. Tissues in the human body are comprised of uneven planes, so we electrospun PMMA fibers onto the glass films to mimic bodily tissues. Half of our samples were plated on films with fibers, while half were left on flat surfaces to compare the possible differences. Using an Evos FL microscope, we composed time lapse videos of each cell line using sets of seven images per hour. Four cell lines were examined: DPSC on fiber, DPSC on thin film, SAOS-2 on fiber and SAOS-2 on thin film. The Evos microscope took clear images, enabling the viewing of the microscopic movement of cells (figures 1 + 2.)

In the future, we plan to quantify the cells migration using a MetaMorph operated CoolSNAP HQ camera attached to a Nikon Diaphot-TMD inverted microscope fitted with a 37 °C stage incubator and a 10 x objective lens. This program will assess the movement of individual cells over one hour periods to further analyze their migration patterns.

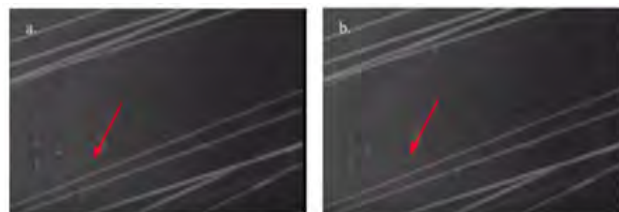


Figure 1: Evos image of Osteosarcoma cells. Image (a) was taken ten minutes prior to image (b) showing the movement of cancerous cells off their fibers.

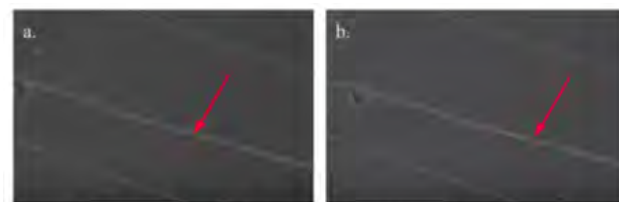


Figure 2: Evos image of dental pulp stem cells. Image (a) was taken ten minutes prior to image (b) showing the movement of healthy cells along their fibers.

[1] Qin, Sisi & Clark, Richard & Rafailovich, Miriam. (2012). Role of fiber functionality and angle on cell migration

Investigating Neurogenic Differentiation of Dental Pulp Stem Cells using Novel PLA and Graphene Thin-Film and Electrospun Fiber Scaffolds *in Vitro*

Nicholas Stabile¹, Michael Stabile¹, Dipen Mehta², Daniel Luo³,
Kuan-Che Feng⁴, Marcia Simon⁵, Miriam Rafailovich⁴

¹Plainedge High School, N. Massapequa, NY 11758; ²George Walton Comprehensive High School, Marietta, GA 30062; ³Monroe-Woodbury High School, Central Valley, NY 10917; ⁴Department of Material Science and Chemical Engineering, Stony Brook University, Stony Brook, NY 11794; ⁵Department of Oral Biology and Pathology, School of Dental Medicine, Stony Brook University, Stony Brook, NY 11794

The nervous system is vital to the survival of humans and animals. Any disturbance or damage done to this system can dramatically disturb essential functions of the body and can have severe and far-reaching consequences.¹ Dental pulp stem cells (DPSCs) are pluripotent cells derived from the cranial neural crest, giving them the ability to differentiate into functional neurons and making them a promising candidate for neuroregenerative therapies because of their ease of availability.² Polylactic acid (PLA) is known to be a biocompatible polymer, especially in relation to stem cells,³ and graphene has been shown to enhance neurogenic differentiation,⁴ most likely through facilitating cellular electrical impulses and synaptic communication through its excellent conductive properties. Previously, morphology⁵, as well as electrical conductivity, have been shown to affect cell differentiation. This experiment investigates the efficacy and mechanisms of PLA and graphene thin-film and fibrous scaffolds in the differentiation of DPSCs into neurons.

To create a proper substrate for the cells, a solution of 15 mg/mL PLA and chloroform was spun-cast onto glass slides using a spin-caster at 2000 rpm for 30 seconds. This was done both with and without graphene at a concentration of 1.5 mg/mL. The glass slides are used for their convenient transparency during analysis. For electrospinning, a 12.5% PLA (by mass) solution in a ratio of 1:2 acetone-chloroform was used, with 3% graphene being used for the PLA with graphene samples. After spinning, approximately 4-5 layers of fiber were produced for each glass slide. In Figure 1, the success of the electrospinning of fibers is seen with and without graphene. The fiber diameters will be analyzed with SEM imaging and the DiameterJ plugin. Following the protocol described in Arthur et al., wells were coated with poly-L-ornithine (10 µg/mL), incubated overnight at room temperature, washed twice with water and then coated with laminin (5 µg/mL) and incubated overnight at 37 °C. Following this, the wells were washed with phosphate-buffered saline (PBS) and growth media before cells were plated. The glass coverslips were placed in 24 well plates and plated with 3×10^4 cells in 1 mL growth media. The DPSCs were cultured in growth medium for 1 week, after which the media was replaced with neurobasal media (Thermo-Fisher Scientific), replacing every 2-3 days for 21 days. They were plated in 4 groups, spuncast PLA and PLA+G film, and electrospun PLA and PLA+G fibers, as well as additional control groups of Tissue Cultured Plastic and No Coating. Neurobasal A media, consisting of 100 U/mL penicillin, 1 x B27 supplement, 100 µg/mL streptomycin, 20 ng/mL epidermal growth factor and 40 ng/mL basic fibroblast growth factor (FGF).⁶

To observe differentiation, the cells will be imaged using optical microscopy during each replacement of the media. After 21 days, cells will be harvested and counted using a hemocytometer. Then, most cells will be lysed. 600 µL of Qiazol will be used to lyse cells and inhibit RNA degradation. RNA will be collected for centrifugation at 1000 rpm for 5 minutes and then used for RT-PCR. Gene expression will be monitored at day 21 and compared to day 0 using primers against the neurogenic markers TBP, Nestin, neurofilament-medium chain, neurofilament-heavy chain, and PSA. This experiment investigates the impact on neurogenesis of growth on PLA with and without graphene. To date, it as indicated by figure 2, it appears that the cells are adherent to the spun-cast samples, but not to the fibers. This will be examined, and its significance will be validated in further research.

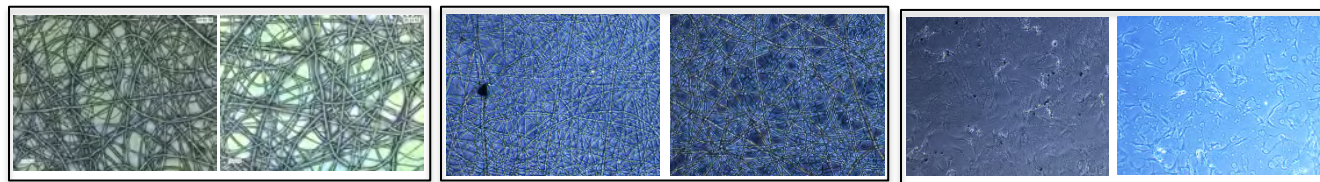


Figure 1 (Left): Fibers with (left) and without (right) graphene

Figure 2 (Middle): Cell growth on electrospun fibers with (left) and without (right) graphene

Figure 3 (Right): Cell growth on thin-film with (left) and without (right) graphene

1. Qin, Weiping, et al. "Bone and Muscle Loss after Spinal Cord Injury: Organ Interactions Bone and Muscle after SCI Qin et Al." *Annals of the New York Academy of Sciences*, vol. 1211, no. 1, Nov. 2010, pp. 66–84. EBSCOhost, doi:10.1111/j.1749-6632.2010.05806.x.
2. Potdar, Pravin D., and Yogita D. Jethmalani. *Human Dental Pulp Stem Cells: Applications in Future Regenerative Medicine*. 2015. EBSCOhost, search.ebscohost.com/login.aspx?direct=true&db=edsbas&AN=edsbas.50E553F9&site=eds-live&scope=site.
3. Wang, Xi et al. "Biocompatibility of biological material polylactic acid with stem cells from human exfoliated deciduous teeth." *Biomedical reports* vol. 6,5 (2017): 519-524. doi:10.3892/br.2017.881
4. Park, S. Y., et al. "Enhanced Differentiation of Human Neural Stem Cells into Neurons on Graphene." *ADVANCED MATERIALS -DEERFIELD BEACH THEN WEINHEIM-*, no. 36, 2011, p. H263. EBSCOhost, search.ebscohost.com/login.aspx?direct=true&db=edsbl&AN=RN298813166&site=eds-live&scope=site.
5. Zhang, Linxi, et al. "Templated Dentin Formation by Dental Pulp Stem Cells on Banded Collagen Bundles Nucleated on Electrospun Poly (4-Vinyl Pyridine) Fibers *in Vitro*." *Acta Biomaterialia*, 2018. EBSCOhost, doi:10.1016/j.actbio.2018.06.028.
6. Arthur, Agnes, et al. "Adult Human Dental Pulp Stem Cells Differentiate Toward Functionally Active Neurons Under Appropriate Environmental Cues." *Stem Cells*, vol. 26, no. 7, 2008, pp. 1787–1795., doi:10.1634/stemcells.2007-0979.

Utilization of Patch Clamping to Investigate the Influence of Graphene on Transmembrane Ion Current in HeLa Cells and the Efficacy of Novel Fluorescent Dye

Daniel Luo¹, Dipen Mehta², Nicholas Stabile³, Michael Stabile³, Hong Zhan Wang⁴,
Kuan-Che Feng⁵, Marcia Simon⁶, Miriam Rafailovich⁵

¹Monroe-Woodbury High School, Central Valley, NY 10917; ²George Walton Comprehensive High School, Marietta, GA 30062; ³Plainedge High School, N. Massapequa, NY 11758; ⁴Department of Physiology and Biophysics, Stony Brook University, Stony Brook, NY 11794; ⁵Department of Material Science and Chemical Engineering, Stony Brook University, Stony Brook, NY 11794; ⁶Department of Oral Biology and Pathology, School of Dental Medicine, Stony Brook University, Stony Brook, NY 11794

Electrophysiology is a vital field of study in relation to cell growth and intracellular interaction, particularly in relation to body systems such as the nervous and cardiovascular systems. The study of ion channel currents and action potentials within stem cells is especially important because of the presence of special electrophysiological properties and markers on differentiated cells.¹ Differentiation of stem cells into tissues such as cardiac and neural tissue is also particularly sensitive to the conductive and electrical properties of the substrates on which they are grown (such as graphene, which is shown to enhance neural differentiation),² making the study of transmembrane currents and electrical activity within cells paramount. Patch clamping is one of the most commonly used techniques to study electrophysiology in a cellular level.³ However, conventional electrophysiology methods such as patch clamping are tedious and difficult procedures to apply to cells such as neurons or dental pulp stem cells, among other limitations.³ This experiment attempts to study the effects of graphene on cell membrane ion currents using patch clamping and test a novel fluorescent dye that fluoresces in response to high ion channel activity and current by comparing its activity with the patch clamping results.

The ion current activity of the cells was measured through patch clamping, which uses current and voltage to measure membrane potential. This was done with HeLa cells (parental and CX43) cultured in standard growth media (10% FBS, 1% Pen Strep). After the HeLa cells were grown in standard growth media, solutions of 7 mg/ml P4VP and 7/mg/ml P4VP + 3% graphene were spuncast on glass wafers. After plating those cells, we analyzed their concentrations. Our preliminary results of patch clamping HeLa cells (each group having sample size ranging from n=1 to n=3), as shown in **Figure 1**, may indicate that graphene is in fact successful in promoting growth via increased conductivity and cellular communication. **Figure 2** shows that cells grown on P4VP+graphene have a significantly more positive current density when compared to cells grown on just P4VP. These results will be further investigated with more patch clamping in the near future. These cells will then be tested with a fluorescent dye which can then be used comparatively to patch clamping on neural cells to demonstrate the ion current activity of the neural cells. Previous research done with the dye has indicated that it would fluorescently label any areas that had high concentrations of ion channels and current, meaning that dye fluorescence should correlate to patch clamping. Patch clamping utilizes electrodes to measure the amount of current passed through cells, so if the dye works, it would achieve similar results to the data that patch-clamping yields.

If the dye successfully functions on the HeLa cells when utilized under the same conditions that the patch-clamping was done at, then it is safe to assume that the dye would also be applicable to a broad range of other cells, such as dental pulp stem cells and neurons, breaking the limitations posed by conventional electrophysiological methods.

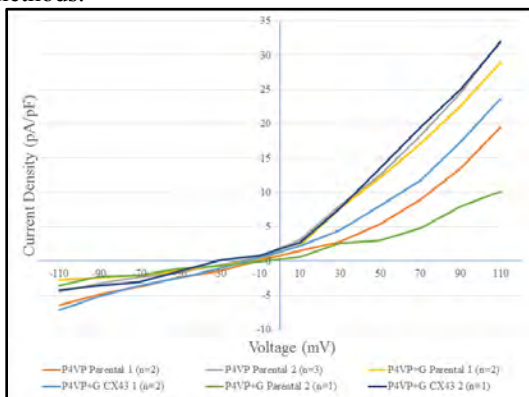


Figure 1: The following graph shows the preliminary results of patch clamping a few cells from each experimental group. The slope of the lines, plotted with current density against voltage, indicate the transmembrane capacitor leakage current rate.

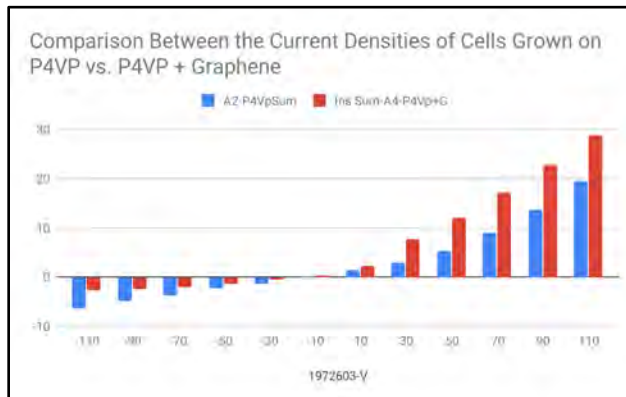


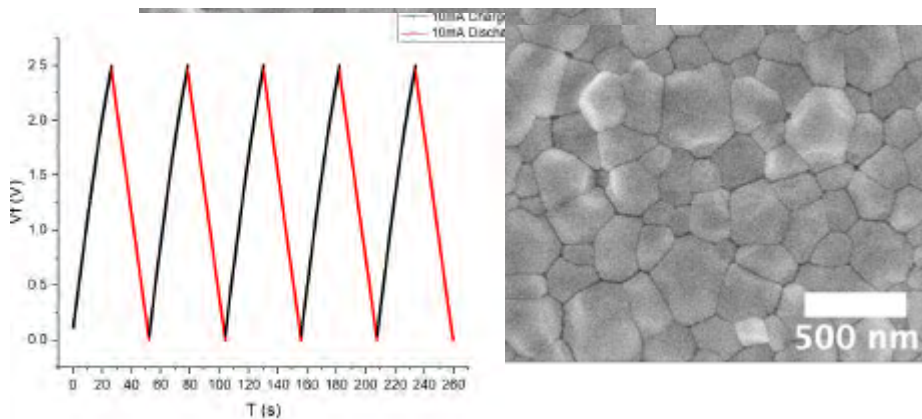
Figure 2: The following graph is the comparison of the current densities of parental HeLa cells grown on P4VP with and without graphene. The cells grown on P4VP with graphene have a more positive current density, which possibly indicates that graphene greatly increases the amount of transmembrane ion activity in cell membranes.

1. Ma, Junyi, et al. "High Purity Human-Induced Pluripotent Stem Cell-Derived Cardiomyocytes: Electrophysiological Properties of Action Potentials and Ionic Currents." *American Journal of Physiology-Heart and Circulatory Physiology*, vol. 301, no. 5, 2011, doi:10.1152/ajpheart.00694.2011.
2. Zhang, Linxi, et al. "Effect of Graphene on Differentiation and Mineralization of Dental Pulp Stem Cells in Poly(4-Vinylpyridine) Matrix in Vitro." *ACS Applied Bio Materials*, vol. 2, no. 6, 2019, pp. 2435-2443., doi:10.1021/acsabm.9b00127.
3. Anson, Blake D., and William M. Roberts. "A Novel Voltage Clamp Technique for Mapping Ionic Currents from Cultured Skeletal Myotubes." *Biophysical Journal*, vol. 74, no. 6, 1998, pp. 2963-2972., doi:10.1016/s0006-3495(98)78003-8.

Session 9:

Perovskites & Graphene: Photovoltaics & Energy Storage

Chairs: Yuchen Zhou
Yifan Yin



Optimization of EDLC Supercapacitors via a Comparison of Acetonitrile and Diethyl Carbonate - Ethyl Carbonate - Tetraethylammonium Tetrafluoroborate Electrolytes with the effects of Graphite-AC, CNT-AC, and CNT-GNP in Supermaterial Electrodes

Samuel Padwa¹, Rishabh Raniwala², Nyle Garg³, Shi Fu⁴, Vladimir Samuilov⁴, Miriam Rafailovich⁴

¹Bronx High School of Science, Bronx, NY 10471, ²Wilton High School, Wilton, CT 06897, ³Greenwich High School, Greenwich, CT 06830, ⁴Department of Materials Science and Chemical Engineering, Stony Brook University, Stony Brook, NY 11790

In the following work, various combinations of electrolytes and carbon-based electrodes were tested to find optimal performance for a supercapacitor. Three different electrodes were tested: a mixed adhesive and active layer consisting of Carbon Nanotubes (CNT) and Graphene Nanoplatlets (GNP), a adhesive layer of CNT and an active layer of Active Carbon (AC), and an adhesive layer of Graphite and an active layer of AC¹. All three of these electrodes were tested with two different electrolytes, one consisting of Diethyl Carbonate, Ethyl Carbonate, and Tetraethylammonium Tetrafluoroborate (DECEC), and the other consisting of Acetonitrile (AN)². The structure of each electrode was characterized via a scanning electron microscope (SEM) in order to predict the capacitance behavior of each type of electrode through observation of pore size and specific area.

Each supercapacitor cell underwent three electrochemical tests for characterization. The Electronic Impedance Spectroscopy (EIS) found both the parallel resistance and equivalent series resistance (ESR) of the supercapacitor, as well as the phase angle of the impedance at frequencies ranging from 100000 Hz to 0.01 Hz. The Cyclic Voltammetry (CV) found the supercapacitor's capacitance, the current flowing for five different voltage per second scan rates, and whether or not the cell remained stable up to 2.5 volts. The Cyclic Charge and Discharge (CCD) once again showed the capacitance, the time the supercapacitor took to charge and discharge, and the voltage dropped in each cycle. These measures allowed each variant supercapacitor to be compared to each other quantifiably in order to find the most optimal from the tested materials.

The most successful cell contained the AN electrolyte and the CNT-AC electrodes. It showed the highest specific capacitance of any cell at 3.32837 F/g as measured through CCD at a current of 10mA (Figure 2) and 3.47105 F/g as measured through CV at a scan rate of 50 mV/s (Figure 3). It also showed the lowest self-discharge at 0.047 V with a 10mA current (Figure 2), thus retaining more of its charge than any other cell tested. Moreover, this cell demonstrated a very low ESR of (Figure 1), which prevents a large voltage drop and allows the supercapacitor to have a higher power density and capacitance. Generally, the best electrodes for ensuring high capacitance, low self-discharge, and a low ESR were the CNT-AC electrodes, followed by the Graphite-AC, followed by the CNT-GNP. The highest measured specific capacitance from either CNT-GNP cell was 1.68724 F/g, far less than 3.47105 F/g from the AN CNT-AC cell or the 2.6338 F/g from the DECEC Graphite-AC cell. Other than the DECEC Graphite AC, cells with AN as the electrolyte consistently outperformed their DECEC counterparts, demonstrating an average specific capacitance 2.97% higher as measured by CCD, and 10.37% higher as measured by CV.

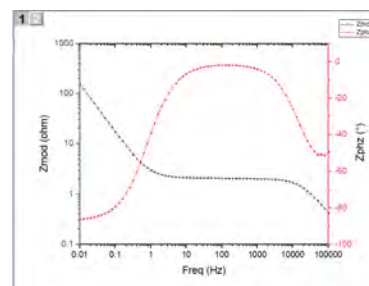


Figure 1 – EIS Graph for an AN CNT/AC cell from 10^5 Hz to 10^{-2} Hz

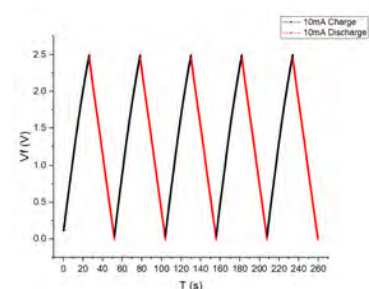


Figure 2 - CCD Chart for an AN CNT/AC cell at 10mA

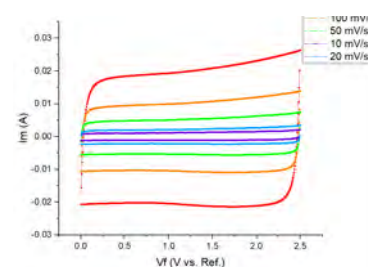


Figure 3 - CV Chart for an AN CNT/AC cell at 50mV/s

¹ Zhang, Li Li, and X. S. Zhao. "Carbon-Based Materials as Supercapacitor Electrodes." *Chemical Society Reviews*, vol. 38, no. 9, 12 June 2009, doi:10.1039/b813846j.

² Zhong, Cheng, et al. "A Review of Electrolyte Materials and Compositions for Electrochemical Supercapacitors." *Chemical Society Reviews*, vol. 44, no. 21, 8 June 2015, pp. 7484–7539., doi:10.1039/C5CS00303B.

Preparation of MAPbI₃ Perovskite via Hot-Casting Technique for Photovoltaic Application

Jasmine Li¹, Aidan York², Yifan Yin³, Yuchen Zhou³, Miriam Rafailovich³

¹ Fairview High School, Boulder, CO 80305

² Kellenberg Memorial High School, Uniondale, NY 11553

³ Department of Materials Science and Chemical Engineering, Stony Brook University, Stony Brook, NY 11794

Solar energy offers a solution to the growing problem of global warming and greenhouse gases. Conventional silicon solar cells display remarkable efficiencies; however, since silicon solar cells are too costly to be considered a legitimate alternative to fossil fuels in larger markets, there has been a demand for alternatives. Perovskite, a family of materials with crystal structure ABX₃, has shown great promise in maximizing efficiency and minimizing cost ever since its introduction in 2009.¹ Nonetheless, one of the greatest problems facing perovskite is the instability of the perovskite crystal quality during the fabrication process. To address this issue, previous research has shown that hot-casting the perovskite layer is a viable technique to promote larger crystal growth and thus decrease grain boundaries and defects.² Thus, the purpose of this study was to investigate the effect of the hot-casting technique as opposed to the conventional post-annealing process on the performance of planar, methylammonium lead iodide (MAPbI₃) perovskite solar cells (PSCs).

To maximize the size of perovskite grains, hot-casting of the photoconductive perovskite layer was utilized because spin-casting and annealing occur simultaneously. The perovskite precursor was prepared at three different concentrations, 0.24 M, 0.4 M, and 1.2 M. PSCs were later on built using FTO glass, TiO₂, MAPbI₃, and spiro-OMeTAD as the conductive substrate, electron transfer layer, photoactive layer and hole transfer layer, respectively. Au was coated via physical vapor deposition to act as an electrode at the end. The devices were prepared to test surface morphology, optical properties, grain size, substrate coverage, and power conversion efficiency (PCE).

Compared to conventionally prepared samples, hot-casted samples featured larger average grain sizes in scanning electron microscopy (SEM) images (Fig. 1). Atomic force microscopy (AFM) gave conclusive evidence that higher concentration solutions formed a more uniform surface morphology. SEM and AFM images show formation of edges because of collisions between large grains that form a compact, fully covered, and highly crystalline surface. Peaks & indices seen in the x-ray powder diffraction (XRD) analysis indicated that the crystal structure of perovskite contained no impurities and degradation (Fig. 3). A more uniform morphology of the photoconductive MAPbI₃ gives potential to achieve a greater PCE due to much fewer grain boundaries, defects, and traps. J-V curves display the greater efficiency of hot-casted samples compared to those of conventionally post-annealed perovskite, achieving a PCE approaching 14% (Fig. 4). In conclusion, hot-casting, particularly at higher concentrations, has proven to be an effective method to maximize grain size and increase efficiencies of PSCs.

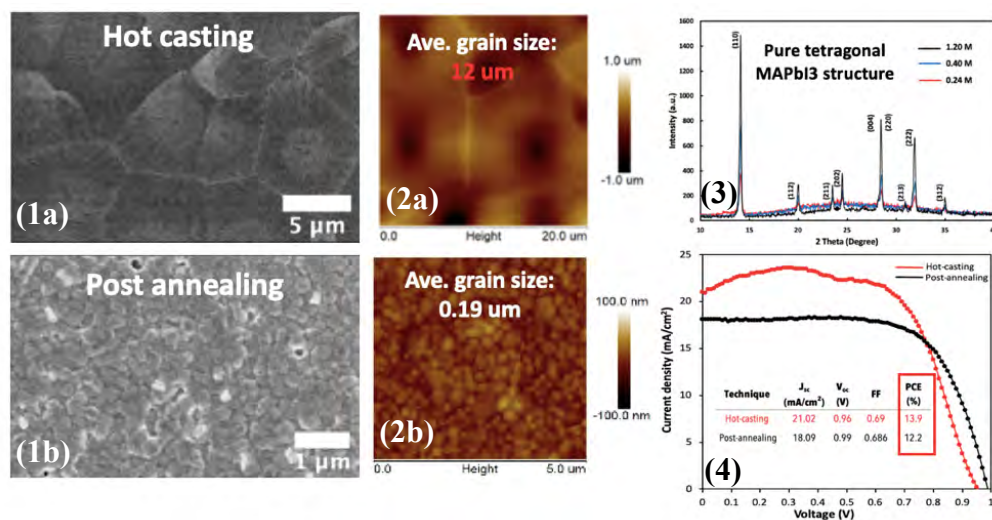


Fig. (1a) SEM of hot-casted MAPbI₃ (1b) SEM of conventionally prepared MAPbI₃ (2a) AFM of hot-casted 1.2 M MAPbI₃ (2b) AFM of MAPbI₃ prepared by post-annealing. (3) XRD analysis of pure MAPbI₃. (4) J-V curves of post-annealed & hot-casted 1.2 M MAPbI₃.

¹ Kojima, A., et al. (2009). Organometal halide perovskites as visible-light sensitizers for photovoltaic cells. *Journal of the American Chemical Society*, 131(17), 6050-6051.

² Nie, W. et al. (2015). Solar cells: High-efficiency solution-processed perovskite solar cells with millimeter-scale grains. *Science*. 347, 522-525.

Stability Enhancement of Perovskite Solar Cells Using Mixed Cation/Halide Perovskite

Ethan Eisenberg¹, Jack Cox², Yifan Yin³, Yuchen Zhou³, and Miriam Rafailovich³

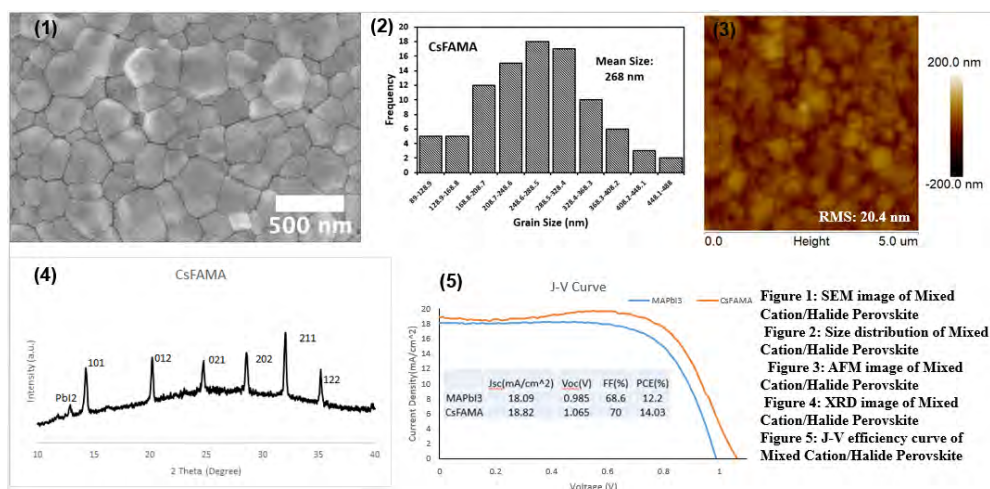
¹George W. Hewlett High School, Hewlett, NY USA ²South Side High School, Rockville Centre, NY USA

³Department of Materials Science and Chemical Engineering, Stony Brook University, Stony Brook, NY USA

Through the past several years, perovskite (PVSK) has emerged as a solar cell material rivalling those of silicon and quantum dots due to their increasing power conversion efficiency (PCE) [1]. They serve as the active layer within a planar PVSK solar cell and have the common hybrid organic inorganic halide structure ABX_3 , with A representing an organic cation, B representing a metal cation, and X indicating a halide anion. The increasing efficiency of these cells can be attributed to several optoelectronic characteristics such as a high absorption coefficient, tunable bandgap and ambipolar carrier transport [1]. However, PVSK are limited because one of the most classic structures, $MAPbI_3$, is unstable. The organic cation of methylammonium (MA) is hygroscopic, causing the cell to degrade under conditions of moisture, heat, oxygen, and light [3]. With these limitations, research has shown the promising photovoltaic properties of mixed cation/halide PVSK. These studies investigate the mixed cation/halide structure $CsFAMAPb_{1-x}Br_{1-x}$ on the performance of thin film planar PVSK. MA and Cs were used because they stabilize the PVSK by limiting transformation into its yellow photo inactive phase and preventing facile degradation. Furthermore, FA has a smaller bandgap, and the use of bromine makes the PVSK more resistant to oxidation and allows for the tuning of the band gap [2].

One-step spin coating was used to prepare the PVSK film. PbI_2 , MAI, CsI, FAI, and $PbBr_2$ at a molar ratio of 1:.7:0.15:0.15 were placed in a mixed solvent of DMF and DMSO (8:2). Titanium dioxide was spin coated onto FTO substrates and annealed to induce an electron transport layer (ETL). The precursor PVSK solution was then deposited via spin coating and chlorobenzene was dipped onto the surface acting as an anti-solvent for crystal generation. Spiro-OMeTAD was coated as a hole transport layer (HTL) and physical vapor deposition (PVD) was used to add the gold electrodes.

Results from UV-Visible Spectroscopy indicated that the changing of the cation/halide component will not influence the absorption of the photoactive layer. Scanning electron microscopy (SEM) morphology results showed increased grain size for the mixed PVSK [Fig.1, 2]. Additionally, atomic force microscopy showed correspondent morphologies to SEM results, but with an increase in roughness, which is in an acceptable range after increasing the grain size [Fig.3]. Moreover, XRD results implicated that the mixed PVSK had two possible crystal phases (α and δ phases) in comparison to the single peak of (110) of $MAPbI_3$ PVSK while only the cubic α phase is photoactive [Fig.4]. Therefore, the mixed PVSK layer was annealed at various conditions to optimize the cubic alpha photoactive phase. This is because the partial phase segregation can lead to increased recombination at Iodine rich centers, and would therefore hinder PCE. [3] After the optimization, results revealed that a temperature and time of 120 Celsius and 10 minutes allowed for the preferable crystallization of the mixed PVSK with a strong alpha peak and negligible delta phase (if any). Furthermore, the PCE measurement indicated the mixed PVSK has higher PCE, probably due to increased grain size [Fig.5]. The moisture and heat stability tests (XRD) revealed enhanced



structural stability against excessive heat, supporting the idea that mixed structure can successfully generate better performance and enhance the durability as well.

[1] Correa-Baena, Juan-Pablo, et al. "The Rapid Evolution of Highly Efficient Perovskite Solar Cells." *Energy & Environmental Science*,

vol.10,no. 3, 2017, p. 714., doi:10.1039/c6ee03397k.

[2]Xiao, Jia-Wen, et al. "The Emergence of Mixed Perovskites and Their Applications as Solar Cells." *Advanced Energy Materials*,

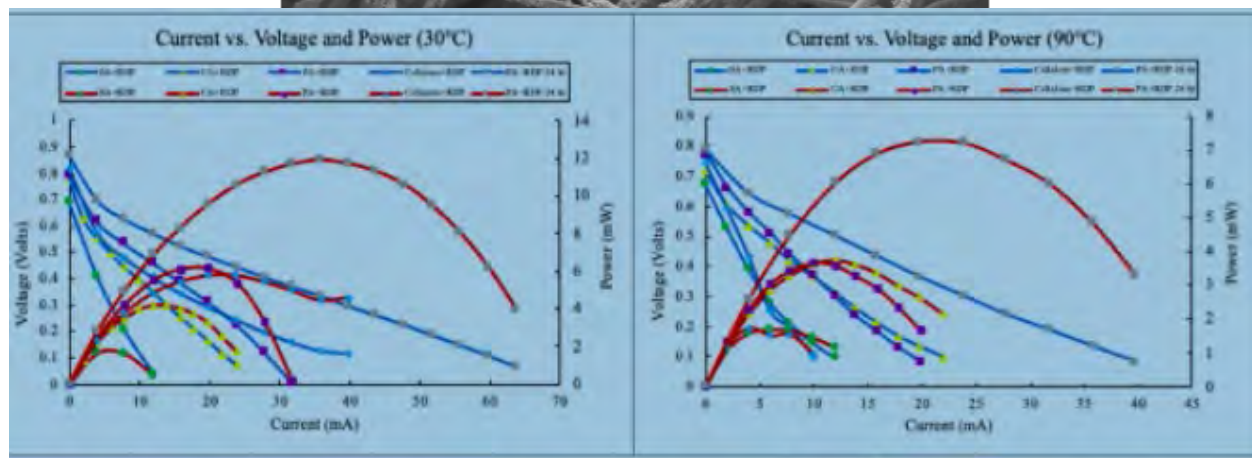
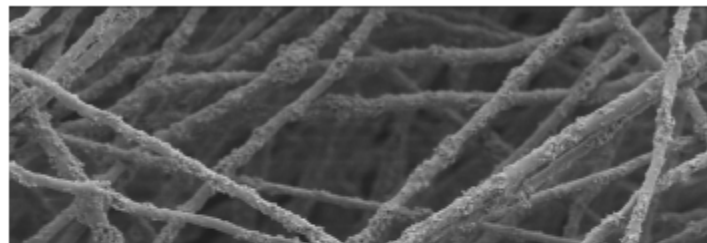
DOI:10.1002/aenm.201700491. Page 1

3. Accessed 22 July 2019

[3]Zhou, Yuanyuan, and Yixin Zhao. "Chemical Stability and Instability of Inorganic Halide Perovskites." *Energy & Environmental Science*, vol. 12, no. 5, 2019, p. 1498., doi:10.1039/c8ee03559h.

Session 10: Fuel Cell Technologies

Chairs: Aniket Raut
Likun Wang



Enhancement of Quaternized Ammonium Polyaromatic Anion Membrane Performance in Alkaline Fuel Cells by Deposition of Graphene Oxide and Catalyst Ink Optimization

Avinash Rao¹, Michael Han¹, Carter Bian², Stoyan Bliznakov³, Miriam Rafailovich³, and Rebecca Isseroff³

¹ Dougherty Valley High School, San Ramon, CA 94582, ² Cupertino High School Cupertino, CA 95014,

³ Department of Materials Science and Chemical Engineering, Stony Brook University, Stony Brook, New York 11790

Current AFC technologies are significantly hindered by various limitations in existing membranes such as increased activation energy for ion transport, substandard mechanical properties, high resistance, and chemical instability, particularly of cationic groups.^[1] Polyaromatic ionomers with quaternary ammonium cationic groups are a particularly well-studied group of ionomers with the potential to compose an efficient alternative to commercial alkaline membranes and eventually proton exchange membranes. However, the ether moieties in many of these ionomers are prone to cleavage, which can diminish the mechanical stability and electrical properties of the ionomer.^[2]

In an attempt to bolster the power density of polyaromatic ionomer membranes in AFCs, two major modifications were made. First, catalyst ink composition was optimized to yield the maximum power performance for the low platinum loading ($.6 \text{ mg/cm}^2$). Previous work and density functional theory calculations have demonstrated that benzene and other aromatic molecules adsorb strongly to Pt and could potentially reduce its catalytic activity.^[2] Consequently, multiple catalyst inks, each containing differing ionomer: catalyst: isopropanol ratios, were prepared and tested on a set of biphenylene (BPN) membranes (Figure 1). It was determined from the tested compositions that an 80:20 (catalyst: ionomer) ratio produced the greatest results for quaternary ammonium biphenyl membranes, yielding an improved 66 mW/cm^2 power density despite reduced back-pressure (Figure 2), comparable to the power density of a commercial PEMFC tested under identical conditions at the same current density (48.2%).

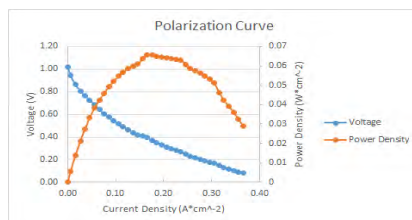


Figure 2: Power density and voltage recorded for MEA prepared from identical anodes and cathodes with $0.6 \text{ mg}_{\text{Pt}}/\text{cm}^2$ and BPN membrane and ionomer. Reached open circuit voltage of 1.02 V and peak power density of 66 mW/cm^2 .

membrane in prior tests. In the future, modifications to membrane structure that increase mechanical stability would allow for thinner membranes to decrease resistance and voltage losses as well as improve durability so significant tests can be made at back-pressures greater than 50 kPa.

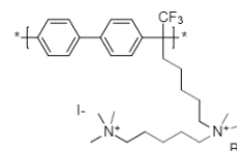


Figure 1: Biphenylene (BPN) ionomer with quaternary ammonium ions on side chains to facilitate anion conductance.

In addition to determining an optimal ink composition, partially reduced graphene oxide (PRGO) was deposited by airbrush onto catalyst-loaded electrodes as a means of improving membrane performance. PRGO has been a staple in PEMFC research, enhancing both current and power density. When applied to the AFC, the performance improved slightly, seeing an increase of peak power density by 1 mW/cm^2 , which was measured at a higher current density.

From these modifications, it was determined that the polyaromatic ionomer membranes based AFCs could be a potential alternative to traditional Nafion based PEMFCs. The membrane electrode assembly reached a power density of 66 mW/cm^2 at a low back-pressure of 50 kPa; likewise, the current density of 400 mA/cm^2 was unprecedented for this particular polyaromatic

¹Gottesfeld, Shimshon, et al. "Anion Exchange Membrane Fuel Cells: Current Status and Remaining Challenges." *Journal of Power Sources*, vol. 375, 31 Jan. 2018, pp. 170–184., doi:10.1016/j.jpowsour.2017.08.010.

²Maurya, Sandip, et al. "Rational Design of Polyaromatic Ionomers for Alkaline Membrane Fuel Cells with $>1 \text{ W/cm}^2$ Power Density." *Energy & Environmental Science*, vol. 11, no. 11, 2018, pp. 3283–3291., doi:10.1039/c8ee02192a.

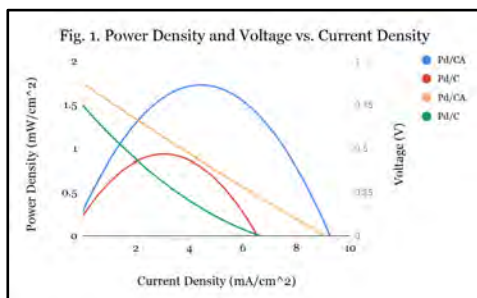
³ Wang, Xin, et al. "N-Cyclic Quaternary Ammonium-Functionalized Anion Exchange Membrane with Improved Alkaline Stability Enabled by Aryl-Ether Free Polymer Backbones for Alkaline Fuel Cells." *Journal of Membrane Science*, vol. 587, 2019, p. 117135., doi:10.1016/j.memsci.2019.05.059.

Facile Synthesis of Carbon Aerogel and Application as Catalyst Support to Increase Performance of Proton Exchange Membrane Fuel Cells

Kevin Gu¹, Eric Kim², Sunil Sharma³, Likun Wang⁴, Stoyan Bliznakov⁴, Miriam Rafailovich⁴

¹Deerfield Academy, Deerfield, MA 01342; ²Stuyvesant High School, New York, NY 10282; ³Department of Chemistry, Stony Brook University; ⁴Department of Materials Science and Chemical Engineering, Stony Brook University, Stony Brook, NY 11794

Proton exchange membrane fuel cells (PEMFC) offer a clean alternative to fossil fuels and nonrenewable energy. Traditional PEMFCs employ platinum on carbon (Pt/C) as the catalyst, although research has been done on non-platinum metals to increase cost efficiency. [1] Carbon black is used as the catalyst support due to its low cost and ease of production; however, it has drawbacks due to its abundance of micropores, hence limiting diffusion of reactants and products and low performance.

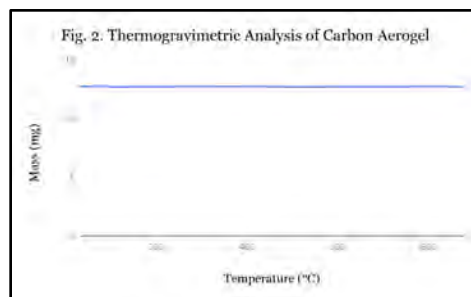


Carbon aerogels are a viable replacement because they have a high surface area, high electrical conductivity, and controllable pore structure which can be easily adapted to electrochemical applications such as supercapacitors and fuel cell electrodes. In this study, carbon aerogel was prepared and impregnated with palladium. The aerogel's catalytic activity was compared with palladium on commercial carbon black (Vulcan XC72R), measured by peak power and current density for a 30% wt Pd loading catalyst ink.

We report a novel method for synthesis of carbon aerogel using the freeze-drying technique. A resorcinol-formaldehyde gel (1:2 ratio) is formed through sol-gel polymerization using sodium carbonate as catalyst. After gelation, we perform solvent exchange on the gels with DI water and age for three days. Then, the gels are freeze dried in a vacuum at -30 °C for 24 h, -10 °C for 24 h, 0 °C for 24 h. Finally, the organic aerogel is carbonized in N₂ atmosphere at 800 °C for 2 hours at a heating rate of 10 °C/min. After carbonization, the furnace was allowed to cool to room temperature.

Figure 1 shows the catalytic activity of palladium on carbon aerogel compared to palladium on carbon black. The aerogel showed an increase in current and power density in comparison to commercial carbon black at 43% and 106%, respectively.

To test the aerogel's thermal stability, the carbon aerogel was put into the thermogravimetric analysis machine. As seen in figure 2, even at 900 °C, the carbon aerogel exhibited little to no mass loss, illustrating its thermal stability in high temperature environments.



Future work includes testing the mechanical durability of the carbon aerogel as catalyst support compared to commercial options. We also hope to synthesize a new batch of nitrogen-doped carbon aerogel or possibly post-dope the carbon aerogel and observe improvements of durability. Previous literature has also shown that aerogels possess excellent CO₂ adsorption as well as hydrophobic characteristics. [2] These features can be adapted to address the poisoning and electrolyte crossover issues present in alkaline anion exchange membrane fuel cells.

[1] Antolini, Ermete. "Palladium in Fuel Cell Catalysis." *Energy & Environmental Science*, vol. 2, no. 9, 2009, pp. 915–931., doi:10.1039/b820837a.

[2] Alhwaige, Almahdi A., et al. "Carbon Aerogels with Excellent CO₂ Adsorption Capacity." *ACS Sustainable Chemistry & Engineering*, vol. 4, pp 1286–1295., doi:10.1021/acsschemeng.5b01323.

Citric Acid Crosslinking of Carboxycellulose Nanofiber Membranes to Enhance Proton Exchange Membrane Fuel Cell Performance

George Cai¹, Songze Wu², Songtao Li³, Likun Wang⁴, Aniket Raut⁴,
Sunil Sharma⁵, Priyanka Sharma⁵, Miriam Rafailovich⁴

¹Wayzata High School, Plymouth, MN 55446, ²High School Affiliated to Renmin University of China, Beijing, China, ³Princeton International School of Science and Mathematics, Princeton, NJ 08540, ⁴Department of Materials Science and Chemical Engineering, Stony Brook University, Stony Brook, NY 11794, ⁵Department of Chemistry, Stony Brook University, Stony Brook, NY 11794

Proton exchange membrane fuel cells (PEMFCs) are clean, efficient electrochemical energy storage devices based on the spontaneous reaction between hydrogen and oxygen. Hydrogen gas can be reliably generated by solar and wind power, while atmospheric oxygen is sufficient, so PEMFCs can store and provide stable power from intermittent sources. However, there are barriers to competitive pricing and efficiency for widespread use in vehicles and other applications¹. Carboxycellulose nanofibers (CNFs) promise to be a green, cheap alternative membrane material that conducts protons via carboxylic acid groups. CNF membranes have excellent mechanical and hydrogen gas barrier properties, but the performance (maximum power density of 0.79 mW/cm²) is around 3 orders of magnitude lower than Nafion (maximum power density of ~450 mW/cm²)². Additionally, nanocellulose swells significantly with high relative humidity and temperature, compromising mechanical stability.

In this study, citric acid, a naturally occurring, biodegradable tricarboxylic acid, was used to crosslink CNF membranes to enhance both performance and mechanical stability in PEMFCs. CNF membranes were prepared by solvent casting 70 mL CNF suspension with 0 or 0.3 mL 1M citric acid, and then hot-pressed and cut into 3 cm x 3 cm PEMs. The PEMs were tested in a custom fuel cell test station at 80°C and 100% relative humidity with 5 cm² electrodes of 0.1 mg/cm² Pt/C on carbon paper. The resulting polarization curves showed a 3044% increase in maximum power density (27.7 mW/cm² vs 0.91 mW/cm²) and 2236% increase in maximum current density (111.8 mA/cm² vs 5.0 mA/cm²) of the crosslinked membrane compared to the uncrosslinked control. Thermogravimetric analysis showed that the onset temperature of thermal decomposition was 170 °C for the crosslinked membrane, which is well above the operating temperature range of PEMFCs. In Fourier-transform infrared spectroscopy, the C=O peak was significantly larger in the citric acid crosslinked membrane, providing further evidence of crosslinking.

Further data is being collected on *in situ* proton conductivity. Mechanical properties will be characterized with temperature scanning DMA and tensile strength testing. Morphological and chemical characterizations such as 3D focused ion beam SEM, AFM, TEM, BET surface area, C¹³ NMR, zeta potential, ion exchange capacity, and x-ray diffractometry are ongoing.

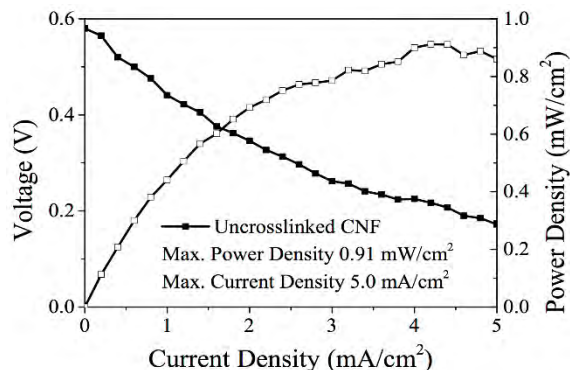


Figure 1 Polarization curve for unmodified CNF membrane

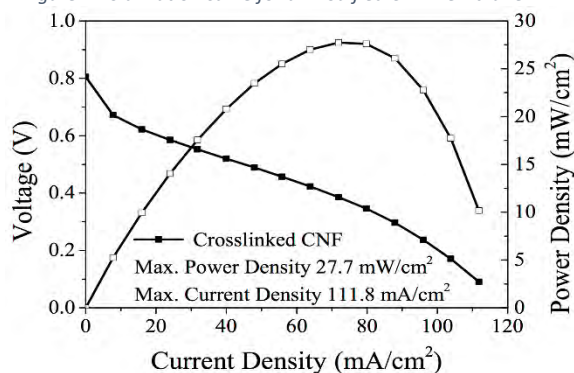


Figure 2 Polarization curve for citric acid crosslinked CNF membrane

¹ Yee, R. S. L., Rozendal, R. A., Zhang, K., & Ladewig, B. P. (2012). Cost effective cation exchange membranes: A review. *Chemical Engineering Research and Design*, 90(7), 950–959. <https://doi.org/10.1016/j.chemd.2011.10.015>

² Bayer, T., Cuning, B. V., Selyanchyn, R., Nishihara, M., Fujikawa, S., Sasaki, K., & Lyth, S. M. (2016). High temperature proton conduction in nanocellulose membranes: Paper fuel cells. *Chemistry of Materials*, 28(13), 4805–4814. <https://doi.org/10.1021/acs.chemmater.6b01990>

Enhancing the Performance of Novel Cellulose Membranes for the Proton Exchange Membrane Fuel Cell

Christine Kong¹, Bhawan Sandhu², Likun Wang³, Aniket Raut³, Rebecca Isseroff², Dr. Sunil Sharma⁴, Dr. Priyanka Sharma⁴, Dr. Miriam Rafailovich³

¹Commack High School, Commack, NY 11725

²Lawrence High School, Cedarhurst, NY 11559

³Department of Materials Science and Chemical Engineering, Stony Brook University, Stony Brook, NY 11794

⁴Department of Chemistry, Stony Brook University, Stony Brook, NY 11794

Fossil fuels, non-renewable energy sources, damage the environment by increasing carbon emissions. Hydrogen Proton Exchange Membrane Fuel Cells (PEMFCs) provide an alternative way of producing clean energy using the reduction-oxidation reaction of hydrogen and oxygen gas. These fuel cells are extremely desirable because the only byproduct is H₂O. This research project examines the creation of a fuel cell membrane using cellulose filter paper and Resorcinol bis(diphenylphosphate) (RDP). RDP has recently been shown to be a proton conductor.¹

Ahlstrom cellulose filter papers with a 1.5 micron pore size were functionalized using sulfuric acid (H₂SO₄), citric acid (C₆H₈O₇), and phosphoric acid (H₃PO₄), respectively, by submerging them in 100 ml of 1M concentration of each acid for 30 minutes. A different set of membranes was also created by submerging the membranes in acids heated to 80°C and then soaked for 24 hours at room temperature in their respective acid. All membranes were dried overnight at room temperature. Membranes were coated with RDP by dropping six drops of RDP on one side of the membrane and three drops of RDP on the other side using a plastic pipette. The pipette and tweezers were used to spread the liquid RDP. Membranes were then placed in an oven at 150°C for 20 minutes to uniformly disperse the RDP across the membrane.

Membranes were tested on the Fuel Cell Testing Station (FuelCellsEtc) under 100% humidity with oxygen introduced from the air. Membranes were tested under varying temperatures, 30°C, 60°C, 80°C, and 90°C. Standard carbon electrodes with platinum catalysts cut to an area of 5 cm² were used.

Table 1 shows the highest power output of each of the membranes tested at various temperatures in milliwatts. The membrane soaked in phosphoric acid (H₃PO₄) for 24 hours and then treated with RDP had the highest power output at each temperature and

Table 1. Highest power density value for each membrane tested at 30, 60, 80, and 90°C.

	30°C	60°C	80°C	90°C
SA+RDP 30 min	1.623	2.66	2.542	1.67
CA+RDP 30 min	4.190604	4.5471	4.53468	3.7452
PA+RDP 30 min	6.14394	10.68162	6.367116	3.671
Cellulose+RDP	5.7618	9.9852	8.112	1.732
PA+RDP 24 hr	11.87844	12.98674	13.26932	7.2468
Percent Increase	106.158%	30.060%	63.576%	318.406%

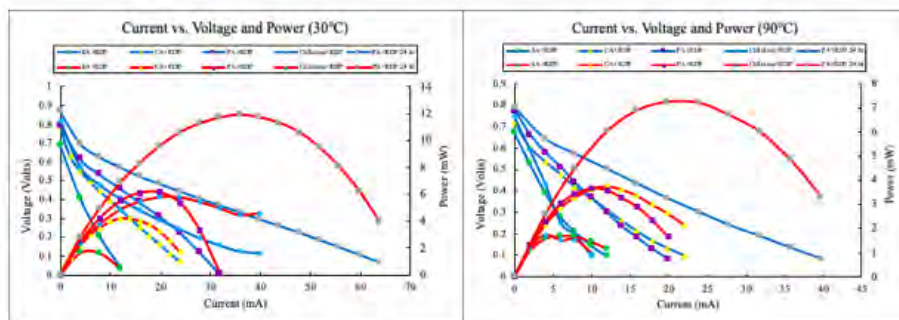


Figure 1. Polarization curves for each membrane tested at 30°C and 90°C.

displayed a significant percent increase compared to the control.

In the future, we would like to measure the Ion Exchange Capacity (IEC) through titration and compare the 30 minute membranes with the 24 hour membranes. Further testing is also required for membranes soaked in 24 hours. Finally, we would like to test membranes with a higher molarity of acid (5M, 7M) and explore methods of enhancing RDP function.

¹Wang, Likun, et al. "Operation of Proton Exchange Membrane (PEM) Fuel Cells Using Natural Cellulose Fiber Membranes." *Sustainable Energy & Fuels*, The Royal Society of Chemistry, 30 July 2019, pubs.rsc.org/en/Content/ArticleLanding/2019/SE/C9SE00381A#!divAbstract.

Optimization of Pt/C Catalyst Nanofibers Electrospun on Nafion 117 Membranes in Polyelectrolyte Membrane Fuel Cells

Surya Rajan¹, Edward O'Keefe², David Lederer³, Aniket Raut⁴, Likun Wang⁴, Miriam Rafailovich⁴

¹California High School, San Ramon, CA, ²Ridgewood High School, Ridgewood, NJ, ³Hebrew Academy of the Five Towns and Rockaway, Cedarhurst, NY, ⁴Department of Materials Science & Chemical Engineering, Stony Brook University, NY

Polyelectrolyte Membrane Fuel Cells (PEMFCs) have been of great interest as a potential source of alternative energy due to their high power output and zero-emission activity, yet their low cost efficiency relative to combustion engines has impeded commercial success.¹ Research concerning the improvement of PEMFC performance has largely focused on optimizing the catalysis of the oxidation and reduction reactions in the cell. While the Pt/C catalyst is traditionally deposited on the electrodes of the fuel cell, this study explores electrospinning Pt/C onto the commercially-used Nafion 117 membrane and finely tuning the deposition and composition of the nanofiber structures to increase electrochemically active surface area and proton conductivity in the fuel cell.²

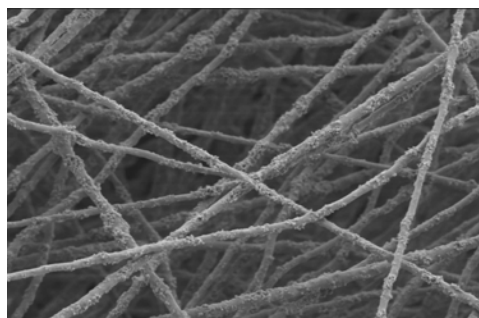


Fig. 1: SEM image of 30.0 Pt/C wt. % nanofibers

SEM and 3D laser microscopy imaging revealed that flow rate and Pt/C wt. % were positively correlated with platinum agglomeration and nanofiber diameter, respectively (Fig. 1). Optical microscopy confirmed that uniform coating and consistent fiber patterns were maintained throughout the nanofiber structures.

The Nafion 117 nanofiber-coated membranes were tested in an H-tech PEMFC kit in an open-air environment at the cathode and with pure hydrogen flowing at 80 ccm into the anode. The peak power density achieved by the 32.5% wt. Pt/C nanofibers indicated an optimal fiber diameter of approximately 1.25 μm . At all Pt/C wt. %, the 0.5 mL/hr nanofiber-coated membranes performed better than or equal to the 1.0 mL/hr nanofiber-coated membranes in terms of power density, supporting the agglomeration reduction theory derived from SEM imaging. Overall, tests showed a 62% increase in maximum power density with 32.5% wt. Pt/C nanofibers extruded at 0.5 mL/hr onto Nafion 117 membranes when compared with commercially-used Nafion 117 membranes (Fig. 2). Further work will concern optimizing components of the (Nafion 117)-PAA-Pt/C solution and implementation of this work in Anion Exchange Membrane Fuel Cells (AEMFCs).

Catalyst ink solutions were made from Nafion 117, poly(acrylic acid) (PAA), and Pt/C as solutes in an isopropanol-water solvent, with Pt/C catalyst wt. % varying from 20% to 40%. Solutions were then electrospun onto Nafion 117 membranes at a potential difference of 15.0 kV, maintaining a platinum loading of approximately 0.1 mg/cm^2 . Flow rates of 0.5 mL/hr and 1.0 mL/hr were employed at each Pt/C wt. %.

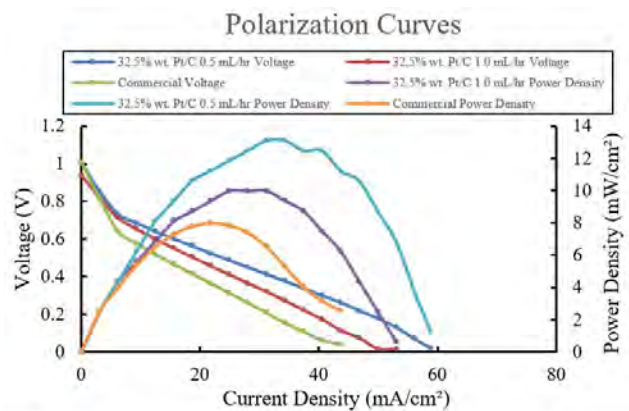


Fig. 2: Power density and polarization curves of PEMFCs with 32.5% wt. Pt/C nanofibers electrospun onto membranes at varied flow rates

[1] Iain Staffell, et al. "The Role of Hydrogen and Fuel Cells in the Global Energy System." Energy & Environmental Science, Royal Society of Chemistry, 10 Dec. 2018, pubs.rsc.org/en/content/articlehtml/2019/ee/c8ee01157e

[2] Ramakrishna S., Fujihara K., Teo W., Yong T., Ma Z., & Ramaseshan R. "Electrospun Nanofibers: Solving Global Issues." *Materials Today*, Elsevier, 18 Feb. 2006, www.sciencedirect.com/science/article/pii/S136970210671389X.

Reduction of Carbon Monoxide Poisoning in Proton Exchange Membrane Fuel Cells via Application of Gold/Ruthenium Nanoparticle Monolayer

Luca Leger¹, Ryan Meehan², Mark Zhang³, Likun Wang⁴, Miriam Rafailovich⁴

¹Medfield High School, Medfield, Massachusetts 02052, ²Sachem High School East, Farmingville, New York 11738, ³Green Valley High School, Henderson, Nevada 89012, ⁴Department of Materials Science and Chemical Engineering, Stony Brook University, Stony Brook, New York 11794

Proton exchange membrane fuel cells (PEMFCs) are a promising alternative to traditional forms of energy, such as fossil fuels, due to their environmental friendliness. PEMFCs utilize the reduction-oxidation reaction $2\text{H}_2(\text{g}) + \text{O}_2(\text{g}) \rightarrow 2\text{H}_2\text{O}(\text{g}) + \text{energy}$. However, one issue currently plaguing cell efficiency is that hydrogen fuel inevitably contains carbon monoxide (CO) contaminant¹. CO can further be formed within the PEMFC through the reaction $\text{H}_2(\text{g}) + \text{CO}_2(\text{g}) \rightarrow \text{CO}(\text{g}) + \text{H}_2\text{O}(\text{g})$ that occurs at the cathode¹. Unfortunately, due to the fact that the bonding of CO to Pt is energetically preferable to that of H₂ to Pt¹, CO adsorbs to active sites on the platinum catalyst, blocking hydrogen fuel conversion and rapidly reducing cell efficiency.

Gold (Au) and Ruthenium (Ru) nanoparticles (NPs) have proven to be effective at oxidizing CO and reducing its detrimental effects on PEMFCs²; however, their joint effect is largely unstudied.

Here, we synthesized gold ruthenium nanoparticles through the two-phase method developed by Brust et al². Monolayers of the AuRu nanoparticles were deposited on Nafion membranes at various surface pressures using the Langmuir-Blodgett method. Following this, each membrane was tested using a hydrogen fuel cell demonstration kit.

Examining membranes coated at surface pressures of 1 mN/m, 2 mN/m, and 5 mN/m, we find that every membrane coated with AuRu nanoparticles experienced an increased maximum power output. The membrane coated



Fig. 2: Top-view TEM micrograph of assembled AuRu NPs at surface pressure of 2 mN/m.

at a surface pressure of 2 mN/m achieved the highest maximum power density in all testing environments. Under atmospheric oxygen conditions, the surface pressure 2 mN/m membrane achieved a 47.3% increase over the control (see figure 1) and with pure oxygen intake, it achieved a 21.5% increase over the control. The AuRu coated membranes experienced less improvement in pure oxygen conditions due to the fact there was no CO₂ present to form CO, meaning the improvements due to oxidation of CO were less pronounced. The results come as some of the first direct proof of the viability of gold ruthenium nanoparticles as a method of mitigating CO poisoning in proton exchange membrane fuel cells.

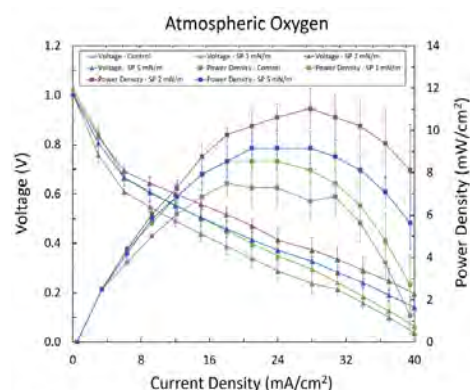


Fig. 1: Polarization and power curves of PEMFCs with membranes coated with AuRu NPs at various surface pressures (SPs)

[1] Wang, Likun, et al. "Suppression of Carbon Monoxide Poisoning in Proton Exchange Membrane Fuel Cells via Gold Nanoparticle/Titania

Ultrathin Film Heterogeneous Catalysts." *ACS Applied Energy Materials*, vol. 2, no. 5, 2019, pp. 3479–3487., doi:10.1021/acsaem.9b00264.

[2] Brust, Mathias, et al. "Synthesis of Thiol-Derivatized Gold Nanoparticles in a Two-Phase Liquid-Liquid System." *J. Chem. Soc., Chem. Commun.*, no. 7, 1994, pp. 801–802., doi:10.1039/c39940000801.

Thin Film Applications of SiC in the Space Program:

- Silicon nitride ceramic matrix composite (SiC CMCs)
- Current SiC CMCs tend to degrade when exposed to several stresses such as intense temperature. Due to this deficiency, an engineered matrix composite was designed to offer resistance to cracking by converting oxygen into a sealant.
- Provides a durable material able to withstand extreme temperatures.
- High Voltage Silicon Carbide Power Devices
- Silicon carbide power devices can enhance the efficiency and power management of aircraft systems.
- High temperature SiC electronics will reduce spacecraft heating.
- Can be applied to future space nuclear power systems.
- The reduction of heating in heat resistant SiC ceramic will allow for the placement of the electronics in closer proximity with the reactor.

Common Applications of SiC CMCs:

- Jet Engine Exhausts
- Land based power generation
- Nuclear reactors

Figure 1: Representation of heat exchangers, a notable use of SiC/SiC CMCs





Figure 2: A 3mm x 3mm SiC circuit chip



Benefits:

- SiC Power Devices
- With hard gap semiconductor
- Provides large bandgap
- Higher thermal conductivity
- Higher junction temperatures
- Self-healing allows for
- Reliable higher thermal conductivity
- High resistance matrix
- Cost Effective: Enabling allows for longer runtimes of the composite
- Flexible
- Easily adaptable

References:

- ["Thin Film Applications of SiC in the Space Program."](#)
- ["Current SiC CMCs tend to degrade when exposed to several stresses such as intense temperature. Due to this deficiency, an engineered matrix composite was designed to offer resistance to cracking by converting oxygen into a sealant."](#)
- ["Provides a durable material able to withstand extreme temperatures."](#)
- ["High Voltage Silicon Carbide Power Devices"](#)
- ["Silicon carbide power devices can enhance the efficiency and power management of aircraft systems."](#)
- ["High temperature SiC electronics will reduce spacecraft heating."](#)
- ["Can be applied to future space nuclear power systems."](#)
- ["The reduction of heating in heat resistant SiC ceramic will allow for the placement of the electronics in closer proximity with the reactor."](#)
- ["Jet Engine Exhausts"](#)
- ["Land based power generation"](#)
- ["Nuclear reactors"](#)

Michael Han
ABOUT WD-40



WD-40 multi-use aerosol, 12 oz.
// WD-40 Company, inc.

- Water Displacement, 40th formula
- Designed as a rust-prevention solvent and degreaser for use in the aerospace industry
- Developed in 1953 in San Diego, CA, by the Rocket Chemical Company (renamed WD-40 Company inc. after its sole product)
- In 1993, it was found that 4 of every 5 households had at least one can of WD-40

SM-65 ATLAS AND USE IN THE SPACE PROGRAM

WD-40 was first used in the aerospace industry by Convair, an aerospace contractor, to protect the outer surface of the Atlas missile. It was designed to deliver nuclear warheads from long distances, which had been difficult to achieve due to the weight of the warhead as well as the distance. The Atlas missile had a range of 14,000 km with a CEP of 3.7 km and carried a 1.5 MT W49 thermonuclear warhead.

Unfortunately, with advances in missile technology, the Atlas missiles became obsolete. However, from 1962, they were used extensively by NASA in their space programs. Of the six crewed flights conducted during the Mercury program, the last four, Mercury 6, 7, 8, and 9, used Atlas rockets. Notably, Friendship 7, the craft that carried John Glenn, the first American in orbit, to space in 1962, was propelled by an Atlas rocket.

The Gemini Program followed the Mercury Program. The Gemini Program pioneered a new capsule that held two astronauts, which gave the program its name. Although the Gemini program used the more powerful Titan rocket to lift the larger and heavier capsule, Atlas rockets still saw use as cargo rockets during the program.



Atlas 2E Missile
// San Diego Aerospace Museum



Gemini/Titan II launch vehicle
// NASA

COMPOSITION

According to the MSDS provided by the WD-40 Company, WD-40 Multi-Use Product Aerosol is composed of:

- 45-50% low vapor pressure aliphatic hydrocarbons (to decrease viscosity and increase penetration into cracks)
- <35% petroleum base oil
- <25% aliphatic hydrocarbons
- 2-3% carbon dioxide (propellant)

All percents indicate percent mass. The exact composition of WD-40 is a trade secret.)

References:

- Dunbar, Brian. "Mercury Manned Flights Summary." NASA, NASA, 17 Mar. 2015, www.nasa.gov/pdf/mercury/mis/misna/manned_flights.html
- "Gemini: Dodge to the Moon." NASA, NASA, www.nasa.gov/specials/gemini_gallery/
- "SM-65 Atlas." Atlas: The Road to Space, www.nasa.gov/pdf/atlantis/atlantis/
- "WD-40 Multi-Use Product Aerosol Material Safety Data Sheet." WD-40 Company, 5 Mar. 2019.
- "WD-40." Wikipedia. "WD-40 Backlist & Brand History: WD-40." "WD-40." WD-40 Company, www.wd40.com/history/

MATERIALS CHALLENGE BY MICHAEL HAN

Memory Foam/Tempur Foam

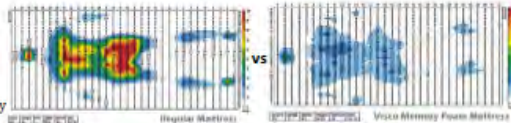
Top-Secret NASA Space Program

- Make customizable seats for astronauts to reduce the effects of high gravitational forces especially during takeoff and landing for the Apollo 11 mission
- Improve uncomfortable seats made from hard materials
- Keep the astronauts from being smashed
- Improve crash protection for airline pilots and passengers



Officially Declassified

- Entrepreneurs pushed for commercialization
- Used as pads & toppers in ER hospital beds to alleviate bed injuries where the body gets irritated from staying stationary



Modern Consumer Products

- Protection in helmets, comfortable prosthetic limbs, shock absorber in bulletproof vests
- Luxurious items like furniture, chairs, shoe pads, mattresses, and pillows



References:

- 1. "About Visco Foam." Visco Memory Foam Mattress, www.visco-memoryfoammattress.com/about-visco-foam/
- 2. Dunbar, Brian. "Memory Foam." NASA, NASA, www.nasa.gov/offices/lp/office/memfoam.html

The Prize Winners:
Victoria Levy
Megha Gopal
Ethan Eisenberg
Bole (James) Pan
Jasmin Li
Frank Gold

Space Blankets

Aka Emergency Blankets
Frank Jin Paul Steven



Gold or aluminium mylar (Polyethylene terephthalate) originally used by NASA as insulation material that protects equipment from infrared as well as UV radiation while being extremely lightweight. Used to protect against the intense heat of the sun on one side of space craft while retaining heat to protect against the frigid cold on the dark side of spacecraft as seen above in the Apollo 11!

References

- Dunbar, Brian. "A Shining Example of Space Benefits." NASA, NASA, www.nasa.gov/mission/earth/technologies/silver_insulation.html
- Bryan, William. "Emergency Blankets." NASA, NASA, 1 Feb. 2016, www.nasa.gov/offices/oct/40-years-of-nasa-spinoff/emergency-blankets

- Now applied to things all around us
- Emergency blankets for refugee camps as well as long distance runners
- Incorporated into heat retaining jackets and clothing
- Has also become a hot topic for fashion designers
- Allowed for a thin yet insulating layer



We gratefully acknowledge support from the Louis Morin Charitable Trust

Muki Shanmyan
Anthony Del Valle
Jonathan Sokolov
George Cai
Ethan Eisenberg
AUDREY CUI
李松涛
William Bertolotti
Eric Kim
Kevin Gu
Jessica Hofflich
吴松涛 林高冲
Vimala S Alayappan
Finnur Christiansen
Ryan Mechem
Avinash RAO
KEVIN YANG
Richard Jin Cai
Richard Li
Jack O'Connell
Mehul Hadik
PK Li
Esther Chai
Julia Miller
Roberto Milan
Addison Liu
Kiana Jang
Miriam Pofai bond
Maira Grajales
Cici Liu
Nina Pollner
Jonathan Ledner
Lauren Stiefel
Jeffrey Wolberg
Sahana Ramrakhiani
Shmuel Z Padwa
Harriet Laverne
Kerui Yang
N. Sath
Diga Rai-Giosappe
Emily Hlavatin
Carter B.
IKShu Pandey
Jessica Somel
Hans Shen
Stella
Ilana Hadik
Alex Krauler
Jaka Gulzer
Rohit Prasad
潘相尔
马子健
Jonathan MARCELIN
James Katherine-Lian
Carl Dan Zy
Christopher Chan
Kevin
Sanya Metta
E. Keefe
Jodor Beismakov
LUI SA PAN

2019